CC 70-243-10

FINAL REPORT

FUNDAMENTALS OF THE OXIDATION PROTECTION OF TANTALUM

by

M. KOLODNEY and R. A. GRAFF

THE CITY COLLEGE
RESEARCH FOUNDATION
THE CITY COLLEGE of
THE CITY UNIVERSITY of NEW YORK

Prepared for
National Aeronautics and Space Administration
Grant NGR 33-013-017

THE CITY COLLEGE RESEARCH FOUNDATION
THE CITY COLLEGE, THE CITY UNIVERSITY OF NEW YORK
NEW YORK, NEW YORK 10031

FINAL REPORT

FUNDAMENTALS OF THE OXIDATION PROTECTION OF COLUMBIUM AND TANTALUM

By
M. Kolodney and R.A. Graff

Prepared For
National Aeronautics and Space Administration
Grant NGR 33-013-017

October 1, 1970

Foreword

The City College Department of Chemical Engineering expresses its gratitude to NASA for supporting this program. We are especially grateful to Robert E. Oldrieve of the Lewis Research Center for his frequent and careful monitoring of the program and for his enthusiastic encouragement.

The authors are particularly appreciative of the efforts of the Chemical Engineering Shop in all phases of the experimental program. Mrs. N. Cohen was of great assistance in the preparation of reports throughout the program. Our thanks are also due to Mrs. P. Wentworth and Mrs. L. Palley for major assistance with this Final Report.

Abstract

A fundamental study of the protection of tantalum by silicides has been performed. Thermodynamic properties of all tantalum silicides have been measured by an EMF method using solid electrolytes. Considerable improvement over older data has been obtained. Measurements have also been made of the degradation of silicide coatings by diffusion of silicon into the tantalum substrate. These measurements permit estimates of time and temperature effects on lifetimes of coatings. Barriers to diffusion have been investigated, but no good ones found. Lastly, the oxidation process has been studied in terms of a silicide ($TiSi_2$) that forms a stable metal oxide. It has been shown that oxidation protection may be retained if the metal oxide can be embodied in the surface silica glass of the coating.

Contents

List of Tables

List of Tables (cont.)

List of Figures

1. Introduction

Refractory metals (metals whose melting points exceed about 3405°F or 1875°C) are required for a variety of applications such as advanced aircraft and space engines. At temperatures below about 2000°F (1092°C) a number of superalloys find application, but there appears to be small likelihood of extending these alloys to higher temperature ranges.

Unfortunately, most proposed high temperature uses of the refractory metals are in oxidizing atmospheres where molybdenum, tantalum, columbium and tungsten display very high loss rates by oxidation. Alloying to improve oxidation resistance has proven unsatisfactory, although alloys with excellent structural properties have been developed (1). Therefore, oxidation protection by coating is essential if these alloys are to attain their true potentials.

Coatings must not only be resistant to oxidation themselves, but if they do oxidize, the film formed must be a bar to the transport of oxygen to the substrate. Damage to the coating surface should be self-healing. In addition, the coating should be adherent to the base and match its expansion characteristics. Silica glass, SiO_2, fulfills the first requirement admirably. When it is formed on compounds such as silicon carbide or silicon nitride it provides excellent protection. Therefore, it is not surprising that refractory metal silicides have been primary candidates for coatings. Although many other coatings have been proposed and tested, the present program devoted itself to the silicides only.

The approach to the study of the fundamentals of silicides was broadly, a two-pronged one. First, it was aimed at the acquisition of thermochemical data and secondly at a study of the mechanism of coating failure.

Thermochemical data are needed to permit the prediction of the possibility of oxidation reactions and their extent. For example, a standard coating for tantalum is the disilicide, $TaSi_2$. Lower silicides, such as Ta_5Si_3 are also known to be stable. Therefore, when $TaSi_2$ oxidizes, does it follow reaction (1)?

$$4\ TaSi_2 + 13\ O_2 = 2Ta_2O_5 + 8\ SiO_2 \qquad (1)$$

Or does it oxidize in accordance with reaction (2)?

$$5\ TaSi_2 + 7\ O_2 = Ta_5Si_3 + 7\ SiO_2 \qquad (2)$$

Furthermore, what is the effect of temperature and of oxygen pressure upon the equilibrium reaction? These questions can be answered with the help of good thermochemical data.

The second area of interest involved the basic modes of coating failures. The present program did not concern itself with failures such as may be caused by mismatch of expansion coefficients or by sharp edges, important as these may be. Instead, it was confined to a study of the mechanisms at the coating-substrate interface and at the gas-coating interface.

One possible mode of failure of a disilicide coating is by loss of silicon to the substrate. In the process of diffusion into the underlying metal, silicon leaves lower silicides behind and may destroy the oxidation resistance of the coating because the properties of the lower silicides are inferior in this respect. It would be desirable to minimize the diffusion of silicon in order to prolong the coating life. Barriers may be of assistance in this respect.

A second mode of failure of the protective coating is by interference with the silica glass. The formation of a silica glass upon oxidation of a refractory silicide is a rather interesting phenomenon. In the first place, although the silicide is crystalline, a glass is formed upon oxidation well below the melting point of the silica. Secondly, in a low temperature region there is frequently a disastrous failure of the silica film. This phenomenon, originally found in the oxidation of molybdenum disilicide, is known as "pest". It is accompanied by destruction of the glass film and has been attributed to the inclusion of the refractory metal oxide in the silica (2). This explanation was tested in the silicide system studied here and found inadequate.

2. Thermochemical Data (S.R. Levine)

2.1 Background and Theory

The work performed in this phase of the program has been described in full detail in the thesis of S.R. Levine (3) and in a published paper (4).

The formation of a stable silica glass is essential for protection of refractory metals such as tantalum. Hence, a desirable reaction is one that produces silica and a lower silicide, as for example, reaction (2) previously given

$$5\ TaSi_2 + 7\ O_2 = 7\ SiO_2 + Ta_5Si_3 \qquad (2)$$

The alternative reaction (1) which results in the formation of

$$4\ TaSi_2 + 13\ O_2 = 2Ta_2O_5 + 8\ SiO_2 \qquad (1)$$

the metal oxide as well as silica may interfere with the integrity of the silica film. However, it has been shown that if the refractory metal oxide is volatile, a protective glass can be formed. In addition, this program has demonstrated that non-volatile oxides may also be tolerated if they can be accommodated by the glass. (See Section 4 of this report.)

In order to predict and understand the oxidation behavior of refractory metal silicides, accurate free energy of formation data are required for the silicides and their oxidation products. Data for silica and for the refractory metal oxides are available (5), but data for silicides are scanty. For many refractory metal silicides only enthalphies of formation are available. Thermodynamic information on the tantalum-silicon system, which is the subject of this study, has been collected by three classical techniques: Brewer and Krikorian (6) determined limits for

the stability of refractory silicides by direct reaction of the compounds with carbides and nitrides. Robins and Jenkins (7) measured the heats of formation of some transition metal silicides from the heat evolved during formation of the compounds from their elements. In the third technique, employed by Searcy and coworkers (8-10), the dissociation pressure of silicon over the silicide of interest was measured by the Knudson effusion method. The vapor pressure data were analyzed by a Second and Third Law approach to obtain enthalpies of formation for the silicides. Data for the tantalum silicides, obtained by these three techniques are presented in Table I. The values listed in column IV are based on an average of the Second and Third Law techniques using a value of -112 kcal for the heat of sublimation of silicon at 298^{o}K. The values in column V are based on the same vapor pressure data as column IV but an improved value of the heat of sublimation of silicon (-108.4 kcal at 298^{o}K) was used and the calculations were made using only the Third Law method (11,12).

In the present work a fourth method was for the first time applied to the determination of the thermodynamic properties of the tantalum silicides. This technique employs a solid oxide electrolyte between a silicide electrode and a reference electrode. Solid electrolytes for the measurement of thermodynamic properties were brought into prominence by Kiukkola and Wagner (13), Schmalzried (14) and others. Oxide electrolytes are binary oxides which conduct almost entirely by transport of oxygen ions over a given temperature-oxygen partial pressure domain. A simple cell employing an oxide electrolyte and an iron-iron oxide (Fe_xO) reference electrode may be formulated as:

$$Pt/Fe,Fe_xO//\text{oxide electrolyte}//M,MO/Pt \qquad (3)$$

where the cell reaction is:

$$M + Fe_xO = MO + XFe \qquad (4)$$

If the cell is reversible, the free energy of the reaction ΔG_R is related to the cell voltage E and to the oxygen partial pressure by

$$\Delta G_R = -nFE = RT \ln \frac{P_{O_2} \text{ (for M,MO)}}{P_{O_2} \text{ (for Fe,Fe}_xO)} \qquad (5)$$

where T is the temperature (^oK) and P refers to the pressures over the respective metal-metal oxide elecrodes. From equations (4) and (5), the standard free energy of formation of MO may be obtained provided that all solid phases are pure (unit activity) and the free energy of formation of the reference oxide Fe_xO is known.

$$\Delta G^o_{MO} = \Delta G^o_{Fe_xO} - nFE \qquad (6)$$

For the more complex reaction of equation (2) a cell using an iron-iron oxide reference electrode would be formulated as follows.

$$Pt/Fe,Fe_xO//\text{oxide electrolyte}//SiO_2,TaSi_2,Ta_5Si_3/Pt \qquad (7)$$

The overall cell reaction is

$$5\ TaSi_2 + 14\ Fe_xO = 7\ SiO_2 + Ta_5Si_3 + 14\ xFe \qquad (8)$$

and the free energy of formation of the highest silicide $TaSi_2$ may be obtained from

$$5\Delta G^o_{TaSi_2} = 7\ \Delta G^o_{SiO_2} + \Delta G^o_{Ta_5Si_3} - 14\ \Delta G^o_{Fe_xO} + nFE \qquad (9)$$

Page 7 is
Blank

Table I

Enthalpy of formation data for the tantalum silicides

kcal/g-atom of silicon

I Compound	II Brewer and Krikorian(5) ΔH^{o}_{298}	III Robins and Jenkins(6) ΔH^{o}_{T}	IV Myers and Searcy(7) ΔH^{o}_{298}	V Searcy and Finnie (10) ΔH^{o}_{298}
½ $TaSi_2$	-12.8 to -32.3	-13.9±1	-11.6±5	-12±3
1/3 Ta_5Si_3	-20 to -77.2	-25.3±1	-26.7±5	-24±4
Ta_2Si	-20 to -90.1	---	-29.3±5	-30.2±4
$Ta_{4.5}Si$	-20	---	-34.4±5	-35.8±4

Obviously, success of the measurement depends upon an accurate knowledge of the free energies of formation of not only SiO_2 and Fe_xO, but also of the lower silicide, Ta_5Si_3. Since the latter is unknown, it becomes necessary to establish free energies for all four of the silicides in the system. Furthermore, oxidation of a silicide to silica and the lower silicide is not the sole possibility. Instead, oxidation may yield Ta_2O_5 and a higher silicide or it may produce both SiO_2 and Ta_2O_5 as in equation (1). All of the possible half-cell reactions for the four silicides of the Ta-Si system ($TaSi_2$, Ta_5Si_3, Ta_2Si and $Ta_{4.5}Si$) are shown in Table II where they are arranged in terms of their reaction products. In addition, this table lists expected EMF values versus an iron-iron oxide (Fe,Fe_xO) reference electrode calculated using the enthalpy data of Searcy and Finnie (11) in lieu of free energies of the silicides. Other thermodynamic data are from Wicks and Block (5).

Examination of the estimated cell voltages of Table II indicates that the silicide pair $TaSi_2$-Ta_5Si_3 should be oxidized only to SiO_2 (compare reactions I and IV). Similarly, from the expected values for reactions II and V for the Ta_5Si_3-Ta_2Si pair, silica appears to be the preferred oxidation product. For the Ta_2Si-$Ta_{4.5}Si$ pair, tantala formation clearly gives the desired free energy minimum as indicated by the expected values for reactions III and VI of Table II.

In order to confirm these expectations, an experimental stability study was conducted. This study was performed at about 1600°C in vacuum using X-ray diffraction to follow changes in the relative amounts of phases. It confirmed the stability of silica in the presence of $TaSi_2$ and Ta_5Si_3 and the stability of tantala in the presence of Ta_2Si and $Ta_{4.5}Si$. However, for the

Page 10
is blank

Ta_5Si_3-Ta_2Si pair, the thermal stability study indicated that tantala rather than silica is the stable oxide.

Since each of the reactions I, V and VI involves a pair of silicides, EMF measurements for these cannot provide individual free energies of formation. However, data for a reaction from group C of Table II would yield the free energy of a single silicide and would thereby permit calculation of all. It may be shown from phase rule considerations that only one reaction in group C is permissible. Since the preferred reaction I yields Ta_5Si_3 and SiO_2, while the preferred reaction V yields Ta_5Si_3 and Ta_2O_5, it appears that reaction VIII is a possible one in group C. In any case, EMF data for four cell reactions are needed to evaluate the individual free energies of formation of all four silicides in the system.

2.2 Experimental

The tantalum silicides were prepared by direct reaction of the elements. The tantalum used in the synthesis was -120 mesh powder obtained from Fansteel Metallurgical Corp. The minimum purity was 99.9%. The silicon was -325 mesh powder of 99.99% purity obtained from United Mineral and Chemical Corp. The tantalum and silicon were weighed out in the desired proportions and mixed in plastic vials in a high speed mixer for a minimum of twenty minutes. They were pressed into 1/2 inch diameter pellets weighing approximately three grams under a pressure of 20 tsi and were reacted in a covered alumina crucible. The crucible, containing a tantalum susceptor, was placed in an induction heated vertical tube furnace connected to a vacuum system. The pellets ignited at about 1125^{o}C with visible evolution of heat. The reaction lasted less than one minute and the rapid evolution of the heat of reaction brought the temperature up to about 1400^{o}C.

During the reaction period, the pressure rose above 10^{-2} Torr because of silicon sublimation, but less than 0.01% of the silicon was lost. The reacted pellets were crushed and mixed with tantalum oxide and/or silica and with less than 1 wt% nickel sintering aid. The tantalum oxide was a purified grade obtained from Fisher Scientific Co. Silica was also obtained from Fisher. The mixed powders were pressed into 2.5 gram pellets in a 1/2 inch diameter die under a pressure of 20 tsi. Because the silicides are extremely hard and brittle, a binder was necessary to provide strength for handling the green pellets. A one per cent solution of poly-methyl-methacrylate in methyl ethyl ketone was used to yield a dry pellet containing approximately 0.2% binder by weight. The pellets were presintered at about 550°C in vacuum to remove the binder and were then sintered on alumina trays in vacuum at about 1625°C for ten minutes. The system pressure was maintained below 10^{-5} Torr. The temperature was measured with an optical pyrometer. With the exception of ($TaSi_2$-Ta_5Si_3-SiO_2) electrodes containing little or no silica, the electrodes sintered poorly. Those electrodes that sintered well were ground and polished to a bright metallic finish. However, the lower silicide electrodes crumbled when ground, so in order to present a dense surface to the electrolyte, these electrodes had to be used in the as sintered condition. However, because of silicon losses their surfaces within a particular batch showed considerable variation in composition. Therefore, electrodes suitable for use in the cells were selected by X-ray diffraction analysis of the surfaces. This permitted a determination of the relative amounts of the lower silicides present.

Reference electrodes for the EMF measurements were prepared from the appropriate metal and metal oxide powders by cold pressing followed by sintering in vacuum. Iron-ferrous oxide electrodes

Table II

Possible half-cell reactions and expected EMF values

with respect to Fe - Fe_xO at 1000°K and 1300°K

Half-cell reactions	Expected voltages (Millivolts)	
A. SiO_2(a)* Is The Oxidation Product:	1000°K	1300°K
I. $5\ TaSi_2 + 14\ O^= = 7\ SiO_2(a) + Ta_5Si_3 + 28e^-$	634 ±65	613 ±65
II. $2\ Ta_5Si_3 + 2\ O^= = SiO_2(a) + 5\ Ta_2Si + 4e^-$	895 ±477	870 ±477
III. $9\ Ta_2Si + 10\ O^= = 5\ SiO_2(a) + 4\ Ta_{4.5}Si + 20e^-$	433 ±113	409 ±113
B. β-Ta_2O_5 Is The Oxidation Product:		
IV. $4\ Ta_5Si_3 + 35\ O^= = 7\ Ta_2O_5 + 6\ TaSi_2 + 70e^-$	548 ±52	528 ±52
V. $6\ Ta_2Si + 5\ O^= = Ta_2O_5 + 2\ Ta_5Si_3 + 10e^-$	475 ±208	457 ±208
VI. $4\ Ta_{4.5}Si + 25\ O^= = 5\ Ta_2O_5 + 4\ Ta_2Si + 50e^-$	617 ±28	598 ±28
C. Complete Oxidation to SiO_2(a) and β-Ta_2O_5:		
VII. $2\ TaSi_2 + 13\ O^= = Ta_2O_5 + 4\ SiO_2(a) + 26e^-$	603 ±20	580 ±20
VIII. $2\ Ta_5Si_3 + 37\ O^= = 5\ Ta_2O_5 + 6\ SiO_2(a) + 74e^-$	577 ±14	556 ±14
IX. $Ta_2Si + 7\ O^= = Ta_2O_5 + SiO_2(a) + 14e^-$	565 ±13	543 ±13
X. $4\ Ta_{4.5}Si + 53\ O^= = 9\ Ta_2O_5 + 4\ SiO_2 + 106e^-$	590 ±7	570 ±7

*SiO_2(a) silica is amorphous as grown on silicide electrodes.

were prepared from 97.1% pure iron powder obtained from the J.T. Baker Chemical Co. The iron was oxidized in air at about 500°C until about one-third of the oxygen required to oxidize all of the iron to FeO had been gained. The powder was then pressed into two-gram pellets in a 1/2" diameter die at 15 tsi and sintered in vacuo at 1250°C for fifteen minutes. Tantalum-ditantalum pentoxide electrodes were fabricated from 99.9% pure tantalum powder and purified grade Ta_2O_5 in the ratio 4:1 by weight. The 1/2" diameter pellets weighing 2.5 grams were sintered in vacuum at 1650°C to 1700°C for fifteen minutes. All reference electrodes were ground flat on emery papers and polished on a napless nylon cloth with 5 micron levigated alumina.

Thoria-yttria electrolytes were fabricated from 99.9% pure thoria powder and 99.9% pure yttria powder obtained from A.D. Mackay, Inc. The powders were weighed out in the desired proportions and mixed for either twenty minutes in a high speed mixer or for 60 hours in a conventional ball mill. The mixed powder was pressed into 1/2" diameter pellets weighing from three to six grams and were sintered in vacuum for 3 to 36 hours at temperatures from 1900°C to 2200°C. The sintered pellets were cut on a diamond wheel to remove the surface layer and any fractured areas. Opposite faces were maintained parallel to within 0.002". The electrolytes were also polished on a napless nylon cloth with 5 micron levigated alumina abrasive. The density, as measured by water displacement, ranged from 87 to 100% of theoretical depending on sintering time, temperature, and the manner in which the thoria and yttria were mixed. The electrolytes were dark green in the as-sintered condition probably because of the trapping of electrons in defects. Heating in air at temperatures as low as 300°C caused the electrolytes to turn white in 30 minutes or less. They also turned white during their use in

the electrochemical cells where the oxygen partial pressure was low.

The EMF apparatus employed in this work was similar to the apparatus used by Kiukkola and Wagner (13) and is shown in Fig. 1. The cell, consisting of three pellets, was assembled between fused quartz rods. The platinum lead wires were brought through the end flanges of the apparatus with teflon lead-throughs. A chromel-alumel thermocouple was used to measure the cell temperature. The cell EMF was measured with a Keithley Model 610B Electrometer with 10^{14} ohm input impedance on the volt scale. Part or all of the cell voltage was biased by a potentiometer in series with the electrometer. The electrometer output was recorded on a potentiometric strip chart recorder. The cell was enclosed in a Vycor tube which was closed off by brass flanges with O-ring seals. The cell was heated by a silicon carbide tube furnace and the temperature was controlled to $\pm$ 5C^{o}. The cell was operated under argon that was purified by passing in succession over anhydrous magnesium perchlorate, zirconium-12.5 atom% titanium chips at 425^{o}C, anhydrous magnesium perchlorate, Zr-12.5 atom% Ti chips at 375^{o}C and tantalum at 600^{o}C. EMF measurements were made over the range of 700^{o} - 1100^{o}C, but most satisfactory measurements were made in the 900^{o}C - 1100^{o}C region.

2.3 Results and Discussion

Test of apparatus and electrolyte

The apparatus was tested by performing EMF measurements on the cell

$$Pt/Ni,NiO//0.925\ ThO_2\text{-}0.075\ Y_2O_3//Fe,Fe_xO/Pt \qquad (XI)$$

over the temperature range of 700^{o}C to 1000^{o}C. The data obtained were in good agreement with the results of other investigators (13,15,16).

Tests of low pressure electrodes were carried out with

$$Pt/Fe,Fe_xO//ThO_2 - Y_2O_3//Ta,Ta_2O_5/Pt \qquad (XII)$$

Results obtained with these cells employing dense Ta,Ta_2O_5 electrodes are summarized in Table III. (Data from cells employing porous electrodes produced with a lower metal:metal oxide ratio or sintered at lower temperatures displayed a strong positive temperature coefficient.) Electrolyte compositions of 1 mole% Y_2O_3 and 7.5 mole% Y_2O_3 in thoria were used. Electrolyte thickness was varied from 0.19 cm to 0.46 cm, while the argon flow rate was varied over the range of 1 CFH to 3 CFH. The electrolyte composition, electrolyte thickness and argon flow rate were found to have no effect upon the results for cells employing dense Ta,Ta_2O_5 electrodes. Therefore, it was concluded that the deviations of the observed EMF from the expected values computed from the data for Fe_xO (15) and Ta_2O_5 (5) were caused by electronic conduction in the thoria-yttria electrolytes. That is, conduction in the electrolyte was not 100% ionic as assumed for equation(5). However, the temperature coefficients of these cells were in excellent agreement with the expected coefficients. Such behavior should be expected if the electrodes are not appreciably polarized by the electronic exchange current. Therefore, EMF data obtained under these conditions are useful if a correction for electronic conduction is made.

This correction may be made by applying an equation derived by Schmalzried (14). Since the oxygen partial pressures over silicide electrodes are not very different from those over Ta,Ta_2O_5 electrodes, the corrections will be closely applicable. The average transport number for ionic conduction, $\bar{t}_i$ is defined simply in terms of the measured and true cell voltages E_m and E, by

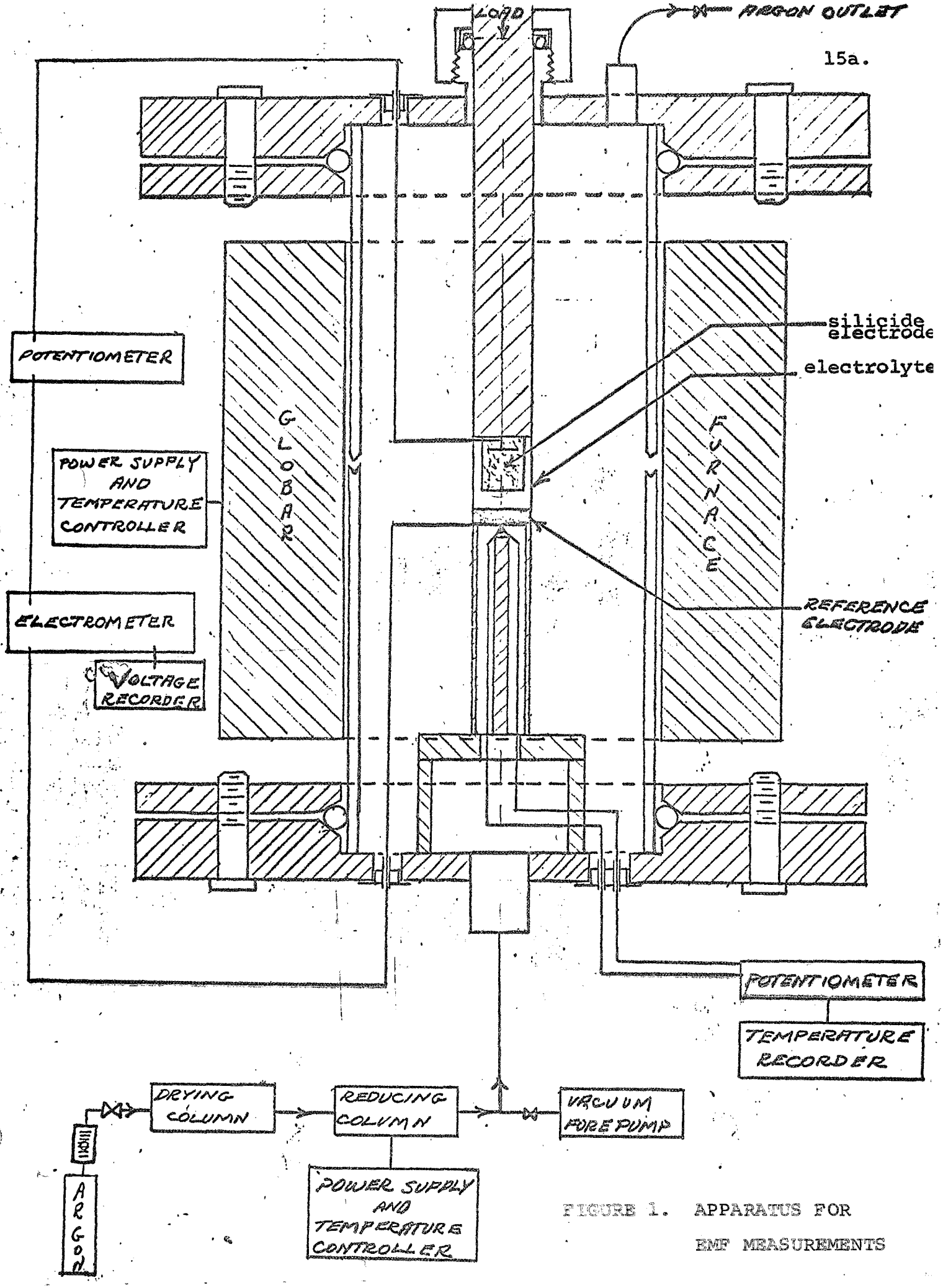

FIGURE 1. APPARATUS FOR EMF MEASUREMENTS

$$\bar{t}_i = \frac{E_m}{E} \tag{10}$$

Now for the present case where the Fe,Fe_xO reference electrode possesses a high oxygen pressure relative to its Ta,Ta_2O_5 mate, E_m may be expressed by

$$E_m = -\frac{mRT}{4F} \left[\ln \frac{P_e^{\frac{1}{m}} + P_{Ta}^{\frac{1}{m}}}{P_{Fe}^{\frac{1}{m}}} \right] \tag{11}$$

where P_e is an oxygen partial pressure characteristic of the electrolyte

P_{Ta} and P_{Fe} are the oxygen partial pressures over the Ta,Ta_2O_5 and the Fe,Fe_xO electrodes

m has a theoretical value of 4.

The value of P_e may be calculated from equation (11) using measured values of E_m and calculated pressures for P_{Ta} and P_{Fe}. At 1300^{o}K, the result is

$$P_e = 2.59 \times 10^{-29} \text{ atmospheres}$$

It then becomes possible to derive E_m as a function of P_{Ta} referred to a fixed P_{Fe}. The true voltage, E, is calculated for the same pressures using equation (5) and appropriate data (5,15). As a matter of interest, a local ion transport number, t_i, may be calculated for the electrolyte at its interface with the low pressure electrode (14).

$$t_i = \exp\left[4F(E_m - E)/mRT\right] \tag{12}$$

The results of the calculations are presented in Table IV. This table may also be used to evaluate corrections for the silicide electrodes where electronic conduction is significant.

Examination of Table IV discloses that the thoria-yttria electrolytes were found essentially free of electronic conduction ($\bar{t}_i \geq 0.99$) down to oxygen partial pressures of about 10^{-24} atmospheres at $1300^{o}K$. This confirms the work of Steele and Alcock (16) and Vecher and Vecher (17), but is in substantial disagreement with the results described by Rapp (18).

Silicide electrodes

A very large number of electrodes was prepared from pairs of silicides in each of the three phase fields. These were mixed with silica and/or tantala to correspond to the reactions of Table II and were tested in cells. Two major kinds of difficulties were encountered. First, many of the mixtures of refractory silicides and oxides did not sinter well even when activated with small amounts of nickel. Consequently, the interior structure was often porous so that the very low partial pressures of oxygen could not be maintained and cell voltages were too low. This was especially true at the lower test temperatures where the electrode-electrolyte reaction was sluggish. As previously explained, this problem was partially overcome by utilizing a dense pressed and sintered surface whose composition was determined by X-ray diffraction. A second difficulty occurred when oxidation of the silicide yielded a silica glass whose high resistivity resulted in ultimate decrease of voltage. Because of these problems, EMF readings were considered reliable only when they were stable, insensitive to the flow rate of the surrounding argon and displayed the expected small negative temperature coefficient. In all cases, corrections for electronic conduction were made using Table IV. The corrected

Table III

EMF measurements (MV)

Temperature °C	700	750	800	850	900	950	1000	1050	1100
Cell I							658±40	648±40	
Cell II			537±4	565±4	578±8	583±4	589±9	585±4	
Cell V						494±3	523±3	521±1	519±3
Cell VI					563±4	562±4	561±4	560±4	559±4
Cell XII	618±2		610±2		604±2		598±2		

Table IV

Transport properties for thoria yttria electrolytes at 1300°K with an Fe,Fe_xO reference electrode

P_{O_2}	E	E_m	$\bar{t}_i$	t_i
10^{-20}	361	361	1	1
10^{-21}	426	425	.998	.990
10^{-22}	490	488	.997	.982
10^{-23}	555	550	.992	.956
10^{-24}	619	612	.989	.939
10^{-25}	685	670	.979	.875
10^{-26}	750	726	.968	.807
10^{-27}	813	775	.953	.712
10^{-28}	878	817	.931	.580
10^{-29}	943	850	.902	.435
10^{-30}	1007	875	.869	.307

measurements are summarized in Table III where the cell numbers correspond to the reactions given in Table II.

$TaSi_2$-Ta_5Si_3 Phase Field

Fifteen electrodes were prepared and tested, but only two points, representing six observations were satisfactory. These are listed under Cell I.

Ta_5Si_3-Ta_2Si Phase Field

Nineteen electrodes were prepared and tested. The ratio of the two silicides was varied while the content of Ta_2O_5 was in the range of 0-25% and that of SiO_2 varied between 0-7% by weight. X-ray and microscopic examinations of the electrodes before and after use led to the conclusion that the anticipated oxidation of Ta_5Si_3 to Ta_2O_5 and SiO_2 (VIII) did not occur. Instead, electrodes that were primarily Ta_5Si_3 were oxidized to SiO_2 and the lower silicide (II). On the other hand, Ta_2Si was oxidized to Ta_2O_5 and the higher silicide, Ta_5Si_3 (V). The corrected potentials measured for these electrodes are given in Table III under the appropriate cell numbers.

Ta_2Si-$Ta_{4.5}$ Phase Field

The expected reaction is VI of Table II. Four electrodes were examined and two performed satisfactorily. The average values are listed in Table III. In this case, correction was made not only for electronic conduction, but also to normalize all measurements to the slightly higher values measured at maximum argon flow rates. Hence, although the variability of the measurements was ± 4 mv., the results were considered reliable to only ± 10 mv.

Evaluation of Free Energies of Formation

The measured EMF values were combined with free energy of formation data for Fe_xO (15) and for Ta_2O_5 and SiO_2 (5) to produce four linear equations which could be solved for the free energies of formation of the individual silicides. An upper bound for Cell I was set by the limitation that its potential may not exceed that of Si,SiO_2 vs the same reference electrode. The results of the calculations are presented in Table V.

Although the free energies are given at three temperatures because measurements were made in the vicinity of these temperatures, it is obvious that the estimated errors are too large to permit calculation of entropy changes. It is worth noting that nearly one-half of the uncertainty in the data for the silicide is attributable to uncertainties in the free energy data for the oxides of iron, tantalum and silicon. This sets a limit on the accuracy that may be achieved.

The free energies of formation may be compared with little error to the enthalpies of formation given in Table I. Since by the Neumann-Kopp rule the formation of a compound from its elements involves no change in heat capacity, then

$$\Delta G_T^o \cong \Delta H_{298}^o - T\Delta S_{298}^o \qquad (13)$$

Furthermore, for the formation of ordered solids from the solid elements, ΔS_{298}^o is very close to zero. Hence,

$$\Delta G_T^o \cong \Delta H_{298}^o \qquad (14)$$

Comparison of the values in Tables I and V shows that for the three lower silicides the results obtained by the EMF method are

Table V

Free energies of formation of the tantalum silicides

(kcal/g. atom silicon)

Temp. ^{o}K	1/2 $TaSi_2$	1/3 Ta_5Si_3	Ta_2Si	$Ta_{4.5}Si$
1200		-24.8 ± 3	-28.1 ± 3.1	-39.2 ± 7.2
1300	$-8.1 \begin{smallmatrix} +1.8 \\ -3.7 \end{smallmatrix}$	-24.0 ± 3	-27.2 ± 3.1	-37.3 ± 7.2
1400		-23.1 ± 3	-26.1 ± 3.1	-35.3 ± 7.2

in substantial agreement with those obtained by effusion. Some improvement in the confidence interval for Ta_5Si_3 and Ta_2Si has been achieved in this work. Furthermore, the results obtained in this investigation are thermodynamically consistent in that the activity of silicon must increase monotonically from the lower to the higher silicides, while the activity of tantalum must decrease. Therefore, EMF's of electrodes where SiO_2 is the oxidation product must increase from the lower to higher silicides, while those where Ta_2O_5 is the oxidation product must fall. This requirement is obeyed by the present results but not by results inferred from earlier data.

2.4 Improved Thermochemical Measurements (G. Halbfinger)

In order to overcome the major difficulties described in the earlier sections, follow-on research has been directed toward the total enclosure of the low pressure electrode. This research has included modification of the electrolyte by the addition of metallic oxides to lower sintering temperatures, the examination of various materials as lead-throughs and the use of cermets as electrodes.

Much of the work has been devoted to reduction of sintering temperature. It has been found that small amounts of the oxides of metals of the first transition series produce dramatic reductions in sintering temperature. However, their effect on ion transport number has not been adequately measured. Nor is the mechanism whereby these oxides aid sintering understood. Both areas are currently being investigated.

3. Substrate-Coating Interaction and Barriers (L.J. Schwartz)

3.1 Background and Theory

The service lifetimes of disilicide coatings are shortened because they interact by diffusion with metallic substrates to form lower silicides, such as Ta_5Si_3. The latter is unable to form the protective glassy oxide, perhaps because of the simultaneous formation of the substrate metal oxide. Therefore, an understanding of the mechanism of growth of the lower silicide layer and its inhibition may increase the coating life.

It has been empirically discovered that additives of elements such as titanium to the coating or substrate can substantially increase coating life. This can be caused by either or both of two mechanisms.

a. The participation of the additive in the oxidation reaction to form a more resistant glass.

b. The performance of the additive as a diffusion barrier to inhibit the growth of the less protective lower silicide.

Therefore an understanding of additive behavior as a barrier to lower silicide growth can help to separate the two mechanisms as well as set up criteria for the selection of additive elements which will act as good diffusion barriers.

When two different metals with extensive solid solubility are interdiffused an alloyed intermediate grows between them. There is a continuous change in concentration from pure A to pure B. This concentration can be followed by means of lattice parameter changes, microhardness profiles, electron microprobe analysis or by radioactive counter methods. Various mathematical expressions have been derived for such cases. Castleman (19) and Kidson (20) give a variety of solutions for different types of systems. These approaches yield an interdiffusion coefficient, $\tilde{D}$. Darken (21), using a non-mechanistic approach has derived the

relationship between this interdiffusion coefficient and the actual diffusivities of the two diffusing species in a binary system with no compound formation.

With the formation of an intermediate compound, discontinuities arise in the concentration profile and Fick's second law cannot be explicitly solved. Instead, the stoichiometric nature of the compound adds the needed condition to Fick's first law. In conjunction with material balances, this leads to the parabolic rate law, relating the thickness of the growing phase to time of diffusion. The method of following this growth is simple (microscopic, X-ray diffraction, electron microprobe) and is called the "moving boundary" technique. The difficulty lies with the more empirical, less basic nature of the parabolic rate constant, k, where k is defined as $(\Delta x)^2/t$, Δx being thickness of the phase grown in time t. This constant must be defined in terms of $\tilde{D}$ to have fundamental significance. This is particularly true when more than one compound grows simultaneously. Janssen and Riech (22), in studying compound formation in the Ni-Al system, used both a "moving boundary" technique and Boltzman-Matano method to calculate D values for four aluminides. Gibbs (23), in a general treatment, considered the total zone of n intermediate phases, assigning an "effective diffusivity", D_β, to the system. He concluded that "only if the n phases have similar diffusion parameters and small miscibility gaps at the intermediate interfaces will D_β approximate some true average diffusivity". Kidson (20) showed that each phase layer obeys the parabolic rate. Roy (24) found D's and k's coupled in a treatment of interstitial systems; and Resnick, Steinitz and Seigle (25) in determining the diffusivity of C in Ta and Cb carbides found the diffusivities in the two growing phases coupled.

In the treatment of substantial compound growth in the Ni/U system, Kimmel, Bar-or and Rosen (26) concluded that the relation between D and k for any growing layer depends only on the homogeneity range and ΔC, the concentration difference, and not on the growth constant of any other phase in the same couple. Wagner (27), recently derived k values for three types of systems. For an intermediate with narrow homogeniety range growing between one compound of higher stoichiometry and one of lower stoichiometry, his k (called k_{II}) value is related to the average diffusivity in a manner similar to the above-mentioned substitutional cases, but is also a function of the mole fractions of the diffusing species in the three compounds. Silicides, being substitutional intermetallics of narrow homogeneity ranges, should fall into the category analyzed by Wagner as long as the silicide grows in a stable fashion.

The diffusivity may be evaluated experimentally by measuring the intermediate rate of growth at constant temperature. One may obtain k from the parabolic rate, $k = (\Delta x)^2/t$. The constant k is a measure of diffusivity from which the fundamental quantity, $\tilde{D}$, may be computed.

As with any rate process, the temperature dependence of k (or $\tilde{D}$) should be of the Arrhenius form: $\tilde{D} = \tilde{D}_o e^{-Q/RT}$, where R is the gas constant and Q is the activation energy for diffusion. Any deviation from this type of dependence would indicate a mechanism consisting of more than one thermally activated step.

To determine the diffusing species, markers may be used. This method is based on marking the original interface in the diffusion couple and measuring the growth on either side of it. Since different reactions are taking place at the interfaces to the left and right of the original interface, a ratio of the

diffusivities of the two species in a binary system results. Any material being used as a marker must be inert to its environment and must not be displaced by any mechanism that would preclude its use as a reference plane. In a review on diffusion in intermetallic compounds, Hagel (28) states "Many correlations were tried to aid in predicting which component of a binary compound would be the faster moving species, and almost without exception it is the element possessing the lower melting point."

$Ta/TaSi_2$ System

From consideration of the Ta-Si phase diagram (Figure 2) it would be expected that three intermediate silicides would grow between $TaSi_2$ and Ta: Ta_5Si_3, Ta_2Si and $Ta_{4.5}Si$. (The α phase of Ta containing a very small concentration of silicon is considered pure Ta.) It has been found, in this investigation and others (29), that as long as $TaSi_2$ is available to supply Si to the growing system, only the trisilicide, Ta_5Si_3, grows in discernible amounts. An analysis including the lower silicides, Ta_2Si and $Ta_{4.5}Si$, assuming that their rate of formation is zero, yields the same result that their exclusion from the analysis predicts. Therefore, it may be considered that the system is Ta_5Si_3 alone growing between $TaSi_2$ and Ta.

FIGURE 3

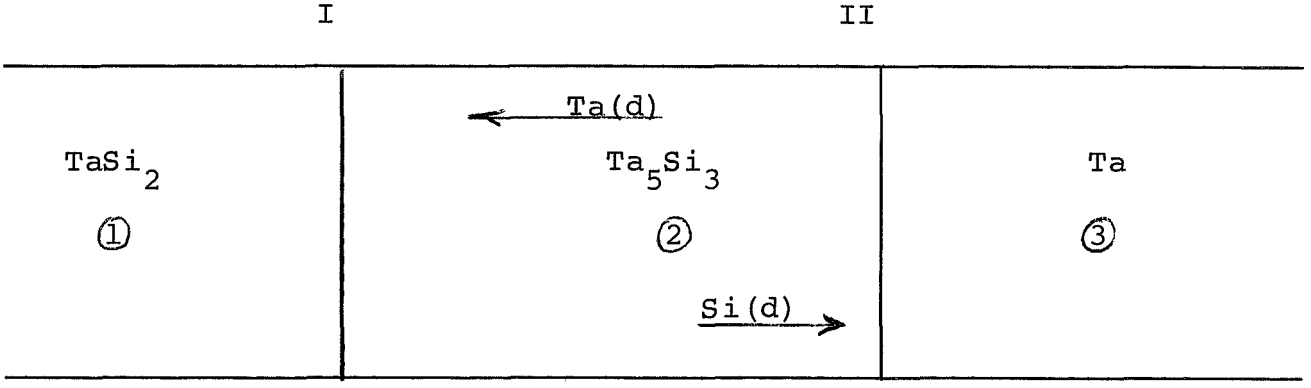

FIGURE 2
Ta-Si PHASE DIAGRAM (30)

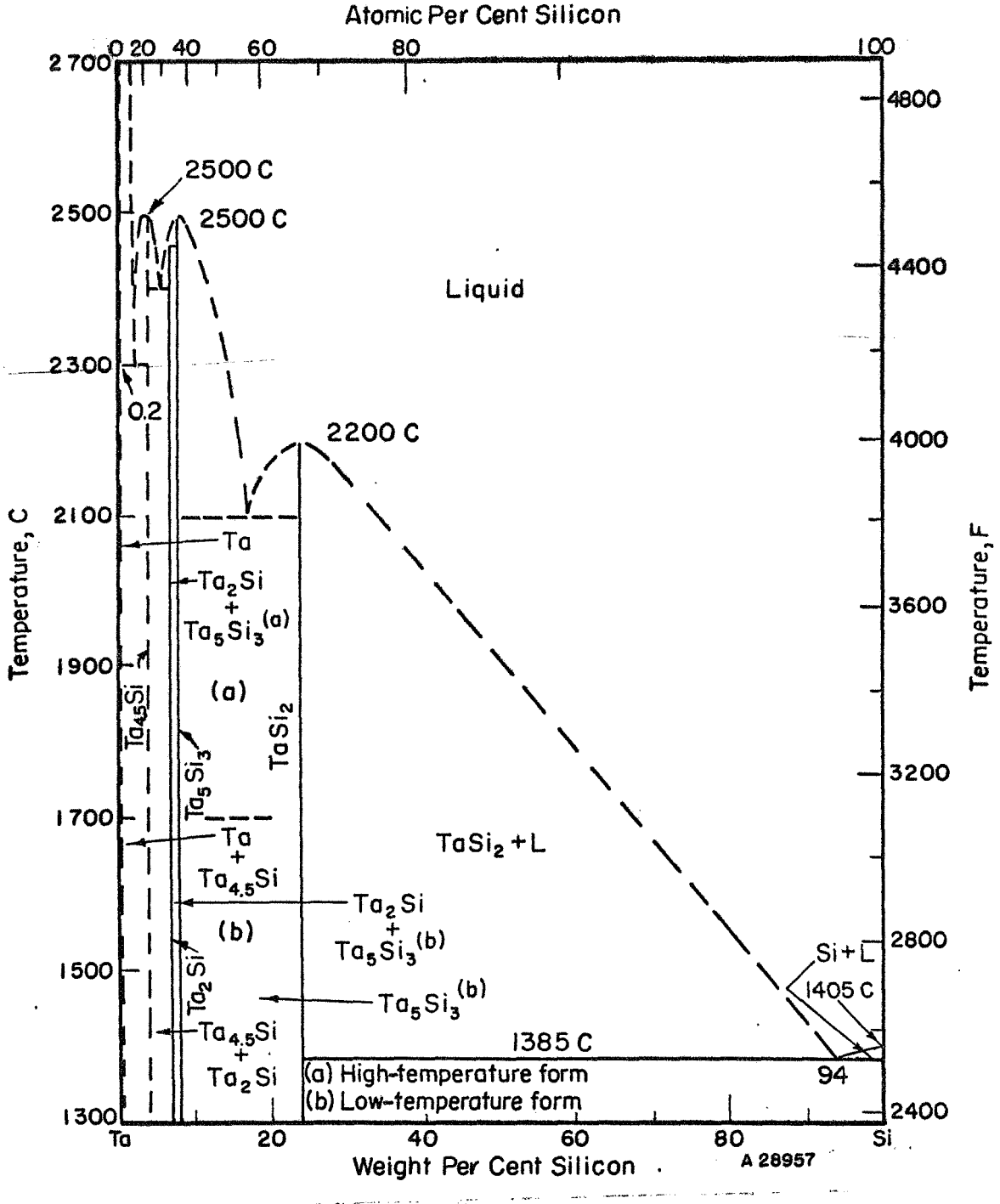

In the figure above ① , ② , and ③ represent the phases and I and II the interfaces. Si(d) indicates Si diffusing from interface I to interface II through phase ② ; and Ta(d) indicates Ta diffusion from interface II to interface I through phase ②. The reactions that may take place at the interfaces are:

$$\text{Interface I:} \quad 5TaSi_2 \rightarrow Ta_5Si_3 + 7Si(d) \tag{15}$$

$$7Ta(d) + 3TaSi_2 \rightarrow 2Ta_5Si_3 \tag{16}$$

$$\text{Interface II:} \quad 5Ta + 3Si(d) \longrightarrow Ta_5Si_3 \tag{17}$$

$$Ta \longrightarrow Ta(d) \tag{18}$$

During the growth of the intermediate phase the reactions are diffusion-controlled and the growth rate of any compound is dependent upon the fluxes, J (moles/cm^{2}sec), of the diffusing components across the phase boundaries. Therefore, taking the flux toward the right as positive, the rate of growth of the trisilicide at interface I is

$$J_I = \frac{1}{7} J_{Si} - \frac{2}{7} J_{Ta} \tag{19}$$

and its rate of growth at interface II is

$$J_{II} = \frac{1}{3} J_{Si}. \tag{20}$$

The total rate of growth of the layer of Ta_5Si_3 is the sum of J_I and J_{II}.

$$J_{total} = \frac{10}{21} J_{Si} - \frac{2}{7} J_{Ta} \tag{21}$$

The fluxes J_{Si} and J_{Ta} may be expressed in terms of their diffusivities (cm^2/sec) and concentration gradients (moles/cm^3/cm).

$$J_{Si} = - D_{Si} \frac{dC_{Si}}{dx} \tag{22}$$

$$J_{Ta} = - D_{Ta} \frac{dC_{Ta}}{dx} \tag{23}$$

It is more convenient to express the concentrations in terms of mole fractions. For example:

$$C_{Si} = \frac{N_{Si}}{V_m} \alpha$$

where N_{Si} = moles Si/(moles Si + moles metal)

V_m = cm^3/mole of compound

and α = (moles Si + moles metal)/mole of compound.

Hence, restating Fick's first law

$$J_{Si} = \frac{-D_{Si}}{V_m} \frac{dN_{Si}}{dx} \alpha \tag{24}$$

$$J_{Ta} = \frac{-D_{Ta}}{V_m} \frac{dN_{Ta}}{dx} \alpha \tag{25}$$

Inserting these fluxes in equation (21)

$$J_{total} \frac{V_m}{\alpha} = \frac{-10}{21} D_{Si} \frac{dN_{Si}}{dx} + \frac{2}{7} D_{Ta} \frac{dN_{Ta}}{dx}. \tag{26}$$

Let $J_{total} V_m = r$ (cm/sec, a velocity of growth of the Ta_5Si_3) and note that for a binary system

$$N_{Si} = 1 - N_{Ta} \text{ and}$$

$$-dN_{Si} = dN_{Ta}.$$

Now for the Ta_5Si_3, the concentration change across the almost

stoichiometric phase is very small* and may be assumed independent of thickness. Therefore, following the usual convention regarding signs,

$$\frac{dN_{Si}}{dx} = \frac{-\Delta N_{Si}}{\Delta x}$$

and

$$\frac{dN_{Ta}}{dx} = \frac{-dN_{Si}}{dx} = \frac{\Delta N_{Si}}{\Delta x}$$

Rewriting equation (26) yields

$$r = \frac{2\alpha}{21} (5 D_{Si} + 3 D_{Ta}) \frac{\Delta N_{Si}}{\Delta x} \tag{27}$$

Defining the interdiffusion coefficient $\tilde{D}$ according to Darken (21)

$$\tilde{D} = N_2 D_1 + N_1 D_2$$

$$\tilde{D}_{Ta_5Si_3} = \frac{5}{8} D_{Si} + \frac{3}{8} D_{Ta}$$

and inserting into equation (27) results in

$$r = \frac{16\alpha}{21} \tilde{D} \frac{\Delta N_{Si}}{\Delta x} \tag{28}$$

The rate of growth can also be expressed as a rate of change in thickness, Δx, of the growing phase.

$$r = \frac{d(\Delta x)}{dt} = \frac{16(8)}{21} \tilde{D} \frac{\Delta N_{Si}}{\Delta x} \tag{29}$$

*It should be emphasized that diffusion occurs down a thermodynamic activity gradient rather than down a concentration gradient. A large activity difference may exist despite a very small concentration difference.

On integration of equation (29) the parabolic rate expression is obtained.

$$(\Delta x)^2 = \frac{256}{21} \tilde{D} \Delta N_{Si} t \qquad (30)$$

Since accurate solvus lines have not been determined for the silicides, the values of ΔN are unknown and cannot be separated from $\tilde{D}$. Then solving for the product $\tilde{D}\Delta N_{Si}$,

$$\tilde{D}\Delta N_{Si} = \frac{21}{256} \frac{(\Delta x)^2}{t} = \frac{21}{256} k \qquad (31)$$

where k is the experimentally determined parabolic rate constant.

The interdiffusion coefficient is directly related to the measured parabolic rate constant by a constant and ΔN. One can be fairly assured that ΔN does not vary significantly over the temperature range of interest and the activation energy from $k = k_o e^{-Q/RT}$ should be the same as the activation energy from $\tilde{D} = \tilde{D}_o e^{-Q/RT}$. But $\tilde{D} = N_2 D_1 + N_1 D_2 = N_2 D_o^1 e^{-Q_1/RT} + N_1 D_o^2 e^{-Q_2 RT}$. Therefore an apparent activation energy, Q, results from a plot of $\ln ((\Delta x)^2/t)$ vs. $1/T_{abs}$, which involves both of the fundamental activation energies, Q_1 and Q_2, and may be temperature dependent. Only if the diffusivity of one species is much greater than the other or if Q_1 and Q_2 are almost equal will $\tilde{Q}$ represent a true activation energy. Therefore, if only silicon diffuses $\tilde{D}$ and $\tilde{Q}$ will represent the actual diffusivity and activation energy for diffusion of Si in Ta_5Si_3.

Markers in the $Ta/TaSi_2$ System

In order to ascertain which of the components predominates in the diffusion process the original interface must be marked. In the $Ta/TaSi_2$ system, as the intermediate layer grows a marker

at the original interface will indicate the relative fluxes of the diffusing species Ta and Si. In this case, the relationship is not as simple as in oxidation experiments because the trisilicide is formed both by loss of Si from the disilicide and by reaction of Si with Ta and of Ta with $TaSi_2$.

FIGURE 4

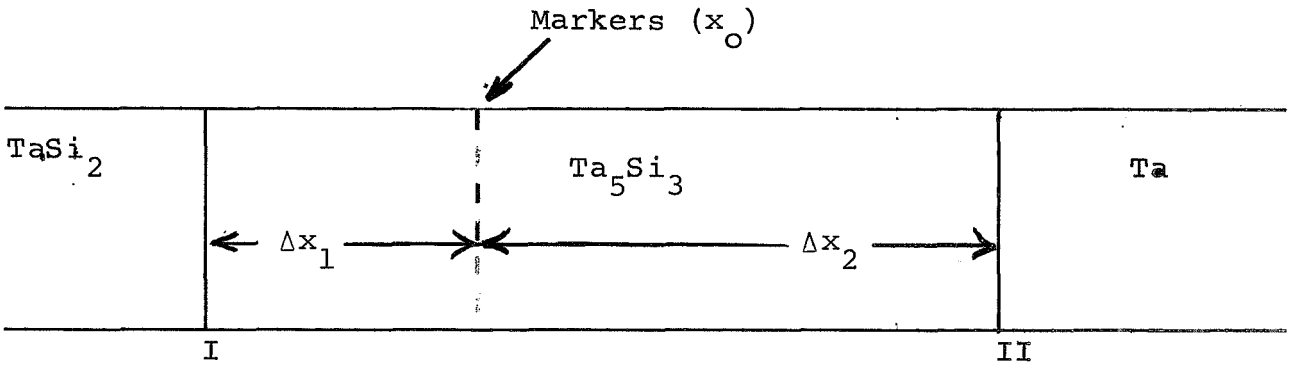

In this analysis, it will be assumed that Ta does not diffuse. Since the markers do not participate in any reactions, the reactions (15) and (17) occur at interfaces I and II, and it is possible to measure the rates of formation at each of the interfaces separately. The following pair of equations result in which k_1 and k_2 are the growth constants for the Δx_1 and Δx_2 zones respectively.

$$(\Delta x_1)^2/t = 2/7\alpha(D_{Si}\Delta N_{Si})_1 = k_1 \qquad (32)$$

$$(\Delta x_2)^2/t = 2/3\alpha(D_{Si}\Delta N_{Si})_2 = k_2 \qquad (33)$$

A simple material balance using reactions (15) and (17) shows that if Ta does not diffuse the thicknesses of the growing phases are stoichiometrically related when molar density is taken into account.

$$\frac{\Delta x_2 V_{m2}}{\Delta x_1 / V_{m1}} = \frac{7}{3} \tag{34}$$

Since the molecular weights of the compound (Ta_5Si_3) are nearly the same in both zones,

$$\frac{\Delta x_2}{\Delta x_1} = \frac{7}{3} = \frac{\rho_1}{\rho_2} \tag{35}$$

where ρ_1 and ρ_2 are the densities (gms/cc) of Ta_5Si_3 in the Δx_1 and Δx_2 zones respectively. Therefore, if measured values of $\Delta x_2/\Delta x_1$ conform to equation (35), it may be said that Ta does not appreciably diffuse.

Dividing equation (23) by equation (32) results in

$$\frac{k_2}{k_1} = \left(\frac{\Delta x_2}{\Delta x_1}\right)^2 = \frac{7}{3} \frac{(D_{Si}\ \Delta N_{Si})_2}{(D_{Si}\ \Delta N_{Si})_1} \tag{36}$$

The following relationship between ΔN and Δx results from solving equations (35) and (36) together.

$$\frac{\rho_2}{\rho_1} \frac{(D_{Si}\ \Delta N_{Si})_2}{(D_{Si}\ \Delta N_{Si})_1} = \frac{\Delta x_2}{\Delta x_1} \tag{37}$$

Therefore, if the diffusivities of silicon in Ta_5Si_3 on both sides of the original interface are the same, the ratio of the stoichiometry ranges across the zones is proportional to the ratio of the thickness of the zones because ρ_2/ρ_1 is a constant close to unity. Since the ratio $\Delta x_2/\Delta x_1$ is known, under the assumptions stated, $\Delta N_2/\Delta N_1$ is known explicitly from

$$\frac{(\Delta N_{Si})_2}{(\Delta N_{Si})_1} = \frac{7}{3}\left(\frac{\rho_1}{\rho_2}\right)^2 \tag{38}$$

Therefore, if it can be shown experimentally that Ta does not diffuse (equation 35 is satisfied) and that the diffusivities in both zones are close, (equations (32) and (33)), the ratio of the ΔN_{Si} values is established by stoichiometry.

$M/TaSi_2$ System

As previously mentioned, $TaSi_2$ on Ta is protective by virtue of the formation of a silica glass at the air interface. If this protective glass is impaired, the $TaSi_2$ acts as a reservoir of silicon for the formation of additional glass. However, the lower silicide, Ta_5Si_3, is not protective, so that the diffusion of silicon out of $TaSi_2$ into the tantalum diminishes the coating life. The thickness of the Δx_1 layer is a measure of the extent of this loss. If it were possible to interpose a silicon-impermeable barrier between the $TaSi_2$ and the Ta, the coating life would be greatly increased. The interpolation of a barrier that merely reduced the flow of silicon would also be desirable. Hence, the measure of the effectiveness of any barrier, M, may be determined from the growth rate of the Δx_1 layer.

In testing the barrier effect of certain additive metals, the growth kinetics of the intermediate zone depends on the fluxes of components in and out of Ta_5Si_3 and one or more M silicides. The system is not truly binary any more and complete analysis is considerably complicated. The growth of the total zone is therefore not easily related to fundamental diffusivities or activation energies. Analysis leads to an apparent activation energy which is related to the activation energies for the growth of the separate phases. Although this analysis has been performed, it will not be presented here. However, $\tilde{D}_{Si_{②}} \Delta N_{Si_{②}}$ is directly related to $k_{②}$ for all cases of diffusion under the assumptions

stated. These values for the growth of Ta_5Si_3 (Δx_1 zones) can be compared with the Δx_1 growth in the Ta/$TaSi_2$ system directly by comparison of the growth constants k. This is exactly the comparison needed to describe the effect of barrier metals on the degradation of $TaSi_2$. Therefore, one can determine the rate of degradation of $TaSi_2$ directly from the rate constants of the Δx_1 zones in any of the barrier systems investigated. Since both the diffusing species (Si) and the medium (Ta_5Si_3) through which it is lost are the same in all cases, differences in growth rates depend on the activities of Si in the M silicides adjacent to the growing Ta_5Si_3.

Previous Work

The only previous comparable work is that by Bartlett (29) and Lavendel and Elliot (31). Both of these used silicide-coated Ta specimens. The $TaSi_2$ coatings were deposited on the Ta substrates by vapor deposition and the coated system was then diffusion annealed to form the lower silicide, Ta_5Si_3. The $TaSi_2$ had cracks, defects and compositional impurities which could affect the results of the studies. Diffusion times were limited by the thickness of the original $TaSi_2$ layer. Bartlett's experiments done in a nitrogen-argon atmosphere resulted in an activation energy of 58,000 cal/mole for the growth of Ta_5Si_3. Lavendel and Elliot performed their diffusion anneal in helium and at higher temperatures. They observed the growth of Ta_2Si as well as Ta_5Si_3 at 3000^{o}F and above, and derived an activation energy of 49,000 cal/mole for the process.

Other diffusion results relevant to this investigation are not directly comparable. Both of the above-mentioned studies included a similar investigation of the Cb/$CbSi_2$ system and both found the activation energy for the growth of Cb_5Si_3 to be the

same as for Ta_5Si_3 in the $Ta/TaSi_2$ system. Koffman and Oglivie (32) calculated the interdiffusion coefficients in Cb containing small amounts of Si and Cb_3Si, using a Wagner analysis based on the coupling of two-phase, arc-melted wafers both of which contained the growing phase. Due to technical difficulties they were not able to determine $\tilde{D}$ for higher silicides. The resulting activation energies are 88,000 cal/mole for Cb/Si solid solution, 166,000 cal/mole for Cb_3Si and 89,000 cal/mole for W/Si solid solution (which was analyzed by the Grube analysis).

Bartlett, Gage and Larssen (33) also investigated the W/Si system and the Mo/Si system by coating WSi_2 and $MoSi_2$ on W and Mo respectively. The method and analysis are similar to those used for $Ta/TaSi_2$ and $Cb/CbSi_2$. The results were: Q = 86,000 cal/mole for both W_5Si_3 and Mo_5Si_3 and 78,000 cal/mole for Mo_3Si.

Bartlett and Gage (34) also measured the growth rate of WSi_2 and $MoSi_2$ during vapor deposition. Although Si reaches the surface of the substrate by vapor transport, it is solid-state diffusion through the silicide that controls the rate of formation. Marker experiments using ZrO_2 spray indicated that only Si diffused appreciably. The activation energy for the growth of both $MoSi_2$ and WSi_2 was determined to be 25,000 cal/mole. Hashimoto (35) grew WSi_2 on a Si substrate and obtained a Q equal to 22,000 cal/mole for the process. Samsonov, et.al. (36) reported activation energies for deposition of Si on Ta, Mo and Ti as 22,000, 14,000 and 5,000 cal/mole respectively. A general survey of diffusion in intermetallic compounds has been presented by Hagel (28). Although no data for silicides are offered, the wide range of values for Q (4 to 240 kcal/mole) indicates how much variation one can expect in the diffusion properties.

No data on the actual effect of coating-substrate interaction

on coating performance or the effect of barriers on service life have been found. Many empirical studies have been made on the effect of certain additives on oxidation resistance of the refractory silicide coatings. Passmore, et.al. (37,38) have investigated diffusion barriers in refractory metals, but not silicides.

3.2 Experimental

In the present study, diffusion couples consisted of a refractory metal wafer and a $TaSi_2$ wafer. This has several advantages over the coating method used by others. First, $TaSi_2$ can be coupled with any metal to test the barrier effect, whereas the coating method can only yield a M/M silicide couple. Markers can be placed in the couple at the investigator's discretion. The $TaSi_2$ phase can be as thick as necessary to ensure that it is not depleted during the anneal. Lastly, the composition and physical defect variables can be better controlled. The wrought metals used were obtained commercially as high purity, high density rods or sheets with very few physical defects. $TaSi_2$, on the other hand, is commercially available only in the powder form. It was found that the commercial powder could not be fabricated into high density wafers by cold-pressing and sintering. Hot-pressing was considered undesirable because of the contamination by die materials. Therefore, the $TaSi_2$ was synthesized in our laboratory as follows.

a. Tantalum and silicon powders were ball-milled together for one day in stoichiometric amounts plus 1% excess silicon to account for evaporation losses. Ball-milling was in a rubber-lined, 3" D mill containing 1/4" and 1/8" stainless steel balls.

b. Reaction wafers were pressed in a 1" diameter hardened steel die at an optimum load of 15 thousand pounds. Wafers weighed between 10 and 15 grams.

c. Five reaction wafers were reacted at a time producing a yield of about 60 grams of usable $TaSi_2$. Reaction took place in an induction furnace in a vacuum contained by a Vycor tube. The reaction wafers were stacked so that only the lower wafer was in contact with the alumina support ring inside an alumina crucible with a tantalum foil susceptor and a tantalum cover. Reaction

took place below 1200°C and was always violently exothermic, no matter how slowly the mass was brought up to temperature. After reaction and subsequent cool-down, the reacted wafers were cleaned and ground. X-ray diffraction patterns of this powder showed the material to be pure $TaSi_2$.

Wafers were prepared by adding 0.5 weight percent nickel (as sintering aid) to the $TaSi_2$ and ball-milling for 24 hours. A binder of 1% polymethyl methacrylate was added in solution, mixed, dried and screened to 100 mesh. Wafers 1/2" diameter were cold pressed at 10,000 pound load and were presintered by slowly heating in vacuum to 1000°F to remove the binder. Final sintering was performed in a tantalum-heated resistance furnace at about 1600°C (2912°F). Sintered wafers were ground on diamond wheels to mirror finish.

The $TaSi_2$ wafers had densities in excess of 95% of theoretical. Although the finished wafers had a mirror finish, small pores were visible microscopically. The concentration of pores was small and reproducible. X-ray diffraction showed the wafers to be almost pure $TaSi_2$ with trace amounts of Ta_5Si_3 (< 5%). Under high magnification (1250X), the trisilicide was found to be uniformly dispersed across the wafer. No free Si or Ta was found, nor were any other phases detected. The microstructure consisted of small, irregular, grains. About 150 such wafers were produced at various times from five different starting batches.

In addition to the reference wafers described, three other types were produced.

a. Very dense (close to 100% theoretical) wafers containing a high concentration of Ta_5Si_3 with hardly any pores. X-ray diffraction yielded a concentration of about 40-50% Ta_5Si_3. Microscopic examination showed the Ta_5Si_3 dispersed as a web throughout the $TaSi_2$. These were designated * type.

b. Dense (≥ 95% theoretical) wafers containing a high concentration of extremely small pores. No trace of Ta_5Si_3. These were designated "A" type.

c. Low density (< 90% theoretical) wafers containing an average concentration of large pores with trace amounts of Ta_5Si_3 similar to the reference wafers. The grain size was considerably larger and more angular than in any other wafers. These were called "B" type.

Markers

The need to introduce inert foreign markers was obviated by the observation that a line of natural markers was created by pores and traces of foreign matter at the mating surfaces.

Experimental Schedule and Barrier metals

An experimental schedule was set up to retrieve the most information in an allotted time. Figure 5 is a diagram of the schedule followed. The temperature range of interest, as determined by service conditions of the silicides, is up to 2500°F. The lower limit of 2100°F was chosen because bonding between Ta and $TaSi_2$ was poor below this temperature. The range of times was chosen as the widest practical to ensure stability of diffusion zones at the long times and observation of any non-equilibrium effects for the short times.

Each box represents one run made at a particular temperature for a particular time. The schedule called for 25 runs. The encircled number at the top of the box represents the chronological order of the runs chosen at random. The number 1 or 2 in the lower right-hand corner of the box identifies the diffusion anneal furnace for the runs.

The criteria for selection of barrier metals were:

1. Metals that were known to improve oxidation resistance of

FIGURE 5

EXPERIMENTAL SCHEDULE

Temperature (°F)

Time (Hrs.)	2100	2200	2300	2400	2500
4	(6) Ti,Zr,Nb 1	(19) Ti,Zr,Mo 2	(17) Ti,Zr,Nb 1	(23) Ti,Zr,Mo,Nb 1	(11) Ti,Zr,Mo,Nb 2
24	(18) Zr,Nb,Mo 2	(8) Re,Mo,Nb 2	(16) W,Zr,Nb,Mo 2	(5) Re,Ti,Mo,Nb 2	(2) W,Ti,Zr,Nb 2
48	(7) W,Re,Zr,Mo 1	(12) W,Ti,Zr,Nb 1	(1) Re,Ti,Nb,Mo 1	(13) W,Re,Zr 1	(15) W,Re,Ti,Nb 1
72	(22) W,Re,Ti,Mo 2	(10) W,Re,Zr,Nb 1	(4) W,Re,Ti 2	(25) W,Ti,Mo,Nb 2	(21) Re,Zr,Mo 1
100	(24) W,Re,Ti,Nb 1	(14) W,Re,Ti,Mo 2	(20) W,Re,Zr,Mo 2	(3) W,Re,Zr 1	(9) W,Re,Mo 2

Each cell contains Ta.

Cell 1-1, Run #6 (4 hrs. @ 2100°F)

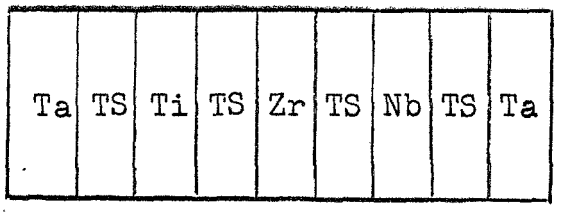

"Sandwich"

Barrier Metals

m.p. of Ta → Ti, Zr, Nb, Mo, Re, W (increasing m.p.)

silicide coatings.

2. Metals with a wide range of melting points bracketing the melting point of tantalum.

3. Metals available in high purity in rods or sheet.

These criteria led to the selection of six barrier metals: tungsten, rhenium, molybdenum, niobum (columbium), zirconium and titanium.

Since $Ta/TaSi_2$ was the system of primary interest, each of the 25 runs contained a $Ta/TaSi_2$ couple. Three runs at each of the temperatures were made for each of the barrier metals. A group of couples to be annealed were stacked in a sandwich arrangement and run under exactly the same conditions. Therefore, the three or four metals listed in the center of each box on the schedule indicate which $M/TaSi_2$ couples were run together with $Ta/TaSi_2$ at that particular time and temperature. The distribution of barrier metal couples throughout the schedule is semi-random, the restriction being that the higher melting point metals (W, Re and Mo) be run for long times at low temperatures. This was necessary because these materials exhibited poor bonding at the lower temperatures.

An example of how the wafers are stacked in sandwich form is shown below the schedule in Figure 5, which is for couples run at $2100^{\circ}F$ for four hours. All couple sandwiches were stacked in the same way: Ta wafers at the ends and four or five $TaSi_2$ wafers (TS on sketch) alternating with three or four barrier metal wafers. Each wafer measured approximately ½" diameter by 1/16" thick; therefore, the total sandwich was a cylinder about ½" in diameter by ½" high.

Before the diffusion anneal the wafers to be used in the sandwich were ground flat and parallel and polished. They were

then mechanically or chemically fine polished, cleaned with water and acetone and stored in acetone. The wafers were dried and stacked in a tantalum sheet basket and held in a molybdenum clamp. This device applied pressure by differential thermal expansion. The top of the clamp, lubricated with MoS_2, was screwed down tightly against the wafers and the assembly was ready for diffusion annealing.

Diffusion Apparatus

The diffusion annealing was performed in two identical SiC-heated tube furnaces. The temperature was controlled to within $\pm$ 10^{o}F by a powerstat through a controller and was measured by a potentiometer connected to a calibrated Pt/Pt-10%Rh thermocouple. The same thermocouple was used for control and measurement. The furnaces were heated over a weekend before the annealing to assure thermal steady state. The temperature was recorded continuously.

The Mo clamp assembly consisting of the clamp suspended on a molybdenum rod was fed through a small O-ring seal connected to the top flange on a mullite furnace tube. Annealing took place in an argon atmosphere. The system was flushed and the pressure in the tube made slightly above atmosphereic. To further protect the specimens the clamp was completely surrounded by a cylinder of tantalum sheet and refractory chip getter. The specimens were retained in the cold region until the furnace had returned to temperature and then the specimens were rapidly lowered to the center of the furnace.

After the diffusion anneal, the specimens were pulled up to the top of the tube and quickly cooled with the aid of a blower. Time at temperature was within $\pm$ 5 minutes and no corrections need be applied.

Measuring Techniques

The specimen sandwich was removed from the clamp, mounted in a room temperature-curing resin and sectioned using a small high speed circular saw. The section was taken as close to a diameter of the cylinder of couples as possible and perpendicular to the mating surfaces. One-half of the sandwich was used for X-ray diffraction analysis and the other ground, polished and etched.

The composition of the growing phases was determined by X-ray diffraction. The general method was to analyze and grind successively through the diffusion zone in steps, starting with pure metal and ending with pure $TaSi_2$. The wafers were split at the original interfaces and the separated surfaces were subjected to full scans (17-72^{o}) in a Norelco diffractometer using CuKα radiation to determine the phases present by comparison with the ASTM file (39). Each wafer was successively ground and analyzed until pure metal was reached in one half and pure $TaSi_2$ in the other. Measurements of amount of material ground off were made with a micrometer to $\pm$0.0001".

3.3 Experimental Results

General Description

Generally the most difficult interface to identify accurately was the $TaSi_2/Ta_5Si_3$ interface because the appearance of the trisilicide closely resembles that of the disilicide and grows on the grains of the latter.

Parabolic growth constants, k, are tabulated for each of the systems investigated. In each table, k values are listed for isothermal growth at each of the experimental temperatures. They are given for the total diffusion zone and for each of the partial zones composing it. The data were analyzed by performing a least-squares analysis on the equations

$$(\Delta x)^2 = k_o t$$

and

$$(\Delta x)^2 = k_s t + b.$$

The variance is expressed as a 95% confidence interval (C.I.) and therefore the first two values tabulated are:

Parabolic constant (through origin) = $k_o \pm$ 95% CI. of k_o and

Parabolic constant (best straight line) = $k_s \pm$ 95% C.I. of k_s; $b \pm$ 95% C.I. of $\sqrt{b}$ where k's are in cm^2/sec and $\sqrt{b}$ values are in microns.

The second equation (best straight line) was tested to ascertain if there were delay times for the formation of any phases. This would correspond to a negative value for b. Positive values of b have no physical significance since this would require a finite thickness of the growing phase to be present before the diffusion anneal was started. The sign of b was retained before the $\sqrt{b}$ for this purpose.

The third value, C_{test}, is a result of a linear regression analysis performed on the equation: $(\Delta x)^2 = kt$. This analysis yields a linear regression factor, F_L, which if significant indicates that a straight line should be fitted to the plot of $(\Delta x)^2$ versus t. A departure from linearity factor, F_D, if significant, indicates that a higher order curve can be fitted. Using standard statistical practices, F_D as well as F_L frequently proved to be significant even when F_L was very much greater than F_D and it seemed evident that the best fit should be a straight line. A ratio of the linear factor (or contribution) to the total contribution (linear plus higher order factors) was used and called the C_{test}. Therefore, $C_{test} = F_L/(F_L+F_D)$ and varies between 0 and 1.

The approach of the C_{test} to unity indicates the relative strength of the linear factor and measures the reliability of the assumption of linearity.

The three values described above are the result of the analysis of all the data recorded for a particular temperature. The three values appearing immediately below these (designated k_o, k_s and C_{test}) are the results of the same analysis performed on data omitting poorer wafers. This was to determine the effects of the use of these wafers on the reliability of the data. All of the statistical analyses were performed on an IBM 360 computer.

Specific Systems

1. $Ta/TaSi_2$

This is, of course, the most important combination and for this reason received the greatest attention. The results of the thickness measurements in the $Ta/TaSi_2$ system are shown in Table VI and in Figure 6. It will be observed from Table VI that the parabolic growth constants, k, for the total zone have been measured within fairly narrow confidence limits (approximately $\pm$ 5% to $\pm$ 15% of the average value). (The $Ta/TaSi_2$ system is the only system in which the growth of the total zone has basic significance.) The values for k_s and b indicate that variations of the best straight line through the data about the origin are random, and a line through the origin can be accepted as the best line. The C_{test} values are very close to unity indicating that the growth rate is truly parabolic. Comparing the data for the partial zones, it is clear that the values of the Δx_2 zones (Ta side) are more accurate than those for the Δx_1 zones ($TaSi_2$ side). This stems from the extra difficulty in identifying the $TaSi_2/Ta_5Si_3$ interface. Comparing the complete and the incomplete ($\bullet$) values, it is obvious that the inclusion of data from couples

TABLE VI

$Ta/TaSi_2$ SYSTEM - PARABOLIC RATE CONSTANTS

TEMP. (°F)	TOTAL ZONE	PARTIAL ZONES	
	k's in (cm^2/sec); Δb (μ)	Δx_1 (Ta_5Si_3) $TaSi_2$ Side	Δx_2 (Ta_5Si_3) Ta Side
2100	k_o= $(7.5\pm0.8)\times10^{-12}$ k_s= $(6.7\pm0.8)\times10^{-12}$; 4 ± 4 C_{test} = 0.974	$(4\pm4)\times10^{-13}$ $(-1\pm4)\times10^{-13}$; 4 ± 3 0.387	$(5\pm1)\times10^{-12}$ $(4\pm1)\times10^{-12}$; 5 ± 4 0.855
	k_o^*= $(7.5\pm0.9)\times10^{-12}$ k_s^*= $(6.6\pm0.8)\times10^{-12}$; 4 ± 4 C^*_{test} = 0.973	same	$(4.6\pm0.9)\times10^{-12}$ $(4.1\pm0.8)\times10^{-12}$; 3 ± 5 0.945
2200	$(1.5\pm0.3)\times10^{-11}$ $(1.1\pm0.2)\times10^{-11}$; 8 ± 4 0.949	$(3\pm2)\times10^{-12}$ $(1\pm8)\times10^{-13}$; 4 ± 2 0.492	$(7.7\pm0.9)\times10^{-12}$ $(6.3\pm0.8)\times10^{-12}$; 3 ± 2 0.940
	$(1.5\pm0.3)\times10^{-11}$ $(1.0\pm0.2)\times10^{-11}$; 9 ± 7 0.932	$(3\pm2)\times10^{-12}$ $(-1\pm1)\times10^{-12}$; 6 ± 3 0.377	$(8\pm1)\times10^{-12}$ $(6\pm1)\times10^{-12}$; 4 ± 3 0.924
2300	$(5.5\pm0.5)\times10^{-11}$ $(6.0\pm0.4)\times10^{-11}$; -10 ± 10 0.990	$(6\pm2)\times10^{-12}$ $(7\pm2)\times10^{-12}$; -5 ± 7 0.934	$(2.6\pm0.2)\times10^{-11}$ $(2.7\pm0.2)\times10^{-11}$; -4 ± 7 0.993
	$(5.2\pm0.7)\times10^{-11}$ $(6.5\pm0.6)\times10^{-11}$; -17 ± 12 0.955	$(4\pm1)\times10^{-12}$ $(6\pm1)\times10^{-12}$; 5 ± 6 0.912	$(2.7\pm0.3)\times10^{-11}$ $(3.2\pm0.2)\times10^{-11}$; -10 ± 7 0.973
2400	$(1.27\pm0.08)\times10^{-10}$ $(1.31\pm0.08)\times10^{-10}$; -9 ± 9 0.994	$(1.3\pm0.3)\times10^{-11}$ $(1.8\pm0.3)\times10^{-11}$; -11 ± 8 0.879	$(6.2\pm0.3)\times10^{-11}$ $(5.6\pm0.3)\times10^{-11}$; 10 ± 8 0.997
	$(1.27\pm0.09)\times10^{-10}$ $(1.34\pm0.09)\times10^{-10}$; -12 ± 15 0.992	same	$(6.1\pm0.4)\times10^{-11}$ $(5.8\pm0.4)\times10^{-11}$; 8 ± 9 0.999
2500	$(2.5\pm0.3)\times10^{-10}$ $(2.0\pm0.2)\times10^{-10}$; 28 ± 16 0.973	$(2.3\pm0.6)\times10^{-11}$ $(1.5\pm0.5)\times10^{-11}$; 12 ± 11 0.922	$(1.21\pm0.09)\times10^{-10}$ $(1.07\pm0.08)\times10^{-10}$; 16 ± 13 0.983
	$(2.5\pm0.3)\times10^{-10}$ $(2.1\pm0.2)\times10^{-10}$; 26 ± 23 0.962	$(2.2\pm0.5)\times10^{-11}$ $(1.6\pm0.5)\times10^{-11}$; 10 ± 10 0.870	$(1.21\pm0.09)\times10^{-10}$ $(1.05\pm0.08)\times10^{-10}$; 17 ± 13 0.982

FIGURE 6

PARABOLIC RATE ~ $\Delta x = k' \sqrt{t}$

$Ta/TaSi_2$ SYSTEM. TOTAL ZONE

COMPLETE - ALL DATA

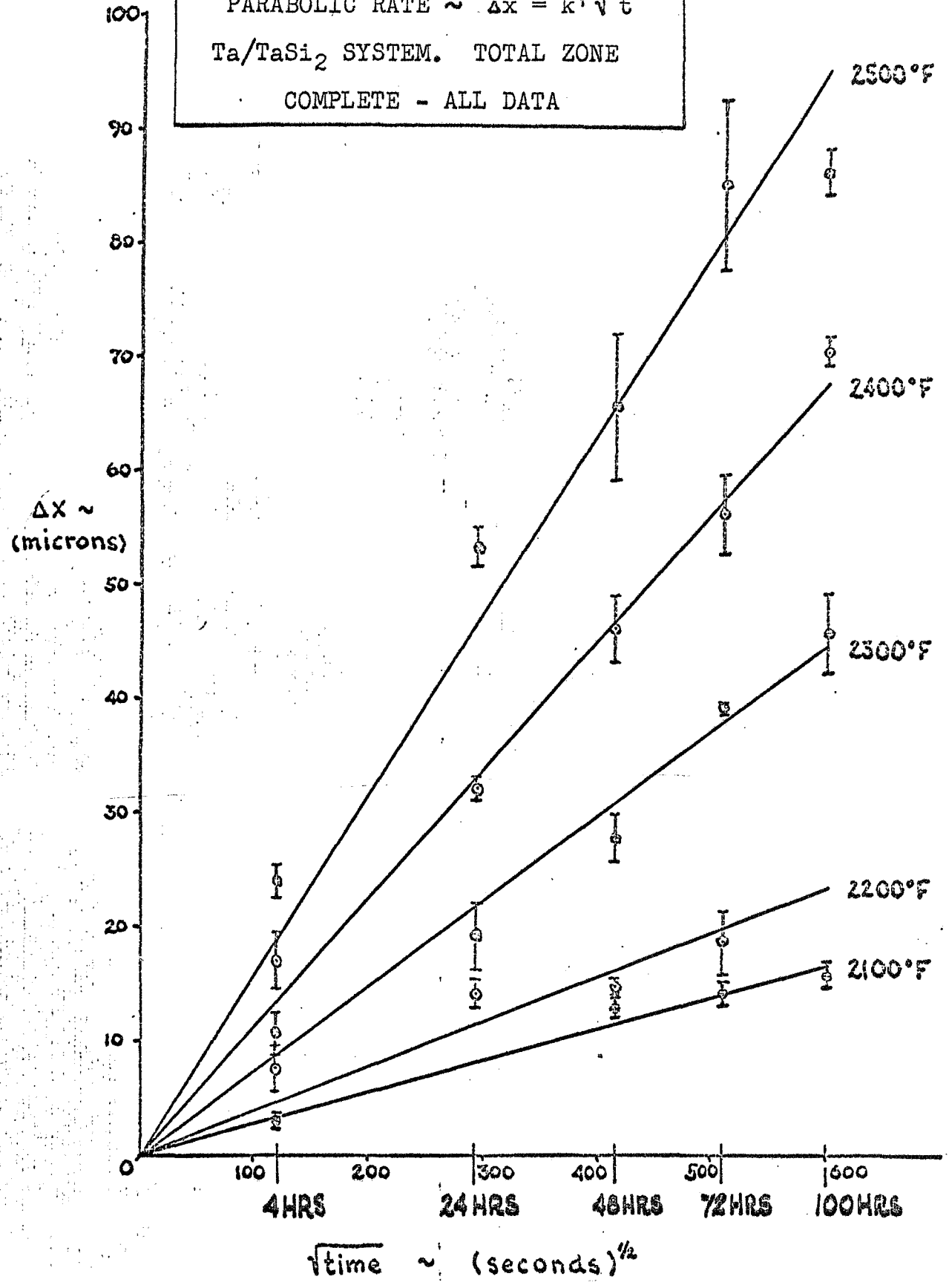

employing poorer $TaSi_2$ wafers has a negligible effect on the overall reliability.

Figure 6 is an example of the parabolic plots obtained. Each point represents an average of about ten pieces of data. The lines drawn are the least-squares lines through the origin utilizing all of the data, and the scatter for individual points is shown in Figure 6 as $\pm \sigma_o$. The overall quality of the data may best be inferred from the k values in Table IV.

The Arrhenius plot of the data for the total zone growth in the $Ta/TaSi_2$ system is shown in Figure 7. The line drawn is the least-squares fit of all the data (not the k_o values alone) and each point represents an average of approximately fifty pieces of data. The slope and intercept of the line were computed using the same statistical approach applied in the determination of parabolic growth constants, and the statistical limits of the values expressed as a 95% confidence interval. The expression for the least-squares line is $k = 5e^{-77,000/RT}$ where Q (the activation energy) = 77,000 $\pm$ 3,000 calories/mole and the pre-exponential constant = $5\ ^{+6}_{-3}$ cm/sec.

The $Ta/TaSi_2$ system has some interesting features. First, Ta_5Si_3 was found to grow in two different crystallographic forms: tetragonal and hexagonal. Bartlett (29) found only tetragonal Ta_5Si_3 in his couples, Nowotny, et.al. (40) reported Ta_5Si_3 as having a hexagonal structure. On the other hand, Knapton (41) and Parthe, et.al. (42,43) reported that pure Ta_5Si_3 is normally tetragonal and that the hexagonal form is an impurity-stabilized phase. In this research, when Ta_5Si_3 formed in small amounts during the synthesis of $TaSi_2$, it was found to be hexagonal; whereas the trisilicide formed by loss of Si from the $TaSi_2$ wafer surface during sintering was found to be tetragonal. The ratio of

FIGURE 7

TEMPERATURE DEPENDENCE OF THE PARABOLIC RATE CONSTANT

$Ta/TaSi_2$ SYSTEM. TOTAL ZONE, COMPLETE DATA

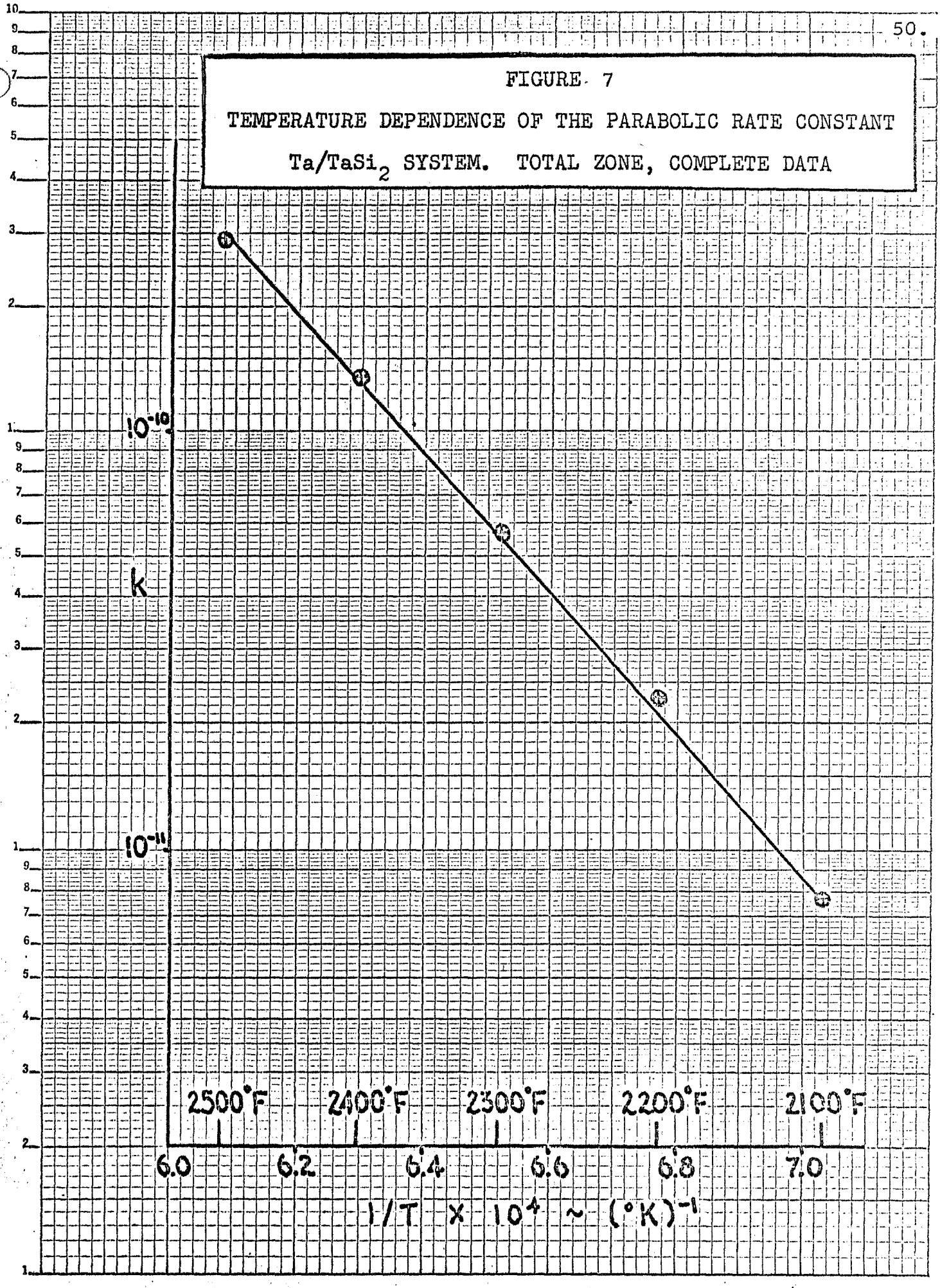

hexagonal Ta_5Si_3 to tetragonal Ta_5Si_3 was always higher in the Δx_1 zone ($TaSi_2$ side) than in the Δx_2 zone (growing from Ta).

2. Diffusion Barrier Systems

As stated earlier, this work had two main aims. First was the measurement of the rate of loss of silicon to tantalum from $TaSi_2$. The second purpose was the search for a diffusion barrier to minimize this loss. For the latter, it was preferable to examine the behavior of a substantial number of candidate metals rather than make precise measurements on a few. Therefore, the number of couples tested in the $M/TaSi_2$ systems were fewer and the results are less reliable. Nevertheless, they are more than adequate for the purpose. In addition, the nature of the intermediate layers was investigated.

a. $Nb/TaSi_2$

Niobium resembles tantalum in its properties and forms similar silicides; $NbSi_2$ (hexagonal crystal structure), hexagonal and tetragonal Nb_5Si_3. Although the metal-rich side of the Nb-Si phase diagram is not as clearly defined as that of the Ta-Si phase diagram and Nb and its silicides melt at considerably lower temperatures, the similarities between Nb and Ta make analysis of the $Nb/TaSi_2$ system desirable.

It was found that two zones grew on the Nb side of the original interface (Δx_a and Δx_2) as well as the Ta_5Si_3 zone (Δx_1) on the $TaSi_2$ side of the original interface. All the interfaces were readily identifiable and the results of the thickness measurements in the $Nb/TaSi_2$ system appear in Table VII.

It will be noticed in Table VII that the values of the parabolic growth constants, k, are generally an order of magnitude larger than the corresponding values in the $Ta/TaSi_2$ system for both total and Δx_1 (Ta_5Si_3) zones. This indicates that niobium

TABLE VII

$Nb/TaSi_2$ SYSTEM - PARABOLIC RATE CONSTANTS

TEMP. (°F)	TOTAL ZONE	PARTIAL ZONES		
	k's in (cm^2/sec); $\bar{\Delta}b$ (μ)	Δx_1 (Ta_5Si_3)	Δx_2	Δx_a
2100	$k_o=$ $(1.3\pm0.2)\times10^{-10}$ $k_s=$ $(0.9\pm0.1)\times10^{-10}$; 23 ± 17 C_{test} = 0.867	$(3.3\pm0.9)\times10^{-11}$ $(1.5\pm0.7)\times10^{-11}$; 17 ± 12 $\bar{0}.642$	$(1.4\pm0.1)\times10^{-11}$ $(1.5\pm0.1)\times10^{-11}$; -4 ± 5 $\bar{0}.991$	$(4.0\pm0.7)\times10^{-12}$ $(2.5\pm0.5)\times10^{-12}$; 5 ± 3 $\bar{0}.847$
	$k_o^*=$ $(1.02\pm0.08)\times10^{-10}$ $k_s^*=$ $(1.03\pm0.08)\times10^{-10}$; -4 ± 14 C_{test}^* = x (2 points)	$(2.1\pm0.3)\times10^{-11}$ $(2.1\pm0.3)\times10^{-11}$; -3 ± 9 $\bar{x}$ (2 points)	$(1.5\pm0.2)\times10^{-11}$ $(1.5\pm0.2)\times10^{-11}$; -3 ± 7 $\bar{x}$ (2 points)	$(3.3\pm0.5)\times10^{-12}$ $(2.8\pm0.4)\times10^{-12}$; 3 ± 3 $\bar{x}$ (2 points)
2200	$(1.8\pm0.2)\times10^{-10}$ $(1.6\pm0.2)\times10^{-10}$; 20 ± 20 $\bar{0}.982$	$(4.0\pm0.8)\times10^{-11}$ $(3.3\pm0.8)\times10^{-11}$; 11 ± 12 $\bar{0}.968$	$(1.7\pm0.6)\times10^{-11}$ $(0.8\pm0.5)\times10^{-11}$; 12 ± 10 $\bar{0}.625$	$(7\pm1)\times10^{-12}$ $(5\pm1)\times10^{-12}$; 6 ± 4 $\bar{0}.914$
	same	same	same	same
2300	$(3.8\pm0.8)\times10^{-10}$ $(2.3\pm0.7)\times10^{-10}$; 36 ± 28 $\bar{0}.754$	$(1.6\pm0.7)\times10^{-10}$ $(-2\pm2)\times10^{-11}$; 40 ± 14 $\bar{0}.439$	$(4\pm2)\times10^{-11}$ $(-0.9\pm0.5)\times10^{-11}$; 20 ± 10 $\bar{0}.400$	$(2.6\pm0.8)\times10^{-11}$ $(6\pm4)\times10^{-12}$; 13 ± 7 $\bar{0}.581$
	2.7×10^{-10} Only 1 Point	6.6×10^{-11} Only 1 Point	1.6×10^{-11} Only 1 Point	1.9×10^{-11} Only 1 Point
2400	$(5.4\pm0.7)\times10^{-10}$ $(5.0\pm0.7)\times10^{-10}$; 21 ± 32 $\bar{0}.993$	$(1.0\pm0.3)\times10^{-10}$ $(0.9\pm0.3)\times10^{-10}$; 12 ± 21 $\bar{0}.970$	$(8\pm1)\times10^{-11}$ $(10\pm1)\times10^{-11}$; -13 ± 12 $\bar{0}.954$	$(2.0\pm0.4)\times10^{-11}$ $(1.1\pm0.3)\times10^{-11}$; 10 ± 6 $\bar{0}.798$
	$(5.3\pm0.9)\times10^{-10}$ $(4.9\pm0.8)\times10^{-10}$; 24 ± 38 $\bar{0}.992$	$(1.0\pm0.3)\times10^{-10}$ $(0.8\pm0.3)\times10^{-10}$; 15 ± 24 $\bar{0}.962$	$(8\pm1)\times10^{-11}$ $(10\pm1)\times10^{-11}$; -15 ± 14 $\bar{0}.943$	$(2.0\pm0.5)\times10^{-11}$ $(1.0\pm0.3)\times10^{-11}$; 11 ± 7 $\bar{0}.773$
2500	$(6\pm1)\times10^{-10}$ $(5\pm1)\times10^{-10}$; 37 ± 33 $\bar{0}.941$	$(1.1\pm0.4)\times10^{-10}$ $(0.9\pm0.3)\times10^{-10}$; 16 ± 20 $\bar{0}.943$	$(3.3\pm0.7)\times10^{-11}$ $(1.9\pm0.5)\times10^{-11}$; 11 ± 7 $\bar{0}.843$	$(6.6\pm0.8)\times10^{-11}$ $(5.7\pm0.8)\times10^{-11}$; 9 ± 9 $\bar{0}.985$
	$(7\pm1)\times10^{-10}$ $(4.5\pm0.5)\times10^{-10}$; 37 ± 20 $\bar{0}.904$	$(1.1\pm0.3)\times10^{-10}$ $(5\pm2)\times10^{-11}$; 20 ± 12 $\bar{0}.745$	$(3.9\pm0.8)\times10^{-11}$ $(2.3\pm0.5)\times10^{-11}$; 10 ± 6 $\bar{0}.850$	$(7.1\pm0.7)\times10^{-11}$ $(6.4\pm0.7)\times10^{-11}$; 7 ± 8 $\bar{0}.987$

would probably make a poor barrier material. The confidence limits for the parabolic growth constants listed in Table IV are somewhat higher than those obtained in the $Ta/TaSi_2$ system. Again, the values of b indicate that there is no incubation period for any of the zones. Most of the C_{test} values are close to unity indicating parabolic growth.

X-ray examination of the $Nb/TaSi_2$ samples showed a similarity to the $Ta/TaSi_2$ system in that two crystallographic forms of the trisilicide appear: tetragonal Nb_5Si_3 and hexagonal Nb_5Si_3. Knapton (41) assigns a tetragonal structure to the pure silicide and calls the hexagonal Nb_5Si_3 an impurity-stabilized phase. In this work it was found that both forms of trisilicide grew with the hexagonal phase increasing in amount relative to the tetragonal phase as the zone grew thicker. Some $NbSi_2$ was found near the original interface, although $NbSi_2$ should be unstable between Ta_5Si_3 and Nb_5Si_3 (if Si activities in Ta and Nb silicides of the same stoichiometry are close, as assumed). This is observed only at high temperatures when rapid Si transport can occur. Besides $NbSi_2$ and two forms of Nb_5Si_3 another phase was detected as represented by one unidentified X-ray peak not characteristic of any Nb silicides in the ASTM file.

b. $Zr/TaSi_2$

Zirconium is a very active metal and forms many silicides. Because it has been used as an additive to help increase the protectiveness of silicide coatings, its effectiveness as a diffusion barrier was studied. Zirconium metal goes through a phase transition from hexagonal to cubic crystal structure at 860°C and is therefore cubic at the diffusion anneal temperatures.

The results of the thickness measurements for the $Zr/TaSi_2$ system are listed in Table VIII, and the k values can be seen

TABLE VIII

$Zr/TaSi_2$ SYSTEM - PARABOLIC RATE CONSTANTS

TEMP. (°F)	TOTAL ZONE	PARTIAL ZONES		
	k's in (cm^2/sec); $\sqrt{b}$ (μ)	Δx_1 (Ta_5Si_3)	Δx_2	Δx_a
2100	$k_o=$ $(1.5\pm0.4)\times10^{-10}$ $k_s=$ $(1.0\pm0.3)\times10^{-10}$; 20 ± 20 C_{test} = 0.714	$(3\pm2)\times10^{-11}$ $(1\pm1)\times10^{-11}$; 14 ± 12 0.377	$(3.5\pm0.6)\times10^{-11}$ $(4.3\pm0.5)\times10^{-11}$; -8 ± 7 0.938	$(3\pm1)\times10^{-12}$ $(2\pm1)\times10^{-12}$; 1 ± 3 0.971
	$k_o^{\circledast}=$ $(1.1\pm0.1)\times10^{-10}$ $k_s^{\circledast}=$ $(1.0\pm0.1)\times10^{-10}$; 5 ± 12 $C_{test}^{\circledast}$ = x (2 points)	$(1.5\pm0.4)\times10^{-11}$ $(1.2\pm0.3)\times10^{-11}$; 5 ± 7 x (2 points)	$(3.8\pm0.6)\times10^{-11}$ $(4.2\pm0.6)\times10^{-11}$; -6 ± 8 x (2 points)	$(3\pm1)\times10^{-12}$ $(2\pm1)\times10^{-12}$; 2 ± 3 x (2 points)
2200	$(1.6\pm0.2)\times10^{-10}$ $(1.4\pm0.2)\times10^{-10}$; 17 ± 19 0.952	$(2.3\pm0.7)\times10^{-11}$ $(1.2\pm0.6)\times10^{-11}$; 12 ± 10 0.646	$(4\pm1)\times10^{-11}$ $(3\pm1)\times10^{-11}$; 8 ± 15 0.876	$(1.2\pm0.4)\times10^{-11}$ $(1.3\pm0.4)\times10^{-11}$; -4 ± 8 0.985
	1.7×10^{-10} Only 1 Point	2.5×10^{-11} Only 1 Point	2.5×10^{-11} Only 1 Point	1.2×10^{-11} Only 1 Point
2300	$(4\pm1)\times10^{-10}$ $(1.5\pm0.6)\times10^{-10}$; 70 ± 40 x (2 points)	$(3\pm4)\times10^{-11}$ $(-4\pm2)\times10^{-11}$; 40 ± 21 x (2 points)	$(6\pm3)\times10^{-11}$ $(2\pm3)\times10^{-11}$; 29 ± 28 x (2 points)	$(1.5\pm0.8)\times10^{-11}$ $(1.0\pm0.8)\times10^{-11}$; 10 ± 14 x (2 points)
	6.2×10^{-10} Only 1 Point	7.3×10^{-11} Only 1 Point	1.3×10^{-10} Only 1 Point	2.6×10^{-11} Only 1 Point
2400	$(6.3\pm0.6)\times10^{-10}$ $(5.2\pm0.6)\times10^{-10}$; 40 ± 30 0.958	$(8\pm1)\times10^{-11}$ $(6\pm1)\times10^{-11}$; 17 ± 16 0.927	$(8\pm1)\times10^{-11}$ $(5.4\pm0.6)\times10^{-11}$; 20 ± 12 0.925	$(5.7\pm0.7)\times10^{-11}$ $(5.3\pm0.6)\times10^{-11}$; 8 ± 12 0.981
	same	same	same	same
2500	$(1.0\pm0.2)\times10^{-9}$ $(6\pm2)\times10^{-10}$; 80 ± 60 0.815	$(1.3\pm0.7)\times10^{-10}$ $(-1\pm5)\times10^{-11}$; 45 ± 29 0.488	$(1.5\pm0.3)\times10^{-10}$ $(9\pm2)\times10^{-11}$; 29 ± 15 0.916	$(1.1\pm0.1)\times10^{-10}$ $(0.9\pm0.1)\times10^{-10}$; 16 ± 14 0.966
	$(1.5\pm0.4)\times10^{-9}$ $(1.0\pm0.2)\times10^{-9}$; 68 ± 50 0.834	$(2.2\pm0.8)\times10^{-10}$ $(1.1\pm0.5)\times10^{-10}$; 30 ± 23 0.763	$(1.7\pm0.6)\times10^{-10}$ $(0.8\pm0.4)\times10^{-10}$; 29 ± 23 0.702	$(1.3\pm0.2)\times10^{-10}$ $(1.2\pm0.2)\times10^{-10}$; 9 ± 13 0.986

to be of the same order of magnitude as in the Nb/$TaSi_2$ system for both total and Δx_1 zones. Therefore, zirconium does not act as a diffusion barrier. The confidence intervals for k_o are generally in the same range as for the Nb/$TaSi_2$ system.

Although X-ray diffraction analysis fairly well determined the composition of the Δx_1 zone as Ta_5Si_3, as in other couples, identification of the other two zones that were found was not successful. There are a number of reasons for this difficulty. The Zr-Si phase diagram indicates the existence of seven Zr silicides. In addition to these, the ASTM Powder Diffraction File gives X-ray diffraction data for two other Zr silicides and Karpinskii and Evseev (44) report even another Zr silicide, Zr_5Si_4. Therefore, a total of ten Zr silicides have been reported to exist. Diffraction studies on the diffusion couples showed no evidences of $ZrSi_2$, ZrSi, Zr_3Si_2 or Zr_5Si_3. Some of the X-ray peaks could be associated with Zr_2Si and Zr_3Si, but most of them remained unidentified.

c. $TiSi_2$

The additive which has been empirically shown to be most effective in increasing the protectiveness of silicide coatings is titanium and so the effectiveness of Ti as a diffusion barrier was examined.

The results of the thickness measurements for the Ti/$TaSi_2$ system are presented in Table VI. From the values for k it can be seen that the total zone grows at a rate close to that for both the Nb/$TaSi_2$ and Zr/$TaSi_2$ systems, but the Δx_1 zone grows at a much higher rate on a comparative scale. Therefore, titanium's effectiveness as an additive in commercial coatings is probably not a result of diffusion barrier action. The confidence limits listed for the data that have been recorded are in the same range as the

TABLE IX

$Ti/TaSi_2$ SYSTEM - PARABOLIC RATE CONSTANTS

TEMP. (°F)	TOTAL ZONE	PARTIAL ZONES		
	k's in (cm^2/sec); $\bar{b}$ (μ)	Δx_1 (Ta_5Si_3)	Δx_2	Δx_a
2100	$k_o=$ $(1.0\pm0.2)\times10^{-10}$ $k_s=$ $(1.1\pm0.2)\times10^{-10}$; -14 ± 24 C_{test} = 0.778	$(3\pm1)\times10^{-11}$ $(4\pm1)\times10^{-11}$; -12 ± 17 0.551	$(1.0\pm0.2)\times10^{-11}$ $(1.0\pm0.2)\times10^{-11}$; -2 ± 8 0.960	$(1.2\pm0.5)\times10^{-12}$ $(0.7\pm0.5)\times10^{-12}$; 3 ± 3 0.465
	$k_o=$ $(1.2\pm0.2)\times10^{-10}$ $k_s=$ $(1.2\pm0.2)\times10^{-10}$; 10 ± 20 C_{test} = x (2 points)	$(4.8\pm0.7)\times10^{-11}$ $(4.7\pm0.7)\times10^{-11}$; 5 ± 13 x (2 points)	$(1.1\pm0.2)\times10^{-11}$ $(1.1\pm0.2)\times10^{-11}$; 2 ± 8 x (2 points)	$(7\pm1)\times10^{-13}$ $(4\pm1)\times10^{-13}$; 2 ± 2 x (2 points)
2200	$(1.8\pm0.2)\times10^{-10}$ $(2.0\pm0.2)\times10^{-10}$; -18 ± 21 0.974	$(8\pm2)\times10^{-11}$ $(8\pm2)\times10^{-11}$; -9 ± 22 0.998	$(1.2\pm0.4)\times10^{-11}$ $(1.4\pm0.4)\times10^{-11}$; -6 ± 10 0.960	$(1.3\pm0.4)\times10^{-12}$ $(1.1\pm0.4)\times10^{-12}$; 2 ± 3 0.913
	$(1.8\pm0.3)\times10^{-10}$ $(2.0\pm0.2)\times10^{-10}$; -22 ± 25 0.965	Same	Same	$(1.2\pm0.5)\times10^{-12}$ $(1.2\pm0.5)\times10^{-12}$; 1 ± 3 0.895
2300	$(5.0\pm0.8)\times10^{-10}$ $(5.1\pm0.8)\times10^{-10}$; -16 ± 36 0.863	$(2.6\pm0.4)\times10^{-10}$ $(2.4\pm0.4)\times10^{-10}$; 17 ± 27 0.910	$(2.7\pm0.9)\times10^{-11}$ $(3.5\pm0.8)\times10^{-11}$; -11 ± 12 0.639	$(1.2\pm0.3)\times10^{-12}$ $(0.9\pm0.3)\times10^{-12}$; 2 ± 2 0.858
	$(5\pm3)\times10^{-10}$ $(10\pm1)\times10^{-10}$; 100 ± 50 x (2 points)	$(2\pm1)\times10^{-10}$ $(4\pm1)\times10^{-10}$; -63 ± 45 x (2 points)	$(3\pm3)\times10^{-11}$ $(8\pm2)\times10^{-11}$; -33 ± 20 x (2 points)	$(1\pm1)\times10^{-12}$ $(-1\pm9)\times10^{-13}$; 5 ± 4 x (2 points)
2400	$(1.1\pm0.1)\times10^{-9}$ $(1.2\pm0.1)\times10^{-9}$; -40 ± 40 0.964	$(4.9\pm0.4)\times10^{-10}$ $(4.5\pm0.4)\times10^{-10}$; 21 ± 24 0.993	$(1.0\pm0.3)\times10^{-10}$ $(1.3\pm0.2)\times10^{-10}$; -21 ± 20 0.781	$(1\pm5)\times10^{-11}$ $(1\pm5)\times10^{-11}$; -11 ± 36 x (2 points)
	$(1.1\pm0.2)\times10^{-9}$ $(1.3\pm0.1)\times10^{-9}$; -52 ± 48 0.953	$(4.9\pm0.5)\times10^{-10}$ $(4.5\pm0.5)\times10^{-10}$; 23 ± 29 0.992	$(1.0\pm0.4)\times10^{-10}$ $(1.4\pm0.3)\times10^{-10}$; -26 ± 23 0.737	Same
2500	Melting	Melting	Melting	Melting

previously mentioned $M/TaSi_2$ systems.

In addition to Ta_5Si_3, two other zones are formed. The one listed as Δx_2 was Ti_5Si_3, while the other shown as Δx_a is probably a eutectoid mixture. The upper temperature of use is limited by the formation of a eutectic at 2426°F (1330°C).

d. $W/TaSi_2$

Tungsten has the highest melting point of all true metals and this property alone makes it a candidate barrier material. From the results of the thickness measurements, presented in Table X, it should be noted that the values for k (total and Δx_1), although an order of magnitude higher than in the $Ta/TaSi_2$ system at low temperatures, are close to the values for $Ta/TaSi_2$ at high temperatures. Most noticeable are the low values for C_{test} which show that the parabolic growth rate was not followed. Confidence limits on k_o reflect a large amount of scatter about a straight line through the origin; but in most cases, the limits on k_s are considerably better indicating that a straight line through the origin is a poor fit of the data. The quality of the results improves at higher temperatures. For this reason, data are presented only for the total and Δx_1 zones, although measured on those grown in the tungsten as well. At low temperatures and for short times at higher temperatures, a WSi_2 phase was found. This was probably produced by vapor transport of silicon from $TaSi_2$. In addition, the W_5Si_3 phase was found to form probably as the result of solid state diffusion.

e. $Mo/TaSi_2$

Molybdenum silicides are the best known and most carefully studied compounds in the silicide family. The melting point of molybdenum is between those of Ta and Nb. These qualifications

TABLE X

$W/TaSi_2$ SYSTEM - PARABOLIC RATE CONSTANTS

TEMP. (°F)	TOTAL ZONE	PARTIAL ZONES (to be continued)
	k's in (cm^2/sec); b (μ)	Δx_1 (Ta_5Si_3)
k_o= k_s= 2100	$(2\pm3)\times10^{-10}$ $(-4\pm1)\times10^{-10}$;120±60 C_{test} = 0.112	$(4\pm8)\times10^{-11}$ $(-4\pm7)\times10^{-11}$;47±46 x (2 points)
k_o^*= k_s^*=	$(2\pm3)\times10^{-10}$ $(-4\pm1)\times10^{-10}$;130±50 C^*_{test}=0.130	$(4\pm11)\times10^{-11}$ $(-10\pm9)\times10^{-11}$;66±52 x (2 points)
2200	$(4\pm3)\times10^{-10}$ $(-3\pm2)\times10^{-10}$;130±70 0.177	2×10^{-11} Only 1 Point
	Same	Same
2300	$(5\pm3)\times10^{-10}$ $(6\pm3)\times10^{-10}$;-60±80 0.696	$(9\pm3)\times10^{-11}$ $(6\pm3)\times10^{-11}$;22±22 x (2 points)
	$(3\pm1)\times10^{-10}$ $(2\pm1)\times10^{-10}$;43±48 x (2 points)	$(9\pm4)\times10^{-11}$ $(6\pm3)\times10^{-11}$;24±27 x (2 points)
2400	$(3\pm3)\times10^{-10}$ $(1\pm3)\times10^{-10}$;70±90 0.243	$(5\pm8)\times10^{-11}$ $(0.7\pm8.0)\times10^{-11}$;35±47 0.139
	$(1.7\pm0.9)\times10^{-10}$ $(1.0\pm0.8)\times10^{-10}$;43±48 0.815	$(3\pm2)\times10^{-11}$ $(1\pm2)\times10^{-11}$;20±19 0.761
2500	$(2.4\pm0.4)\times10^{-10}$ $(2.3\pm0.4)\times10^{-10}$;10±30 0.986	$(4\pm2)\times10^{-11}$ $(0.8\pm1.5)\times10^{-11}$;26±19 0.602
	$(2.5\pm0.5)\times10^{-10}$ $(2.3\pm0.5\times10^{-10}$;23±35 x (2 points)	$(4\pm2)\times10^{-11}$ $(0.7\pm1.0)\times10^{-11}$;27±16 x (2 points)

make Mo a choice candidate to be tested as a barrier material.

The results of the thickness measurements are presented in Table XI for this system. Low temperature values for k are the highest of any of the systems tested being two orders of magnitude higher than the results for $Ta/TaSi_2$. At high temperatures, however, the k values are only one order of magnitude higher than in the $Ta/TaSi_2$ system, or about the same as in most of the other $M/TaSi_2$ systems. The high confidence limits on the 2100°F results can be attributed to paucity of data at this temperature and the results are consequently in considerable doubt. Results at 2200°F, 2300°F and 2400°F are almost as good as those for the $Ta/TaSi_2$ system. Confidence limits are generally low and the high values for C_{test} indicate that up to 2400°F growth follows the parabolic rate. The two zones found and measured metallographically were shown by X-ray to be Mo_5Si_3 (Δx_2) and Mo_3Si (Δx_a).

f. $Re/TaSi_2$

Rhenium was chosen for testing as diffusion barrier because of its high melting point and high density. Re is the densest metal and has a melting point between W and Ta. It was also of interest to investigate a metal with a hexagonal crystal structure as a barrier. (Re was the only metal tested which was not cubic at the annealing conditions.) However, because of cracking and loss of material from the diffusion zones, only a few pieces of data could be recorded and, therefore, no results for the growth kinetics in the $Re/TaSi_2$ system were obtained. The reason for the incompatibility in the $Re/TaSi_2$ couples is probably mechanical and a result of the properties of both Re metal and its silicides at the temperatures of interest.

TABLE XI

$Mo/TaSi_2$ SYSTEM - PARABOLIC RATE CONSTANTS

TEMP. (°F)	TOTAL ZONE	PARTIAL ZONES		
	k's in (cm^2/sec); $\sqrt{b}$ (μ)	Δx_1 (Ta_5Si_3)	Δx_2	Δx_a
2100	k_o= $(7\pm18)\times10^{-10}$ k_s= $(-1.3\pm0.4)\times10^{-9}$; 200 ± 90 C_{test} = x (2 points)	$(2\pm4)\times10^{-10}$ $(-4\pm1)\times10^{-10}$; 112 ± 54 x (2 points)	$(1\pm3)\times10^{-10}$ $(-2.8\pm0.4)\times10^{-10}$; 93 ± 31 x (2 points)	$(1.3\pm0.9)\times10^{-12}$ $(1.6\pm0.7)\times10^{-12}$; -3 ± 4 x (2 points)
	k^*_o= 1×10^{-9} k^*_s= C^*_{test} = Only 1 Point	3×10^{-10} Only 1 Point	2×10^{-10} Only 1 Point	1.2×10^{-12} Only 1 Point
2200	$(1.0\pm0.1)\times10^{-9}$ $(1.0\pm0.1)\times10^{-9}$; -14 ± 52 0.999	$(2.3\pm0.4)\times10^{-10}$ $(2.5\pm0.4)\times10^{-10}$; -18 ± 28 0.990	$(1.6\pm0.2)\times10^{-10}$ $(1.6\pm0.2)\times10^{-10}$; 3 ± 20 0.997	$(3.2\pm0.5)\times10^{-12}$ $(2.6\pm0.4)\times10^{-12}$; 3 ± 3 0.963
	$(1.0\pm0.2)\times10^{-9}$ $(1.0\pm0.2)\times10^{-9}$; 25 ± 75 x (2 points)	$(2.3\pm0.6)\times10^{-10}$ $(2.5\pm0.6)\times10^{-10}$; -22 ± 40 x (2 points)	$(1.6\pm0.3)\times10^{-10}$ $(1.5\pm0.3)\times10^{-10}$; 15 ± 29 x (2 points)	$(3.1\pm0.8)\times10^{-12}$ $(2.4\pm0.7)\times10^{-12}$; 4 ± 4 x (2 points)
2300	$(1.6\pm0.2)\times10^{-9}$ $(1.4\pm0.2)\times10^{-9}$; 50 ± 80 0.956	$(5\pm1)\times10^{-10}$ $(4\pm1)\times10^{-10}$; 58 ± 47 0.894	$(2.9\pm0.9)\times10^{-10}$ $(3.7\pm0.9)\times10^{-10}$; -42 ± 46 0.862	$(1.1\pm0.8)\times10^{-11}$ $(1.1\pm0.8)\times10^{-11}$; 3 ± 11 0.438
	$(1.4\pm0.3)\times10^{-9}$ $(1.1\pm0.2)\times10^{-9}$; 69 ± 70 0.950	$(4\pm1)\times10^{-10}$ $(4\pm1)\times10^{-10}$; 43 ± 48 0.957	$(2.2\pm0.6)\times10^{-10}$ $(2.5\pm0.6)\times10^{-10}$; -21 ± 30 0.891	$(1\pm1)\times10^{-11}$ $(1\pm1)\times10^{-11}$; 7 ± 14 0.338
2400	$(1.8\pm0.2)\times10^{-9}$ $(1.4\pm0.1)\times10^{-9}$; 70 ± 50 0.950	$(4.0\pm0.4)\times10^{-10}$ $(3.5\pm0.4)\times10^{-10}$; 26 ± 27 x (2 points)	$(2.9\pm0.6)\times10^{-10}$ $(2.7\pm0.6)\times10^{-10}$; 14 ± 32 x (2 points)	$(1.7\pm0.4)\times10^{-11}$ $(1.3\pm0.3)\times10^{-11}$; 7 ± 7 0.905
	Same	Same	Same	Same
2500	$(1.5\pm0.8)\times10^{-9}$ $(8\pm7)\times10^{-10}$; 140 ± 140 0.387	$(2\pm1)\times10^{-10}$ $(9\pm13)\times10^{-11}$; 59 ± 60 0.313	$(3\pm3)\times10^{-10}$ $(1\pm2)\times10^{-10}$; 72 ± 81 0.240	$(6\pm2)\times10^{-11}$ $(7\pm1)\times10^{-11}$; -16 ± 20 0.767
	$(8\pm1)\times10^{-10}$ $(6.2\pm0.5)\times10^{-10}$; 62 ± 42 x (2 points)	$(1.0\pm0.2)\times10^{-10}$ $(6\pm1)\times10^{-11}$; 30 ± 20 x (2 points)	$(1.0\pm0.2)\times10^{-10}$ $(0.7\pm0.1)\times10^{-10}$; 26 ± 19 x (2 points)	$(6.9\pm0.7)\times10^{-11}$ $(7.0\pm0.7)\times10^{-11}$; -5 ± 14 x (2 points)

Comparative Results and Effect of Temperature

Tables XII and XIII list the results for the temperature dependence of the growth constants using all data and incomplete data with high quality specimens respectively. The Arrhenius relation of the form $k = k^o e^{-Q/RT}$ is assumed. The parameters k^o and Q are obtained by a least squares analysis of the equation: $\ln k = \ln k^o - Q/RT$, and R is the gas constant. The previously calculated parabolic rate constants (k) were not used; but rather the original thickness measurements themselves were used in the analysis. Therefore, at each temperature there are about fifty values of $(\Delta x)^2/t$ for the $Ta/TaSi_2$ system and about thirty for the $M/TaSi_2$ systems. These data were analyzed by computer using the subroutines for least-squares and departure from linearity analyses employed previously in the computation of parabolic growth constants.

In the tables, the Arrhenius expressions are listed for the total and partial zones for each system. Q, the activation energies for diffusion, are tabulated in the next column together with the 95% confidence intervals. Values for the pre-exponential constants, k^o, appear with their 95% confidence limits in the next column; and C_{test} values are listed in the last column. High values for C_{test} in this case indicate that the data follow the expected exponential temperature dependence. Using C_{test} as criteria for the quality of the data, it can be seen that the best results are those for the $Ta/TaSi_2$ system, and the worst are those for the $W/TaSi_2$ system. It can also be observed that the growth of the Δx_2 zone (Ta side) in the Ta/TaSi system is more accurately known than the growth of the Δx_1 zone ($TaSi_2$ side). This was noticed before and is a result of difficulty in measuring the $TaSi_2/Ta_5Si_3$ interface.

TABLE XII

ARRHENIUS EXPRESSIONS FOR GROWTH RATES (Complete Data)

System	$k = k^o e^{-Q/RT}$	Q ± CI (kcal/mole)	$-k^o < k^o < +k^o$ (cm^2/sec)	C_{test}
$\underline{Ta/TaSi_2}$				
total	$k=5e^{-77,000/RT}$	77 ± 3	2<5<11	0.999
Δx_1	$k=2e^{-81,000/RT}$	81 ± 7	0.2<2<16	0.979
Δx_2	$k=0.6e^{-73,000/RT}$	73 ± 2	0.3<0.6<1.4	0.996
$\underline{W/TaSi_2}$				
total	$k=(4x10^{-10})e^{-2,000/RT}$	2 ± 13	$(0.3<4<52)x10^{-10}$	0.033
Δx_1	$k=(1x10^{-9})e^{-11,000/RT}$	11 ± 14	$(0.1<1<23)x10^{-9}$	0.374
Δx_{a2}	$k=(1.5x10^{5})e^{-120,000/RT}$	120 ± 10	$(0.1<1.5<20)x10^{5}$	0.996
Δx_2	$k=(5x10^{-12})e^{+5,000/RT}$	-5 ± 17	$(0.4<5<80)x10^{-12}$	0.163
Δx_{a1}	$k=(1x10^{-9})e^{-20,000/RT}$	20 ± 45	$10^{-15}<10^{-9}<10^{-3}$	0.110
$\underline{Mo/TaSi_2}$				
total	$k=(4x10^{-6})e^{-25,000/RT}$	25 ± 9	$(0.5<4<31)10^{-6}$	0.873
Δx_1	$k=(2x10^{-7})e^{-20,000/RT}$	20 ± 10	$(0.1<2<60)x10^{-7}$	0.547
Δx_2	$k=(1x10^{-6})e^{-30,000/RT}$	30 ± 10	$(0.1<1<16)x10^{-6}$	0.923
Δx_a	$k=0.4e^{-75,000/RT}$	75 ± 7	0.04<0.4<3.6	0.998
$\underline{Nb/TaSi_2}$				
total	$k=(1.4x10^{-4})e^{-40,000/RT}$	40 ± 6	$(0.4<1.4<4.5)x10^{-4}$	0.987
Δx_1	$k=(4x10^{-6})e^{-30,000/RT}$	30 ± 10	$(0.2<4<68)x10^{-6}$	0.770
Δx_2	$k=(4x10^{-6})e^{-36,000/RT}$	36 ± 9	$(0.4<4<42)x10^{-6}$	0.883
Δx_a	$k=(1.4x10^{-3})e^{-55,000/RT}$	55 ± 7	$(0.2<1.4<12)x10^{-3}$	0.954
$\underline{Zr/TaSi_2}$				
total	$k=(4x10^{-3})e^{-50,000/RT}$	50 ± 5	$(1<4<17)x10^{-3}$	0.991
Δx_1	$k=(3x10^{-5})e^{-40,000/RT}$	40 ± 10	$(0.1<3<76)x10^{-5}$	0.924
Δx_2	$k=(1x10^{-4})e^{-45,000/RT}$	45 ± 9	$(0.1<1<12)x10^{-4}$	0.989
Δx_a	$k=1.2e^{-76,000/RT}$	76 ± 6	0.2<1.2<8.6	0.995
$\underline{Ti/TaSi_2}$				
total	$k=0.8e^{-66,000/RT}$	66 ± 6	0.1<0.8<5.4	0.978
Δx_1	$k=170e^{-84,000/RT}$	84 ± 9	10<170<2600	0.982
Δx_2	$k=(4x10^{-5})e^{-44,000/RT}$	44 ± 9	$(0.3<4<57)x10^{-5}$	0.911
Δx_a	$k=(1x10^{-11})e^{-6,000/RT}$	6 ± 20	$(0.01<1<150)x10^{-11}$	0.254

TABLE XIII

ARRHENIUS EXPRESSIONS FOR GROWTH RATES (Incomplete Data)

System	$k = k^o e^{-Q/RT}$	$Q \pm CI$ (kcal/mole)	$-k^o < k^o < +k^o$ (cm^2/sec)	C_{test}
$Ta/TaSi_2$				
total	$k=6e^{-78,000/RT}$	78 ± 3	$2<6<14$	0.9996
Δx_1	$k=3e^{-84,000/RT}$	84 ± 7	$0.3<3<34$	0.979
Δx_2	$k=0.8e^{-74,000/RT}$	74 ± 2	$0.4<0.8<1.4$	0.998
$W/TaSi_2$				
total	$k=(1x10^{-10})e^{+2,000/RT}$	-2 ± 15	$(0.1<1<21)x10^{-10}$	0.038
Δx_1	$k=(5x10^{-10})e^{-8,000/RT}$	8 ± 18	$(0.1<5<13)x10^{-10}$	0.188
Δx_{a2}	$k=(1.3x10^{5})e^{-120,000/RT}$	120 ± 10	$(0.1<1.3<21)x10^{5}$	0.996
Δx_2	$k=(5x10^{-11})e^{-2,000/RT}$	2 ± 18	$(0.3<5<80)x10^{-11}$	0.022
Δx_{a1}	$k=(3x10^{-10})e^{-20,000/RT}$	20 ± 50	$(2x10^{-17}<3x10^{-10}<4x10^{-3})$	0.063
$Mo/TaSi_2$				
total	$k=(1.3x10^{-7})e^{-14,000/RT}$	14 ± 12	$(0.1<1.3<15)x10^{-7}$	0.605
Δx_1	$k=(1.3x10^{-9})e^{-5,000/RT}$	5 ± 19	$(0.03<1.3<65)x10^{-9}$	0.053
Δx_2	$k=(2x10^{-9})e^{-6,000/RT}$	6 ± 17	$(0.1<2<44)x10^{-9}$	0.263
Δx_a	$k=11e^{-86,000/RT}$	86 ± 9	$(0.6<11<200)$	0.997
$Nb/TaSi_2$				
total	$k=(1x10^{-3})e^{-46,000/RT}$	46 ± 5	$(0.4<1<2.6)x10^{-3}$	0.998
Δx_1	$k=(7x10^{-5})e^{-43,000/RT}$	43 ± 8	$(1<7<49)x10^{-5}$	0.990
Δx_2	$k=(8x10^{-6})e^{-39,000/RT}$	39 ± 9	$(1<8<55)x10^{-6}$	0.927
Δx_a	$k=(2.5x10^{-3})e^{-58,000/RT}$	58 ± 6	$(0.5<2.5<13)x10^{-3}$	0.983
$Zr/TaSi_2$				
total	$k=0.08e^{-58,000/RT}$	58 ± 5	$0.02<0.08<0.33$	0.994
Δx_1	$k=(4x10^{-3})e^{-55,000/RT}$	55 ± 7	$(0.6<4<31)x10^{-3}$	0.986
Δx_2	$k=(8x10^{-4})e^{-50,000/RT}$	50 ± 9	$(0.5<8<120)x10^{-4}$	0.968
Δx_a	$k=0.5e^{-72,000/RT}$	72 ± 5	$(0.1<0.5<2.2)$	0.9992
$Ti/TaSi_2$				
total	$k=0.03e^{-55,000/RT}$	55 ± 5	$0.006<0.03<0.17$	0.956
Δx_1	$k=0.5e^{-66,000/RT}$	66 ± 6	$0.1<0.5<4.1$	0.964
Δx_2	$k=(2.3x10^{-5})e^{-40,000/RT}$	40 ± 10	$(0.1<2.3<53)x10^{-5}$	0.895
Δx_a	$k=(5x10^{-11})e^{-10,000/RT}$	10 ± 20	$(0.01<5<2000)x10^{-11}$	0.394

Comparison of the activation energies for the partial zones in the $Ta/TaSi_2$ system shows that their ranges overlap, although the extremes are substantially different. Hence, it may be concluded that the controlling process is the diffusion of silicon in Ta_5Si_3, even though the reaction producing the Ta_5Si_3 is different in the two zones. This is also true for the Δx_1 and Δx_2 zones in all of the other systems with the exception of the $Ti/TaSi_2$ system, where Q for Δx_1 is considerably greater than Q for Δx_2. In the remaining systems it is the Δx_a zone (closest to the metal) which exhibits a higher activation energy (Δx_{a2} zone in the $W/TaSi_2$ system) than the other partial zones. The activation energies for total and Δx_1 zones in the $Ta/TaSi_2$ system are higher than in any of the other systems (with the exception of the Δx_1 zone in the $Ti/TaSi_2$ system.

Degradation of $TaSi_2$ is best observed by comparing the growth rates of the Δx_1 (Ta_5Si_3) zones. It may be concluded that none of the pure metals tested is clearly a barrier for the loss of silicon from $TaSi_2$, The only competition may be tungsten.

Results of Marker Experiments

1. $Ta/TaSi_2$ System

The results shown in Table XIV are the simple averages of the ratio $\Delta x_2/\Delta x_1$ for each run in the $Ta/TaSi_2$ system in which the partial zones were measurable. Earlier, it was shown that in the $Ta/TaSi_2$ system

$$\frac{\Delta x_2}{\Delta x_1} = \frac{7}{3}\frac{\rho_1}{\rho_2} \tag{35}$$

if $D_{Ta} = 0$ (only Si diffuses). $\Delta x_2/\Delta x_1$ should range from 2.3 to

2.45, depending on whether the Δx_1 zone is tetragonal or hexagonal Ta_5Si_3. X-ray diffraction analysis showed that the Δx_2 zone was ostensibly pure tetragonal Ta_5Si_3 at all conditions, whereas the Δx_1 zone contained varying amounts of hexagonal trisilicide of higher density. ρ_1/ρ_2 varied from unity (homogeneous Ta_5Si_3) to 1.05 (Δx_1 being pure hexagonal Ta_5Si_3) in the extreme. The values of $\Delta x_2/\Delta x_1$ shown in Table XIV are near the expected values. The low values may be expected when the Δx_1 zone develops after short diffusion anneals. Therefore, these results indicate that Ta does not diffuse.

TABLE XIV

RESULTS OF MARKER EXPERIMENTS FOR $Ta/TaSi_2$

AVERAGE VALUES FOR $\Delta x_2/\Delta x_1$

	2100°F	2200°F	2300°F	2400°F	2500°F
4 HRS.	1.6		1.8		1.9
24 HRS.		1.7	1.8	2.9	2.1
48 HRS.	2.2	2.6	2.6	2.4	2.9
72 HRS.			2.5		
100 HRS.				1.9	2.6

2. $M/TaSi_2$ Systems

In the $M/TaSi_2$ systems, it was of primary interest to ascertain whether the metal atom diffused. Marker experiments similar to those made on the $Ta/TaSi_2$ couples need not be made if the phases on each side of the original interface can be identified. In most cases, the original interface was easily located, and identification of the M silicides in the diffusion zone was accomplished. If metal atoms had diffused, M silicides or ternary M, Ta silicides should have been found on the $TaSi_2$ side of the original interface (Δx_1). In all cases but one, only Ta_5Si_3 was found in Δx_1, indicating that the metal did not diffuse appreciably. The exception was the $Ti/TaSi_2$ system in which results clearly indicated Ti_5Si_3 growing in the Δx_1 zone.

3.4 Discussion

The $Ta/TaSi_2$ Couple

1. Comparison of Results

In this work the growth rate of Ta_5Si_3 in the $Ta/TaSi_2$ system has been accurately measured. In the Arrhenius form the parabolic growth constant is

$$k = 5e^{-77,000/RT}$$

where the activation energy is known with 95% confidence to be between 74,000 and 80,000 cal/mole and the pre-exponential constant is known with the same confidence to be between 2 and 11 cm^2/sec. This may be compared with the result obtained by Bartlett (29) who expressed his diffusion constant as

$$\tilde{D}\Delta C = 0.3e^{-58,000/RT}$$

which becomes

$$k = 3.66^{-58,000/RT}$$

There appears to be a substantial discrepancy between the pre-exponential constant in Bartlett's equation and his graphical data.

The rate of degradation of $TaSi_2$ in the $Ta/TaSi_2$ system has also been measured separately. This is identical with the growth rate of Ta_5Si_3 on the $TaSi_2$ side of the original interface (Δx_1) and may be expressed in terms of its parabolic growth constant as

$$k_1 = 2e^{-81,000/RT}$$

where the activation energy is known with 95% certainty to be between 74,000 and 88,000 cal/mole and the pre-exponential constant to be between 0.2 and 16.

The results of the marker experiments indicate that only silicon diffuses. Therefore, there should be only one activation energy for diffusion for k_1, k_2 and k, and the pre-exponential constants should be related through the ratio of k_2/k_1 from equations (35) and (36). The differences in these experimentally determined constants is then a result of experimental error.

2. Significance of Results

In Table XV, times are calculated from the experimentally determined Arrhenius equations which indicate the practical service lifetimes of a $TaSi_2$ coating at 1500°F, 2000°F and 2500°F if the coating could be applied in a dense form similar to the wafers fabricated in this work. The first and second lines are the times required to grow the total Ta_5Si_3 zone 1 mil thick using the

equations from this work and Bartlett's work respectively. The ratio, next line, indicates that a dense $TaSi_2$ layer has a considerably longer lifetime than the porous coating used in Bartlett's work. The total Ta_5Si_3 zone grows from both degradation of $TaSi_2$ and consumption of Ta metal and, therefore, the time required to grow 1 mil Ta_5Si_3 is less than the service lifetime of 1 mil of $TaSi_2$. On the last line (2b) the lifetime of 1 mil layer of $TaSi_2$ has been computed from the results on line 1 assuming the theoretical relationship between k_2 and k_1 from equations (35) and (36). From these equations, k_2 should be approximately six times k_1 and the time to grow a 1 mil Δx_1 zone (or deplete 1 mil $TaSi_2$) would be seven times the time to grow 1 mil total Ta_5Si_3. This may be compared with the lifetime of a 1 mil $TaSi_2$ layer calculated directly from the experimentally determined equation for the growth rate of the Δx_1 zone (2a). The agreement is fairly good and is best at higher temperatures.

In a practical application, lifetimes of about 1000 hours are desired at a temperature of 2500°F. This work shows that it would be necessary to use a minimum coating thickness of about 5 mils merely to compensate for loss of $TaSi_2$ by diffusion.

TABLE XV

CALCULATED TIMES TO GROW A 1 MIL LAYER OF Ta_5Si_3 AND LOSE 1 MIL $TaSi_2$

(For Layers Other Than 1 Mil, Multiply Times by Square of Layer Thickness in Mils)

TEMPERATURE	1500°F	2000°F	2500°F
1. Time to grow 1 mil Ta_5Si_3:			
a) This work	10^6 hrs.	600 hrs.	5.25 hrs.
b) Bartlett	18 hrs.	5 min.	8 sec.
c) Ratio $\frac{t \text{ present work}}{t \text{ Bartlett}}$	50,000	7,500	2,400
2. Lifetime of 1 mil coating of $TaSi_2$:			
a) Using result of k_1	1.4×10^7 hrs.	6,600 hrs.	45 hrs.
b) Using $k_1 = \frac{1}{7} k_{total}$	7×10^6 hrs.	4,200 hrs.	37 hrs.

3. Phases Formed

Table XVI is a summary of the phases found to exist between the metal and $TaSi_2$ in the diffusion zone. It may be noted that in each system but the $Zr/TaSi_2$ system, the trisilicide (M_5Si_3) grew as a measurable zone. This is designated Z in the table. Phases labeled X were not noticeable microscopically, but were observed by X-ray diffraction analysis. The Ta_2Si phase, shown as

X*, grew only under special conditions, previously discussed, near the metal interface. The cross-hatched areas represent phases not reported on the phase diagrams and should, therefore, be non-existent. The double cross-hatched areas are silicides reported in the literature but not represented on the accepted phase diagrams and, therefore, their existence is questionable. Only boxes marked X or Z represent silicides that were found to be present in the diffusion couples studied in this work. Identification of the Zr silicides was difficult and the compositions of the growing zones could not be deduced. Only in the Mo system does the lowest silicide grow as a zone. The growth of the Mo_3Si zone is probably the reason for the unexpectedly high growth rate in that system.

TABLE XVI

SUMMARY OF INTERMEDIATE PHASES FOUND

M	MSi_2	MSi	M_3Si_2	M_5Si_3	M_2Si	M_3Si	M_4Si	$M_{4.5}Si$
Ta	—			Z	X*			—
W	Z			Z				
Mo	X			Z		Z		
Nb	X		Z	Z			—	
Ti	—	—		Z				
Re	Z			Z				
Zr	—	—		—	?	X	No X-ray data	

4. Glass Structure and Growth (F.N. Schwettmann)

4.1 Introduction

The previous section was devoted to studies of interactions between silicide coatings and their substrates. This section describes research to explore the interaction of refractory metal silicides with an oxidizing environment. In order for the silicide coating to provide oxidation resistance, it is necessary for an adherent oxide film to be formed when the material is exposed to an oxidizing atmosphere. The structure of the oxide film, its mechanism and rate of growth, and its protectiveness are of fundamental interest.

A simple coating of $TaSi_2$ formed on tantalum does not provide oxidation resistance (49). In order to obtain a suitable coating, it is necessary to add modifiers such as chromium, titanium, molybdenum and vanadium during the coating preparation (50,51). The final coating is a mixture of the various metal silicides. In some of the more promising systems, the resulting protective layer consists mainly of $TiSi_2$. The mechanism by which $TiSi_2$ enhances the oxidation resistance of the silicide mixture has not previously been determined nor has its oxidation behavior in bulk form been studied.

Determination of the fundamental oxidation mechanism for a silicide when in the form of a coating is difficult because of physical defects in the coating and uncertainties in its chemical composition. Also, interactions between the coating and substrate can be a significant factor in long term oxidation resistance.

In this research, the oxidation of $TiSi_2$ in bulk form has been studied in the temperature range 300-1300^{o}C at oxygen partial pressures of 0.2 to 1.0 atmospheres. Information on the oxidation of TiSi and Ti_5Si_3 was also obtained at 1000^{o}C. The structure of

the growing oxide film was determined by matallography, X-ray diffraction, infrared spectroscopy and electron microscopy.

The observations of this study are not explained by the mechanism previously proposed to account for the oxidation protection of other silicides, particularly $MoSi_2$. Contrary to previous theory, it is apparently quite possible to have a protective oxide film containing both the metal oxide and SiO_2. It is the compatability of the two oxides which is of basic importance.

4.2 Literature Review

Oxidation of Silicides

Little work has been done on the intrinsic oxidation behavior of bulk titanium silicides. Samsonov (52) describes the results of an experiment in which $TiSi_2$ was heated to 1200°C over a four hour period. The weight gain observed was only 0.3 mg/cm^2. An adherent oxide film was formed. The author speculates that the protective nature of this film is due to the formation of an eutectic mixture of titanium silicates. No mention is made of the sample density, quality of surface or any of the other variables significant in oxidation studies.

The silicide whose oxidation has been studied most extensively in bulk form is $MoSi_2$. Wirkus and Wilder (2) have recently summarized the oxidation studies on $MoSi_2$. They show two distinct temperature regions where a characteristic oxide is formed.

Measurable oxidation begins at about 300°C for both bulk and powdered $MoSi_2$. At temperatures of 300-600°C, a duplex oxide of MoO_3 and SiO_2 forms. This region has been termed the "pest" since the oxide spalls from the silicide surface with deterioration occurring at a rapid rate.

Berkowitz-Mattuck et.al. (53) have carried out an extensive

investigation of the oxidation of $MoSi_2$ in the temperature region 450-650°C. The authors studied the oxidation of polycrystalline and single crystal samples made using a zone refining technique. The polycrystalline samples were found to deteriorate when exposed to oxygen, but not nitrogen, carbon dioxide, carbon monoxide or argon. X-ray analysis indicated MoO_3 and SiO_2 were present as the oxidation products. The observed rate of disintegration was extremely sensitive to changes in the oxygen pressure.

One of the major characteristics of pesting is the increase in the number of cracks in the substrate as oxidation proceeds. These cracks are of all kinds, some occurring within single grains and others across or along grains. Single crystal samples of $MoSi_2$ did not exhibit pest.

The authors indicate that the physical nature of the $MoSi_2$ may be the significant factor in the "pest" phenomena. Materials which can be prepared crack free, such as Mo_3Si, do not pest, while those which are difficult to prepare free of cracks, do. WSi_2 (650-2150°C), Nb_5Si_3 (500-1150°C) and Mo_5Si_3 (500-800°C) are materials that do contain cracks and also show pest in an intermediate temperature region.

If the diffusion of oxygen through the oxide to the $MoSi_2$ is involved in the reaction sequence, the newly forming oxide in a crack would exert considerable pressure since the volume expansion would be about 200 percent. This would tend to propagate the crack and result in sample deterioration.

At temperatures above 600°C, the volatility of MoO_3 becomes appreciable. A two-stage mechanism has been proposed for this region. In the initial stage of oxidation, both oxides are formed. The MoO_3 volatilizes, leaving a relatively pure silica film. The oxygen activity at the substrate-oxide interface is considerably

reduced because of the dense, impervious nature of the oxide. Under these conditions, Searcy (54) claims that the reaction

$$5MoSi_2 + 7O_2 = Mo_5Si_3 + 7SiO_2$$

is thermodynamically favored. The Mo_5Si_3 is found in a layer directly below the protective SiO_2 film. This is confirmed by X-ray diffraction and weight change studies. If MoO_3 and SiO_2 were formed, a weight loss would be observed due to MoO_3 volatilization. On the other hand, formation of SiO_2 and the lower silicide would show a weight gain and, this is observed.

The rate determining step appears to be diffusion through the oxide film. Since Mo_5Si_3 forms below the oxide surface, the diffusion of silicon through this layer may be the significant rate determining factor. Wirkus and Wilder discuss this possibility and conclude that the silicon mobility is much larger in the silicide than is the oxygen in SiO_2.

The simplest coating system can be obtained by straight siliciding of the tantalum or columbium metal. It has been found (49), however, that on oxidation $TaSi_2$ and $CbSi_2$ form non-protective scales. For this reason, other materials are added to the silicon powder during the coating preparation to improve the oxidation resistance. Some of the materials which give favorable results when used by themselves or in combination with each other are silicides of titanium, chromium, vanadium and molybdenum. Alternatively, the substrate metal may be alloyed with these metals.

A fundamental study aimed at the composition of the oxide film formed during oxidation of silicide coatings on tantalum was carried out by Bracco, et.al. (50). Two coating systems and two

metal substrates were used in this work. The coatings were prepared by straight siliciding and siliciding with 90Ti-10W in the pack. The substrate materials were tantalum and T-222 alloy (88Ta 2.7Hf 9W). The analytical techniques used for studying the oxide film that was formed on oxidation were X-ray diffraction and electron microprobe analysis.

When the samples that were straight silicided were oxidized, the major oxidation product was found to be Ta_2O_5. At oxidation temperatures of 2800°F (1538°C) α-Ta_2O_2 predominated, while at 2500°F (1371°C), the β-Ta_2O_5 form was the major product. SiO_2 (α-cristobalite) was present in trace amounts when the tantalum-based silicide coating was oxidized at 2800°F (1538°C), while none was found when T-222 samples were similarly treated. Some shifts were noted in the reflectance peaks of Ta_2O_5 which may indicate SiO_2 solution since thermodynamically SiO_2 should be present.

A somewhat different situation resulted in the case where a Ti-W-Si coating system was used. TiO_2 (rutile) and SiO_2 (α-cristobalite) were the major oxide phases formed at 2500°F (1371°C). Tantalum oxides were not found. As in the straight tantalum work, no SiO_2 was found in the 2800°F (1538°C) samples, TiO_2 (rutile) being the main product. In this case, the lack of indication of SiO_2 may be due to its being amorphous and, therefore, not indicated because of interference from the strong orientation in the TiO_2 reflections.

Wimber and Stetson (51) have reported results on a more complex silicide coating formed on tantalum T-222. This coating contained 15Ti-35W-15V-35Mo where the values are in wt. percent. When this coating was oxidized at 2400°F (1316°C) for 400 hours, three oxide phases were observed under microscopic examination. One appeared white, the other light gray and the third dark gray.

An electron microprobe run parallel to the surface indicated that the white phase was TiO_2. The (110) plane was found to be oriented parallel to the sample surface. The light gray phase contained 4 to 6 percent titanium while the dark gray phase contained no titanium. No silicon appeared in the white phase. The light gray contained 10 percent and the dark gray 20 percent. The authors suspect that the dark gray phase was slightly impure, partially devitrified SiO_2 while the light gray phase was a titania-silica glass.

Binary TiO_2-SiO_2 System

There has been little work on interactions in the binary TiO_2-SiO_2 system. The first phase equilibrium study was reported by Bunting (55). He shows the phase diagram as a simple eutectic with no compounds and no solid solubility. The eutectic was given at 1540°C for 10.5 wt. percent TiO_2.

A later, more detailed study was carried out by Ricker and Hummel (56). They report the revised phase diagram shown in Figure 8. Their data relocates the eutectic composition at 21 wt. percent TiO_2 with the same eutectic temperature of 1540°C. In addition, considerable solid solubility is indicated at both the high and low silica concentrations. The maximum values are approximately 10 percent TiO_2 in high cristobalite and approximately 24 percent silica in rutile at the eutectic temperature. At 1500°C, a heat treatment time of 10 hours is reported sufficient to produce equilibrium, while at 1350°C, 30 hours is satisfactory. At 1350°C, X-ray data gave evidence of limited solubility. At 1000°C, even after 168 hours heating, no conclusions could be drawn since equilibrium conditions were probably not obtained.

The refractive index of the cristobalite solid solution was observed to increase as more TiO_2 was included. The average

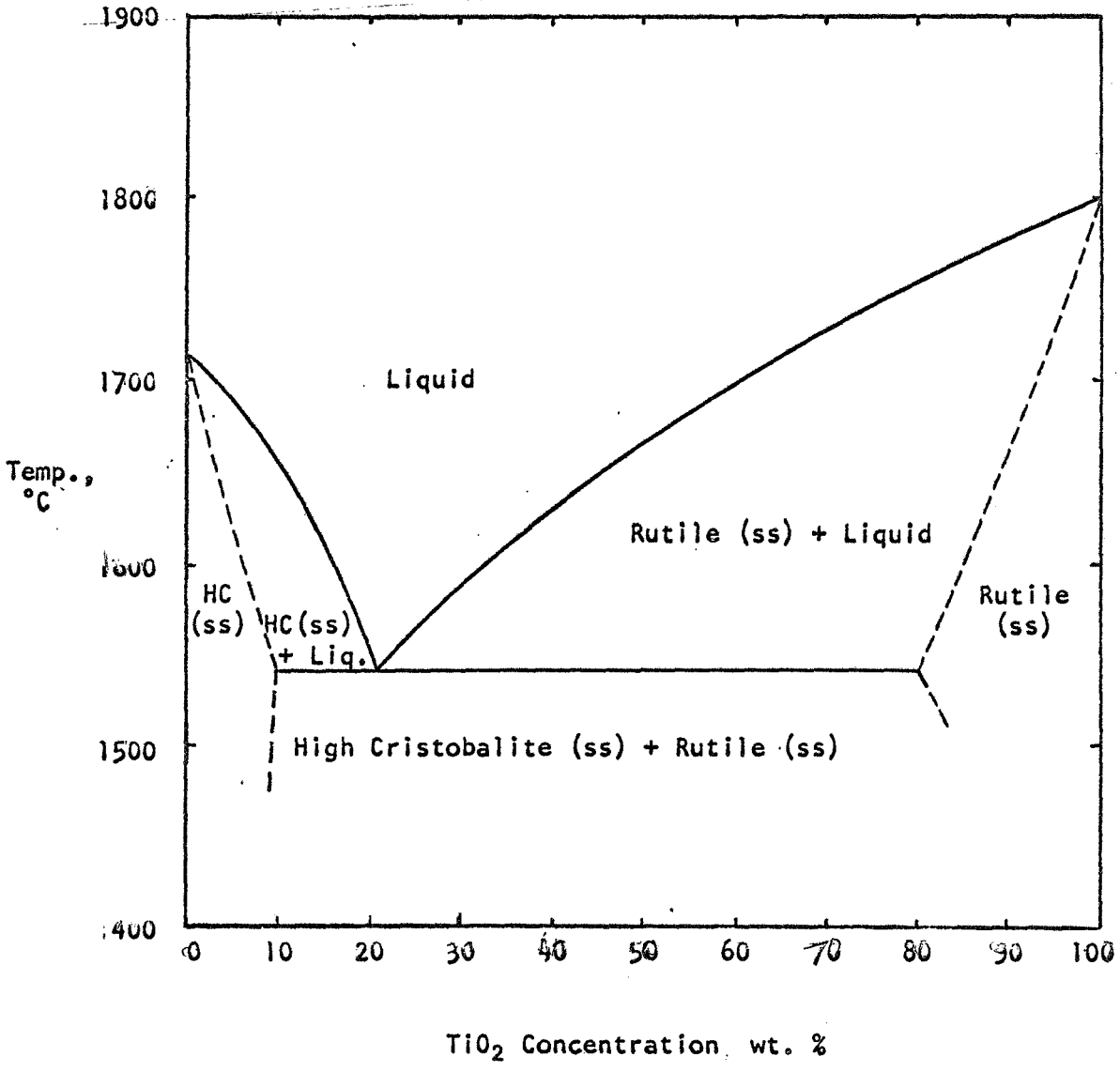

Figure 8 TiO_2-SiO_2 Phase Diagram (56)

refractive index of a solid solution containing 9 percent TiO_2 was 1.490.

Ricker and Hummel also prepared TiO_2-SiO_2 binary glasses by heating samples of the desired composition to 1700°C in platinum and quenching. The glasses were light bluish-gray, transparent when 2-3 mm. thick and opaque at greater thicknesses. The refractive indices of the glasses were given as:

TiO_2 Conc., Wt. %	Refractive Index
9	1.493
13	1.503
20	1.538
25	1.556

The refractive index of pure silica is reported as 1.46. These glasses were annealed at 1575°C for 1.5 hours and then quenched. The samples containing 9 and 13 percent TiO_2 analyzed as cristobalite with extremely small specks of what appeared to be TiO_2. The 20 percent sample remained essentially a glass with only a slight trace of unidentified crystals with the 25 percent sample containing large crystals of rutile.

An important conclusion of this study is that at temperatures over about 1000°C, 10 wt. percent TiO_2 can be dissolved in SiO_2. The resulting solid solution is retained when cooled to room temperature.

Titanium is normally classified as an intermediate ion, i.e., although not usually capable of forming a glass, it can take part in the glass network. Because of its size, it usually assumes a coordination of 6. In order to take part in the silica network, the required coordination would be 4. Many ions exhibit a decrease in coordination as the temperature is increased. Titanium

then could assume the required coordination of 4 at the temperature at which solution occurs. Quick cooling could then freeze the dissolved titanium in the network forming position.

The results of Ricker and Hummel (56) do not indicate whether the TiO_2-SiO_2 glasses with less than 10 wt. percent TiO_2 are homogeneous or whether amorphous phase separation has occurred. Two phase separation has been observed in the MgO-SiO_2 and CaO-SiO_2 systems but not in the Na_2O-SiO_2 and K_2O-SiO_2 systems (57).

Oxidation of Silicon

In exploring the oxidation mechanism of silicides, it is worthwhile to consider a comparison with the oxidation of silicon which has been studied in great detail in recent years. All of the latest studies on the oxidation of pure, single crystal silicon indicate that when clean surfaces are used, the SiO_2 film formed is amorphous. The quality of the amorphous film, in terms of density and defects, is determined by the nature of the surface preparation, oxidation conditions and type of oxident. From the standpoint of oxidation protection, a high density film is desired since this shows a lower growth rate.

Pliskin and Lehman (58) have carried out an extensive transmission infrared study on the structure of SiO_2 films formed by thermal oxidation and evaporation techniques. The infrared spectrum of bulk amorphous SiO_2 shows absorptions at 1100, 800 and 465 cm^{-1}. With a bare silicon wafer in the reference beam, Pliskin and Lehman report a strong Si-O stretching band at 1090 cm^{-1}. The half-width and position of this band was strongly influenced by bonding character, stoichiometry, density and porosity of the film. At 1250 cm^{-1} a slight bump in the broad 1090 cm^{-1} peak was observed. The Si-O-Si bending vibration at 450-460 cm^{-1} was not discussed since it behaves in the same way as the 1090 cm^{-1} peak.

A typical, dense SiO_2 film with a thickness of 1μ had absorption peaks at 1093 and 805 cm^{-1}. A lower density pyrolytic oxide film showed bands at about 1080-1085 cm^{-1}, and 813 cm^{-1}. Films with greater porosity and bond strain show even greater shifts than those indicated above. In comparing oxide films, comparable thicknesses are required since half-widths and band positions vary slightly with thickness.

Murray and Goldsmith (59) in a reflection study of SiO_2 on silicon, showed the effect of film thickness on peak position. Reflection maxima are observed at 1280 and 1120 cm^{-1} with corresponding minima at 1260 and 980 cm^{-1}. The authors indicate that increasing the thickness from 1000 to 10,000Å shifts the reflection peak from 1070 cm^{-1} to 1120 cm^{-1}.

Sata and Shibata (60) have studied the restrahl reflection spectrum of amorphous SiO_2 grown on silicon and presented a mechanism to explain changes in peak position with changes in thickness. The authors also compare the spectrum for amorphous SiO_2 with that of quartz and indicate that the knowledge of the spectral reflectivity of the amorphous form is in its infancy.

The Si-O stretching band at 1100 cm^{-1} and the Si-O bending band in the 470 cm^{-1} region were both observed while the Si-Si stretching bands at 800 and 775 cm^{-1} and the Si-Si bending band at 540 cm^{-1} were either missing or very weak. These latter Si-Si bands are usually quite clear in quartz.

The reflection spectra obtained by Sato and Shibata are similar to that obtained by Murray and Goldsmith (59). Peak position decreased from 1100 cm^{-1} at 5200 Å to 1060 cm^{-1} at 1000 Å. In addition, the reflection intensity decreased until at 1000 Å, the curve was almost flat. At less than 750 Å, the peak became an absorption peak. The back reflection gave, in all cases, an absorption peak.

Sata and Shibata suggest that the shift in peak position is due to silicon with dangling bonds on the surface. If $\overset{\bullet}{\underset{\bullet}{Si}}$ represents silicon bonded to only three oxygen, $\overset{\bullet}{\underset{\bullet}{\overset{\bullet}{Si}}}$ two and $\overset{\bullet}{\underset{\bullet}{Si}}\bullet$ one, then the absorption frequencies would be

$$\nu(\overset{\bullet}{\underset{\bullet}{Si}})>\nu(\overset{\bullet}{\underset{\bullet}{\overset{\bullet}{Si}}})>\nu(\overset{\bullet}{\underset{\bullet}{Si}}\bullet)$$

As the surface of the oxide is approached from within the oxide, the number of "unsaturated" silicon atoms would increase. As the film gets thinner, the silicon with dangling bonds would have a greater effect and the band would be observed at a lower frequency. The backside data show no shift which the authors claim is consistent with the model since there would be no reason to find silicon with dangling bonds at the silicon-silica interface.

Deal (61) reports the following data on SiO_2 films on silicon obtained from thickness and weight change measurements.

Oxidant	Temp., ^{o}C	Density, g/cm^3
Dry O_2	1000	2.27
	1200	2.24
Wet O_2	1000	2.18
	1200	2.21
Steam	1000	2.08(2.00-2.20)
	1200	2.05(2.00-2.20)

Ing. et.al. (63) report on a permeation study designed to determine the imperfections in a thermally grown film on silicon. The authors etched a hole (area $\sim$ 0.01 cm^2) in an SiO_2 film with HF. Upon exposure to chlorine at 800^{o}C, the silicon in the hole was vaporized as $SiCl_4$. Since the SiO_2 film is not attacked by the chlorine, an SiO_2 window is formed at the other end of the hole. A pressure drop was then applied across the film and the

permeation rate measured. For films 5000 Å thick, a (ΔP) of 200 mm was used, while for films of 15,000 Å thick, 760 mm was used. Results were categorized as:

Permeation Constant, cm^3-cm/sec-cm^2-cm-Hg	Mechanism
10^{-3} to 10^{-5}	Flow through microcracks and crystalling boundaries
10^{-7} to 10^{-10}	Flow through microchannels
10^{-15}	True diffusion and permeation

The bulk of the results in the study fell in the 10^{-7} to 10^{-10} range of flow through microchannels. In some of the films, where crystal-like growth appeared, the permeation rate was $\sim 10^{-4}$. These crystallites varied in diameter from 4×10^{-4} to 3.3×10^{-3} cm. When the entire film was etched away, the silicon appeared pitted where the crystals were observed in the film. In addition, it was found that the permeation rate varied with the base used.

In contrast to the single crystal studies, Evans and Chatterji (63) carried out a study on the oxidation of silicon formed by melting powdered silicon in a thoria-lined alumina crucible. The oxidation product upon analysis by X-ray was found to be transparent cristobalite. Evans and Chatterji also observed that silicon reacts with nitrogen at 1200-1360°C to form Si_3N_4. Weight gains as high as 1 mg/cm^2 were observed after three hours in pure N_2.

In determining the mechanism for the oxidation of silicon, three distinct temperature regions are considered. The first is the range from room temperature to 500°C where no noticeable oxidation occurs. In the region from 500-900°C, the oxidation

kinetics are apparently linear, while from 900-1200°C, the kinetics are parabolic.

An excellent summary and interpretation of the rate data on silicon oxidation was recently presented by Deal and Grove (64). Where other authors considered a single rate controlling step for each temperature region, Deal and Grove used a combined mechanism considering all the steps in a single model. The basic assumption was made that the film thickness was large enough so that the effect of space charge conduction was negligible.

In developing the general rate expression, four steps were considered in the reaction sequence. These were: gas phase diffusion of oxygen to the oxide surface; adsorption of oxygen into the oxide film; diffusion through the oxide film; and reaction at the oxide-silicon interface. Using a suitable mathematical expression for each step, the general rate expression

$$X^2 + AX = B(t + \tau)$$

where X = weight gain or oxide thickness, t = time, B = parabolic rate constant, B/A = linear rate constant, τ = constant related to initial condition, was obtained. B is directly related to the effective diffusivity through the film and B/A to the reaction rate constant and gas phase mass transfer coefficient.

Deal and Grove determined the importance of the various parameters in the above reaction. An oxidation study was carried out with dry oxygen (less than 5 ppm water) over the temperature range 700-1200°C. The silicon was Czochralski pulled (single crystal pulled from the melt), p type, boron doped with an (111) surface. Multiple beam interference techniques were used to determine the oxide film thickness.

For the case with dry oxygen, it was found that none of the curves of X versus t extrapolated through the origin. At all

temperatures, a value of X of 230 $\pm$30Å was obtained at t = 0. At 700°C, where the oxidation was extremely slow, an extrapolated value of X = 210 Å was obtained from the linear part of the curve. This value was adopted as the value of X_i, the initial condition.

A plot of ln B vs. 1/T indicated a diffusion activation energy of 28.5 kcal. This compares with a value of 27.0 kcal obtained by Norton (65) and 71.2 kcal by Sucov (66) for the diffusion of oxygen through fused silica. A plot of ln B/A vs. 1/T also gave a straight line with an activation energy of 46.0 kcal.

The parabolic rate mechanism found in the oxidation temperature region 900-1200°C indicates that the diffusion of a particular species is the rate controlling step in the reaction. In this system, the possible diffusants are: the silicon atom or ion; the oxygen atom or ion; or the oxygen molecule. Marker studies (67,68) have shown that some form of oxygen is the diffusing species. The data of Flint (69) indicate that the parabolic rate constant is directly proportional to the oxygen pressure. These results led Deal and Grove (64) to the conclusion that O_2^- is the diffusing species.

The mechanism by which the oxygen is transported through the silica film is not understood. Sucov (66) proposed that the mechanism of oxygen diffusion in silicate glasses and non-stoichiometric silica involves the rupture of a single oxygen bond to silicon and that the diffusion occurs by interstitial motion through the voids formed in the lattice. A calculation shows that at least 50 kcal per mole is required to remove an oxygen from the lattice. Since two bonds must be broken for vacancy diffusion, the activation energy would be at least 100 kcal/mole. This would appear to indicate interstitial diffusion since the experimental value obtained was 71.2 kcal/mole. Similar activation energies are

obtained for oxygen diffusion in soda lime glasses indicating a similar mechanism.

Ligenza (70) carried out a study on the effect of crystal orientation on the oxidation rate of silicon in high pressure steam. The kinetics were linear and directly proportional to the steam pressure.

Properties of the Titanium Silicides

The phase diagram for the titanium-silicon system is shown in Figure 9 (71). Three compounds are indicated. These are $TiSi_2$, TiSi and Ti_5Si_3. A summary of the properties of these materials is given by Samsonov (72).

4.3 Experimental

A. Sample Preparation

The titanium silicide wafers used in this study were prepared using the techniques of powder metallurgy. In the initial phase of the study, $TiSi_2$ powder from CERAC, Inc. was used. This material was -325 mesh with a minimum purity of 99.6 percent. A typical analysis as supplied by the manufacturer is given in Table XVII. These data indicate a silicon excess of 0.68 percent.

Table XVII

Analysis of CERAC $TiSi_2$

	Weight %
Titanium	45.60
Silicon	53.80
Carbon	0.20
Iron	0.10
Oxygen	0.30
	100.00

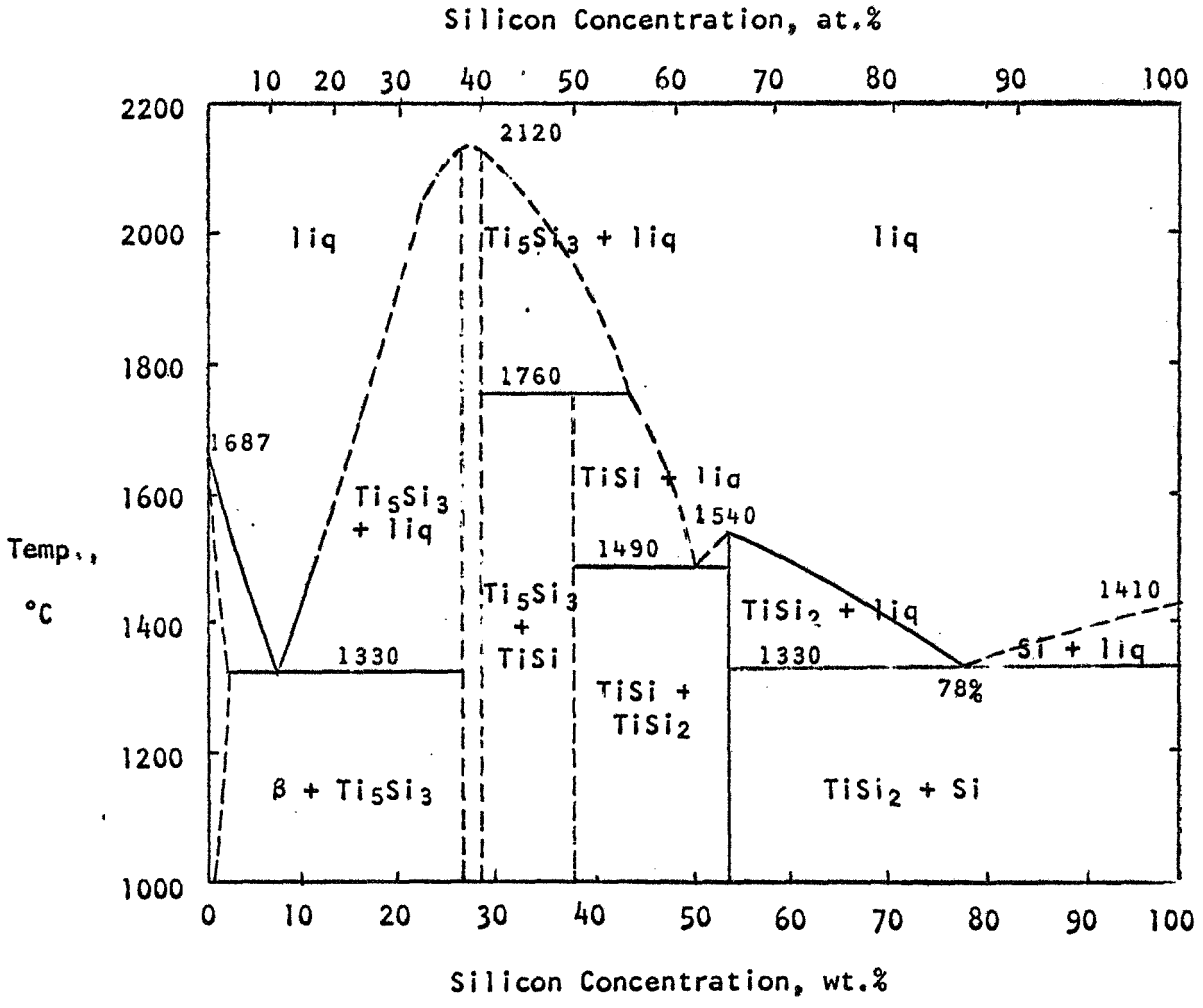

Figure 9 The Titanium - Silicon System (7)

The pressing of one inch diameter wafers directly from the purchased powder proved quite difficult. Pressures of 10-50 tsi were investigated using a hardened steel die. Invariably, the samples cracked on ejection. A number of binders were evaluated using lower pressures. A satisfactory procedure consisted of slurrying the titanium disilicide powder with a sufficient amount of a 5 percent polymethylmethacrylate solution in acetone to give a final dry mixture containing 0.1 percent polymer. After the powder was dried, one inch diameter wafers were pressed at 5-10 tsi. Sample thickness was approximately 0.1 inches.

Densification of the compacted wafer was carried out in two stages. In the presinter, the binder and any residual solvent were removed by heating in vacuum. The pressed wafer was supported on a high density alumina dish which was placed in an impervious silica tube. The tube was evacuated to 10^{-4} Torr and held for 0.5 hours. The temperature was slowly brought up to 900°C over a two-hour period. At the elevated temperature, the polymer "unzips" giving methacrylate monomer which is easily removed at the low pressure. There was no evidence of charring or carburizing of the polymer.

The final sintering was carried out at 1375-1400°C and 5×10^{-5} for 15 minutes.

The faces of the sintered wafers were ground successively on diamond disks of medium, 30 micron and 6 micron coarseness. The ground wafers were then lapped with 6 and then 3 micron diamond paste.

In order to prepare wafers of better quality, two procedures for upgrading the purity of the silicide powder were investigated. The first consisted of reacting the CERAC $TiSi_2$ with a 10 percent NaOH solution. Dilute caustic dissolves the excess silicon but

not the disilicide. The reaction was carried out at 40°C for two minutes. The slurry was immediately centrifuged and the caustic solution discarded. The silicide was then washed several times with water until a solution neutral to pH paper was obtained. The dried silicide powder was ground in a steel die, contacted with a 10 percent HCl solution for two hours to remove iron, centrifuged, washed with water and dried. The powder was sieved with the material passing through the 400 mesh being used for wafer preparation.

In addition to using the CERAC $TiSi_2$, a number of wafers were fabricated from $TiSi_2$ powder prepared by direct reaction of titanium and silicon powder. Titanium powder from CERAC or titanium sponge from United Mineral and Chemical Co. was used in the reaction. The CERAC powder had a purity of 99.6% while the UMC material was 99.9%. The sponge was ground in a hardened steel vial. The -325 mesh portion was obtained from United Mineral and Chemical Co. and had a purity of 99.99%.

The required amounts of each material were weighed out in a plastic vial on an analytical balance. Usually, a slight excess of silicon, 0.1 wt. % was used. The mixed powders were pressed into one inch diameter wafers at pressures of 20-25 tsi. Reaction was carried out in a high density alumina crucible in a vacuum of 10^{-4} Torr.

Reaction began when the sample temperature reached about 900°C. At this point, the heating was discontinued. The reaction, however, is quite exothermic. If the mixture was heated too fast, the reaction temperature quickly exceeded the melting point of the reactants (1350°C) and the resulting molten mass adhered to the alumina crucible. Slow heating gave a controlled reaction with the temperature reaching a maximum of 1000°C. The final product

was a slightly sintered, spongy mass of $TiSi_2$. This was ground and the -400 mesh product used for wafer preparation.

Wafers of TiSi, Ti_5Si_3 and $TaSi_2$ were prepared in a similar fashion.

B. Oxidation Experiments

The oxidation experiments were carried out in vertical tube-type furnaces. The atmosphere in the tube was a mixture of argon and oxygen. The oxygen partial pressures investigated were 0.2, 0.6 and 1.0 using gases purchased directly from Matheson, Inc. The gas was admitted through the bottom of the mullite tube with the rate controlled by a rotameter located at that point.

The samples were supported by a vitreosil holder and suspended from the top of the furnace by a vitreosil rod into the region where the temperature variation was less than $5^{\circ}C$. No reaction was observed between the silicides and the vitreosil holder.

Oxidation rate data were obtained by periodically removing the sample from the oxidation furnace and recording the weight using a microbalance. A precision of ± 5 micrograms was obtained.

C. Analytical Methods

1. Metallography

Photomicrographs of polished and etched silicides and oxide films were prepared with a Leitz model MM5 metallograph. The polished silicides were etched for 15 seconds in a solution consisting of:

5 parts hydrofluoric acid (by volume)
15 parts 5% chromic acid
40 parts 1% potassium permanganate
100 parts water

The samples were observed under both ordinary and polarized light.

The oxide films were etched with "P" etch, a reagent commonly used in the modification of oxide films grown on silicon (58). This etch consists of:

15 parts hydrofluoric acid

10 parts nitric acid

300 parts water

This reagent has been found (58) to etch pure SiO_2 films on silicon at a rate of 2 Å/sec., while impure SiO_2 films etch at a considerably faster rate. A typical example is a phosphosilicate film which etched at 570 Å/sec.

A number of samples were sectioned in order to determine the vertical structure of the growing oxide. -200 mesh alumina powder was added to the usual epoxy resin to prevent rounding of the sample edges during polishing.

2. X-ray Diffraction

X-ray diffraction scans were made on the silicide surface and the oxide film. The diffraction patterns were obtained with a Norelco Geiger counter X-ray spectrometer. CuKα radiation with $\lambda = 1.54050$ was obtained by passing the beam from a copper tube through a nickel filter. The surface of the wafer was scanned by inserting it directly in the sample holder. This non-destructive method allows for many measurements to be made on the same sample. A number of powder patterns were also prepared by grinding the finished wafer.

Several powder patterns were also obtained on the oxide film. In order to remove the oxide, a chlorine etch technique (73) used in studying the oxide formed on silicon was used. The powder patterns yield the same results as the simpler non-destructive method.

A number of mechanical mixtures of SiO_2 and TiO_2 of known concentration were prepared in order to determine the reproducibility of peak positions and intensity in the X-ray method. An approximate calibration curve for the concentration of TiO_2 in 0.5 inch diameter wafers was developed. The minimum amount of TiO_2 which can be detected is approximately 1%.

3. Infrared Spectroscopy

A more detailed analysis of the amorphous region of the oxide film was carried out using infrared spectroscopy. A Perkin-Elmer Micro Specular Reflectance Accessory was used in conjunction with a Perkin-Elmer 621 Spectrophotometer. This provides a 2X absorption spectrum which can be compared with literature data on amorphous silica and glasses.

The infrared analysis of the bulk glasses was carried out using the KBr pellet method. The sample to be analyzed was ground on a Spex Mixer/Mill for about one hour. The powder was collected and 0.4 - 1.4 mg mixed for 30 seconds with 200 mg of KBr on a Spex Mixer. The powder was placed in a standard KBr pellet die, evacuated and pressed for 20 minutes at 20,000 lbs. The KBr pellet was then placed in a holder and inserted directly in the sample beam.

4. Electron Microscopy

A standard replicating technique was used for studying the surface structure of both the $TiSi_2$ and the growing oxide film. A film of nitrocellulose from a 4 percent collodion solution was formed on the sample. The film was separated from the surface by initially forming a square around the desired region with cellophane tape. Breathing on the film supplied moisture which penetrated through the cellulose to the sample surface. The tape

was peeled away, carrying the cellulose replica along. The replica was mounted surface side up on a glass slide. The film was shadowed with chromium or platinum in a vacuum of 10^{-4} Torr. The shadowing angle was varied from 15 to 35°. A thin film of carbon was then deposited, also at 10^{-4} Torr. The specimen was cut with a knife into small squares which were placed on grids, usually copper or nickel (200 mesh). The grids were placed on a piece of filter paper in a flat dish. The filter paper was kept wet with amyl acetate until all the nitrocellulose had dissolved. The carbon replica was then dried.

A Phillips model 300 electron microscope was used in examining the specimens. The carbon replica method provides a resolution of 50 Å.

D. TiO_2-SiO_2 Solid State Reactions

A study was made to confirm the solubility of TiO_2 in SiO_2 and also the glass forming ability of the TiO_2-SiO_2 system as reported by Ricker and Hummel (56). In the solubility study, 0.5 inch diameter wafers were used, while in the glass formation work, the mixed powders were used directly. In both methods, the appropriate amounts of powder were mixed for one hour on a Spex Mixer/Mill. Wafers were prepared by adding polymethylmethacrylate binder to the powder, drying and pressing at 10-15 tsi. The wafers were placed in a silica dish, presintered to remove binder and then heated to the desired temperature in either a Brew furnace at a pressure of 10^{-4} Torr or a Lindbergh furnace at atmospheric pressure.

The pressed samples were placed in the furnace, the system evacuated and the temperature brought slowly to the desired value. Heat-up time was usually 0.5-1.0 hours. After the required time at temperature, the power was shut off and the sample allowed to

cool in vacuum. Cooling time to below red heat was approximately 5 minutes in vacuum. No interaction was observed between the sample and the sample holder when a solid state reaction occurred. When the wafer melted, bonding to the sample holder was observed.

Since the amount of TiO_2 that is formed if $TiSi_2$ was oxidized completely to the oxides is 39.9 percent, concentrations at and below this value were studied.

The wafers were analyzed by X-ray and infrared methods. The X-ray analysis was performed on the wafer while the infrared analysis was carried out on the ground powder using the KBr method.

4.4 Experimental Results

A. Silicon Oxidation

A number of silicon wafers were oxidized to test the oxidation system and the analytical techniques. These wafers were N-type with the 110 face parallel to the surface. The as-purchased lapped wafers were chemically polished in an etch called C.P. 8 consisting of

75 ml. HNO_3

45 ml. HF

45 ml. Acetic acid.

Etching time was 30 seconds. A mirror-like finish was obtained.

Oxidation was carried out at 1000°C in an atmosphere of 0.2 oxygen and 0.8 argon. X-ray analysis after 100 hours at temperature indicates only the silicon substrate. Absorption peaks in the oxide were obtained at 1080, 805 and 460 cm^{-1}. A faint bump on the broad 1080 peak is observed at 1250 cm^{-1}. When using the reflectance unit, a definite absorption is obtained at 1230 cm^{-1}, while reflection peaks are obtained at 1110, 820 and 465 cm^{-1}. These results correspond quite well with those obtained by Pliskin and Lehman (58) and Murray and Goldsmith (59) for an amorphous SiO_2

film thermally grown on silicon.

The infrared spectrum of a sample oxidized at 800°C is similar to that obtained at 1000°C. Since the oxide thickness is considerably lower at this temperature, it would be expected that the Si-O absorption would be shifted to a lower frequency. This is what is observed.

Rate data were obtained for silicon oxidized at 1000°C in an atmosphere with an oxygen partial pressure of 0.20. When the square of the weight gain is plotted against time, a straight line passing through the origin is obtained. The average value of the parabolic rate constant is 1.9×10^{-4} $(mg/cm^2)^2/hr.$ $\pm$ 0.17×10^{-4} $(mg/cm^2)^2/hr.$ Deal and Grove (64) report a value of 1.57×10^{-4} $(mg/cm^2)^2/hr.$ for the parabolic rate constant at 1000°C. This is quite good agreement considering that great care was not taken in preparing the surfaces. These results indicate that the experimental procedure and equipment are suitable for obtaining oxidation rate data for the disilicides.

A few data points were also obtained for silicon oxidized at 800 and 600°C. At 800°C, a weight gain of only 120 μg is observed after 50 hours of oxidation. At this time, the sample exhibits a bright purple interference color. Insufficient data were taken to comment on the oxidation mechanism.

A wafer oxidized at 600°C in an oxygen atmosphere shows a weight gain of only 30 μg after 300 hours. No meaningful rate data could be obtained at this low level. No interference colors are observed with the sample.

B. $TiSi_2$ Oxidation

1. Sample Quality

In order to obtain reliable oxidation rate data, it is necessary that the sample surface be uniformly clean, both chemically

and physically. In a system of the type studied here, it is difficult to prepare wafers that contain only a single compound. As indicated by the phase diagram (Figure 9) there are three compounds in the titanium-silicon system. When preparing either of these materials, a second phase must be present. For example, if a slight excess of silicon is present when preparing wafers of $TiSi_2$, a silicon phase is observed. At the high sintering temperatures used, a loss of one of the elements occurs, in this case silicon. If, therefore, stoichiometric amounts are used, a deficiency of silicon will be observed resulting in the presence of a lower silicide phase.

Since it is also difficult to obtain densities that are equal to the theoretical values using the powder metallurgy technique, physical defects are also to be expected.

Considerable effort was spent developing the technique for preparing the $TiSi_2$ wafers. The method involves sintering the pressed pellet at 1380-1400^{o}C in a vacuum of 5×10^{-5} Torr. Samples made from CERAC $TiSi_2$ have densities of 93-96 percent of theory, as determined by water displacement. When the sample volume is determined by direct measurement with a micrometer, these percentages are lower by 1-2 percent. This difference is probably due to the presence of pores in the sample surface.

As the sintering temperature is decreased below 1380^{o}C, the sample density decreases. At temperatures above 1400^{o}C, the samples warp badly and in some cases adhere to the alumina dish in which they are supported.

Microscopic examination shows a $TiSi_2$ grain size of approximately 50-70 microns. In addition to the $TiSi_2$, there is a second phase which collects at the intersections of silicide grains. X-ray analysis of the surface shows $TiSi_2$ and a small amount of

silicon The silicon is apparently the second phase that is observed. Holes in the sample surface are also seen. These appear to be primarily in the silicon phase and may result from pulling out during polishing. Under polarized light, the $TiSi_2$ grains show up as two distinct shades, possibly indicating two preferred orientations.

The large grain size and apparent preferred orientation result in differences between the observed and ASTM standard X-ray intensities. This is shown by some typical data in Table XVIII. Of greater significance is the fact that the observed angle positions are lower than those given by the ASTM. X-ray patterns obtained with the CERAC powder give similar results. The lower angle indicates that the interatomic lattice distances are larger than those given by the ASTM data. This may be due to silicon interstitially dissolved in $TiSi_2$.

The infrared spectrum of an etched $TiSi_2$ wafer was determined using the microspecular reflectance attachment. An extremely weak absorption was observed at 1040 cm^{-1}. This probably indicates that even after etching an extremely thin film of SiO_2 is present.

The excess silicon (0.68%) was removed from the CERAC $TiSi_2$ powder by treating with a 10% NaOH solution at 40°C. The silicon phase observed with the unwashed CERAC $TiSi_2$ disappears while another smaller, more circular phase forms. X-ray analysis shows only $TiSi_2$, no silicon or lower titanium silicides are indicated. In several samples, Ti_5Si_3 was indicated. The interatomic distances for the $TiSi_2$ were again greater than the ASTM values. They were, however, not as great as those observed with the unwashed CERAC $TiSi_2$. This is consistent with the idea of interstitial silicon since the caustic wash would be expected not only to remove the silicon as a separate phase, but also to some extent remove some of the dissolved silicon.

Table XVIII

Comparison of Observed and ASTM X-ray Data for $TiSi_2$

Experimental		ASTM		
2θ	I/I_1	2θ	I/I_1	Identification (hkl)
23.85	5	-	-	*
28.45	100	28.42	100	Si(111)
30.02	5	-	-	*
39.12	100	39.30	100	$TiSi_2$(311)
42.30	3	42.40	70	$TiSi_2$(004)
43.23	53	43.46	90	$TiSi_2$(022)
47.35	75	47.30	60	Si(220)
49.78	67	50.08	90	$TiSi_2$(313)
68.70	11	69.00	70	$TiSi_2$(331)
71.96	13	72.02	90	$TiSi_2$(602)

*These two peaks were found in all the $TiSi_2$ wafers prepared.

Higher magnification shows another phase between the disilicide and the second phase. If the second phase is Ti_5Si_3, the small intermediate layer would logically be TiSi. There are fewer and smaller holes in these specimens than in those made with the unwashed CERAC $TiSi_2$.

Samples prepared from NaOH-washed CERAC $TiSi_2$ had densities, as determined by water displacement, of 95-98 percent of the theoretical values. Densities obtained by direct measurement with a micrometer were lower, but not as much as with wafers made from the unwashed CERAC $TiSi_2$.

Samples were also prepared from $TiSi_2$ made by direct reaction of titanium and silicon. To the unaided eye, these appear similar to the samples made from caustic-washed CERAC $TiSi_2$. In many samples, there appears to be a second phase which is similar to that observed with the CERAC $TiSi_2$ where excess silicon is present. X-ray analysis, however, shows only $TiSi_2$. The amount of the second phase is considerably lower than that in the unwashed CERAC samples and, as such, it is possible that the X-ray method is not sufficiently sensitive. As in earlier samples, the holes appear to be in either this second phase or at the junction of three grains.

2. Character of the Oxide Film

Wafers of $TiSi_2$ were oxidized at 300-1350°C in oxygen-argon atmospheres where the oxygen partial pressure was varied from 0.2 to 1.0. Below 300°C, negligible oxidation occurs.

At 300°C, where the weight gain is almost negligible, no visible continuous oxide is observed. A few, very small, multicolored crystalline areas are present on the sample surface when viewed at a magnification of 400X. X-ray analysis shows only the $TiSi_2$ substrate which does not change during the course of oxidation.

Under polarized light, the entire field is dark. The few crystalline-appearing areas observed may be due to oxides of impurities in the silicide.

At 600°C and an oxygen partial pressure of 0.2, a multicolored, transparent oxide film is formed. In the initial stage of oxidation, there are usually two or three interference colors that are observed from the oxide when viewed by the unaided eye. On microscopic examination within each color region, it is found that this overall color is a blend of several color areas. Each of these color areas corresponds roughly in size and shape to the $TiSi_2$ grain structure. When a separate silicon phase is present in the substrate, the oxide formed on that phase exhibits a different interference color. This color is usually the same on all silicon areas through the sample.

As the time of oxidation increases, the colors observed on the $TiSi_2$ grains show gradual changes. The color displayed by the oxide on the silicon phase remains a light tan to pale brown throughout the course of a run. Based on interference charts developed for the oxide formed on silicon (74), the light tan color indicates an oxide film thickness ot about 500 Å.

Examination of the oxide film with a light microscope reveals no crystalline regions after 300 hours of oxidation. X-ray analysis indicates only the $TiSi_2$ substrate with interatomic distances that are constant through the oxidation period. Observation under polarized light shows lighter colored areas within the holes in the sample surface.

At 800 hours of oxidation, microscopic examination indicates a number of small, yellow crystalline islands. These are found near the holes originally observed in the $TiSi_2$ surface. X-ray analysis indicates only $TiSi_2$.

Electron micrographs of the oxide formed on $TiSi_2$ during oxidation at 600°C show no observable difference between the oxide growing on the silicon phase and on that growing on the $TiSi_2$ phase. Of particular significance is the lack of amorphous phase separation or crystallization in the oxide on the $TiSi_2$.

At 800°C, a significant change occurs in the structure of the growing oxide film. In the initial stage of oxidation, metallographic and X-ray examination indicate an amorphous film similar to that obtained at 600°C. The interference color is more uniform over the surface compared to 600°C where the thickness varies with grain orientation. After three hours, however, small clumps of crystalline TiO_2 are observed. These clumps are approximately 50 microns in diameter. X-ray diffraction studies show that the TiO_2 is in the rutile form. The crystalline areas are generally found at the phase boundary of the silicon and $TiSi_2$ phases. This is also the region where most of the holes in the surface are observed. As the reaction time increases, more clumps are observed while those formed earlier increase slightly in diameter. Also of interest is the fact that TiO_2 grows up and out of the amorphous silica film. This is easily observed with a light microscope at 400X magnification. Under polarized light, the crystalline areas appear bright yellow, while the surrounding amorphous region is dark.

At 1000°C, the oxide film is similar to that obtained at 800°C. X-ray and metallographic studies indicate an amorphous matrix with crystalline islands of TiO_2 (rutile). The crystallization occurs after about one hour at reaction temperature compared to the three to seven hours observed at 800°C. With wafers made from "homemade" $TiSi_2$, the observable crystallization occurred at a longer time, approximately ten hours. In these samples, there

is a negligible silicon phase. Most of the crystallization occurs at the silicide grain boundaries. The TiO_2 clumps are more numerous and larger in size than those formed at 800°C for comparable oxidation times.

At 1200°C, the characteristic amorphous silica film with crystalline TiO_2 (rutile) islands growing out and above the silica is observed. Crystallization of the TiO_2 occurs within 0.5 hours at temperature. These TiO_2 islands also grow laterally and vertically with time. X-ray analysis indicates that α-cristobalite is also present at 0.5 hours. Many small multi-colored crystalline-like areas also appear in the film after about 30 hours. This is probably the α-cristobalite observed in the X-ray.

In order to characterize the amorphous region of the oxide film, the infrared spectra of a number of samples were obtained. Some typical results are shown in Figure 10 and summarized in Table XIX. More detailed data are given in reference 75. The results shown in Figure 10 and Table XIX were obtained at extended oxidation times where the positions of the absorption maxima have stabilized.

The infrared spectrum of the oxide formed at 300°C is indicated in Figure 10(a). This result was obtained using 5X ordinate expansion. As indicated, there is faint evidence of a very thin silica film. Little can be deduced about the structure from the broad, low intensity absorptions.

The spectrum obtained at 600°C is given in Figure 10(b). The absorption peak normally observed at 1250 cm^{-1} has shifted to 1150 cm^{-1} and has become quite broad. The Si-O vibration at 1100 cm^{-1} has moved to 1040 cm^{-1} while the Si-O-Si bond bending at 460 cm^{-1} has shifted to 435 cm^{-1}. These shifts to lower frequencies are indicative of low density or impurities in the film.

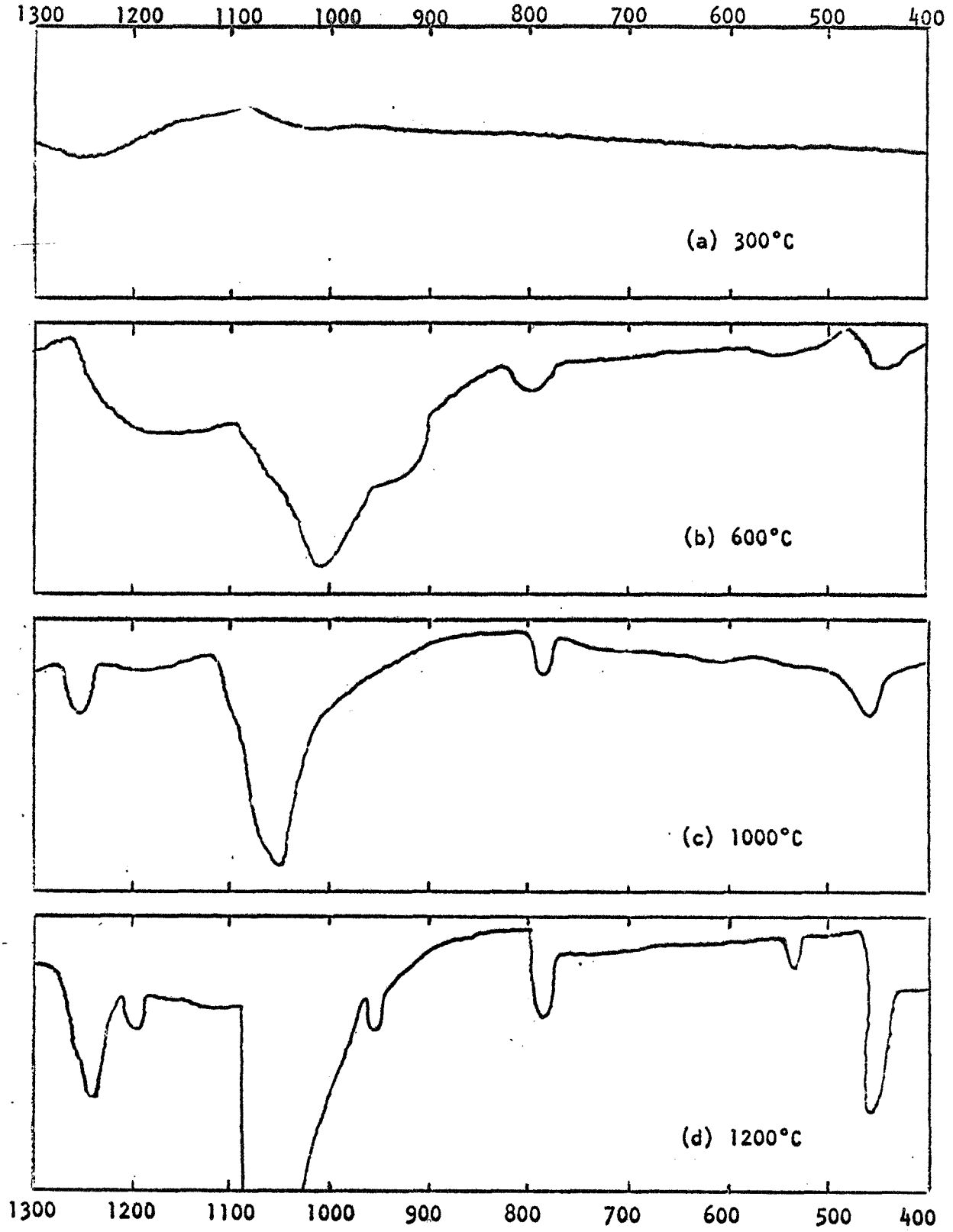

Figure 10. Infrared Spectra of Oxide Grown on $TiSi_2$ at 300-1200°C

Table XIX

Summary of the Infrared Results of the Oxide on $TiSi_2$ Oxidized at 300 - 1200°C

Oxidation Temp., °C	Absorption Maxima, cm^{-1}						
300	1250(VW)	-	1040(VW)	-	-	-	-
600	1200(B)	-	1040	930(B)	800	-	440
800	1255	-	1060	-	780	-	X
1000	1254	-	1065	-	780	-	X
1200	1254	(1195)	1058	950	785	535	465
Amorphous SiO_2 Film(23)	-	-	1100	-	800	-	465

(VW) - Very weak

(B) - Broad peak

X - Region not investigated

The broadness of the peaks also indicates considerable variation in the bonds.

In addition to the shifts in the normal silica vibrations, a significant broad absorption is observed at 930 cm^{-1}. Bulk TiO_2-SiO_2 studies indicate that this is due to a Ti-O-Si vibration. The strength of this peak indicates a considerable amount of this structure. As at 300°C, it was necessary to use 5X ordinate expansion to locate the position of the maximum absorption.

The infrared spectrum was recorded during the course of a 187 hour oxidation run at 600°C. The spectra at 54 and 187 hours of oxidation appear to be identical except for the 940 cm^{-1} absorption which is slightly stronger at the longer time. This indicates that the character of the oxide is not undergoing any appreciable change during this oxidation period.

At 800 and 1000°C, the spectrum is that of silica with the major Si-O vibration at 1060 cm^{-1}. No absorption is observed at 930 cm^{-1}. The increase in frequency from 1040 to 1060 cm^{-1} when the temperature is increased from 600 to 800°C indicates a more dense or higher purity silica film at the higher temperature. The absorption maxima for high purity SiO_2 on silicon is 1090-1100 cm^{-1} (58). The amorphous silica matrix formed at 1000°C on $TiSi_2$ then is not as pure or dense as that formed on silicon when it is oxidized. The lack of an absorption at 930 cm^{-1} indicates a lack of Ti-O-Si bonding in the amorphous region. This is not surprising since TiO_2 has crystallized into small clumps.

The shift in the position of the absorption maxima and the appearance of a new peak are well known in the study of bulk glasses. Simon and McMahon (76) indicated a shift to a lower frequency of the 1100 cm^{-1} Si-O vibration and also the formation of a new peak at 930 cm^{-1} as Na_2O was added to SiO_2.

The spectrum at 1200°C, Figure 10(d), shows silica with additional vibrations at 1190, 950 and 535 cm^{-1}. The 1195 and 950 cm^{-1} peaks appear to be related to the major vibrations at 1245 and 1058 cm^{-1} respectively. The peaks are very much sharper than at lower temperatures indicating a more ordered structure. These three peaks may be additional Si-O stretching modes resulting from the more ordered structure. The fact that the major Si-O vibration is found at 1060 cm^{-1}, which is 40 cm^{-1} less than where pure SiO_2 would be observed, indicates that while the structure is becoming more ordered, the impurity in the network is still present.

The infrared spectra in the initial oxidation period are different from that observed at longer times. This is indicated by the data in Table XX. Up to four hours of oxidation at 1000°C, only the 1250 and 1050 cm^{-1} vibrations are observed. The position of the 1250 cm^{-1} peak is fairly constant during this initial period, while the Si-O stretching frequency increases from 1000 cm^{-1} at 0.5 hours to 1035 at four hours. In each spectrum, a weak absorption is also observed at 900-950 cm^{-1}. For reaction times greater than about 10 hours, the positions of the absorption maxima appear to be relatively stable.

Murray and Goldsmith (59) and Sato and Shibata (60) indicate an increase in the position of the reflection maxima of the Si-O vibration of 50 cm^{-1} when the SiO_2 thickness on silicon is increased from 0.1 to 1.0 microns. This shift has been attributed (60) to the presence of free silicon bonds in the silica as the oxide-air interface is approached. The shift could also be due to an increase in oxide density as the structure assumes its more stable form.

3. Rate Data

The variables that were considered in the rate study were:

Table XX

Effect of Oxidation Time at 1000°C on
Infrared Absorption Maxima Positions

Spectrum	Run	Oxidation Time, Hrs	Wt. Gain, mg/cm^2	Absorption Maxima, cm^{-1}			
25	8	0.5	0.0722	1255	1000		
26	8	1.0	0.1045	1252	1020		
27	8	2.25	0.1455	1250	1030		
30	75	1.0	0.0140	1250	1020		
31	75	4	0.0258	1255	1035		
32	75	100.5	0.123	1255	1050	780	460

surface quality, gas flow rate, temperature and oxygen partial pressure. The quality of the surface was considered qualitatively while the other variables could be investigated quantitatively.

In the initial phase of the study, the effect of gas flow rate was considered. Several wafers of $TiSi_2$ were oxidized at 600 - 1000°C in an atmosphere with an oxygen partial pressure of 0.20. The gas flow rate was varied from 0 to 200 cc/min. Within experimental error, no effect is observed with changing gas rates. These results indicate that mass-transfer through the gas phase is rapid compared to the other steps in the reaction. This same result was obtained by Deal and Grove (64) in their studies of the oxidation of silicon. Since most of the later experiments were carried out at conditions where the oxidation rate would be lower, the effect of gas flow rate could readily be neglected. In all the later studies, the gas flow rate was fixed at 200 cc/min. in order to insure a uniform gas composition in the reactor.

A single sample of $TiSi_2$ prepared from CERAC powder was oxidized at 300°C in order to establish the lower level of observable oxidation. After 20 hours at temperature, a total weight gain of 25 μg is observed. After 320 hours, the weight gain increased to 112 μg. A summary of the data obtained at 300°C is shown by the lower curve in Figure 14.

Based on the analysis of the oxide film described earlier, there appear to be two reactions occurring at 300°C. One is the formation of a very thin amorphous SiO_2 film and the other a localized reaction, possibly of impurities. Assuming an oxide density of 2.2 gms/cm^3, the observed weight gain corresponds to a film 1270 Å thick. Since TiO_2 may be dissolved in the film, the density could be considerably greater. The observed interference color indicates a film less than 500 Å thick if the color charts

developed for silicon oxidation are used (74). If TiO_2 were dissolved in the film, the refractive index would be greater and the film would be thinner than what is indicated by the color charts.

These results indicate that the weight gain due to the point reaction is significant. Since the weight gain associated with this reaction cannot be determined, it is not possible to make a quantitative evaluation of the thin film formation.

Since the sample quality was not good enough, no further studies were made to evaluate the mechanism at 300°C.

Typical weight gain data for $TiSi_2$ oxidized at 600°C are shown in Figure 11. The most noticeable characteristic of the data at this temperature is the sharp break in the curve at about 9 hours. The value of n in the expression $X^n = kt$ for times less than 9 hours is 2-3, while after the break, values of 8-10 are observed.

When these data are replotted as the square of the weight gain versus time, the curves shown in Figure 12 are obtained. If this were a simple diffusion controlled process, a straight line would have been obtained. While this is not the case, the slope does appear to be approaching a constant value. If it is assumed that the slope is constant after 150 hours, a parabolic rate constant equal to 85×10^{-7} $(mg/cm^2)^2/hr$ is obtained.

At 600°C, the oxygen partial pressure was varied from 0.2 to 1.0 atmospheres. Within experimental error, no effect is observed when the oxygen pressure is varied in this range.

The type of powder used, whether CERAC $TiSi_2$, NaOH-washed $TiSi_2$ or homemade $TiSi_2$ does not appear to affect the rate. In addition, varying the sample density of CERAC $TiSi_2$ wafers from 91.5 to 95.2 percent of the theoretical density does not affect

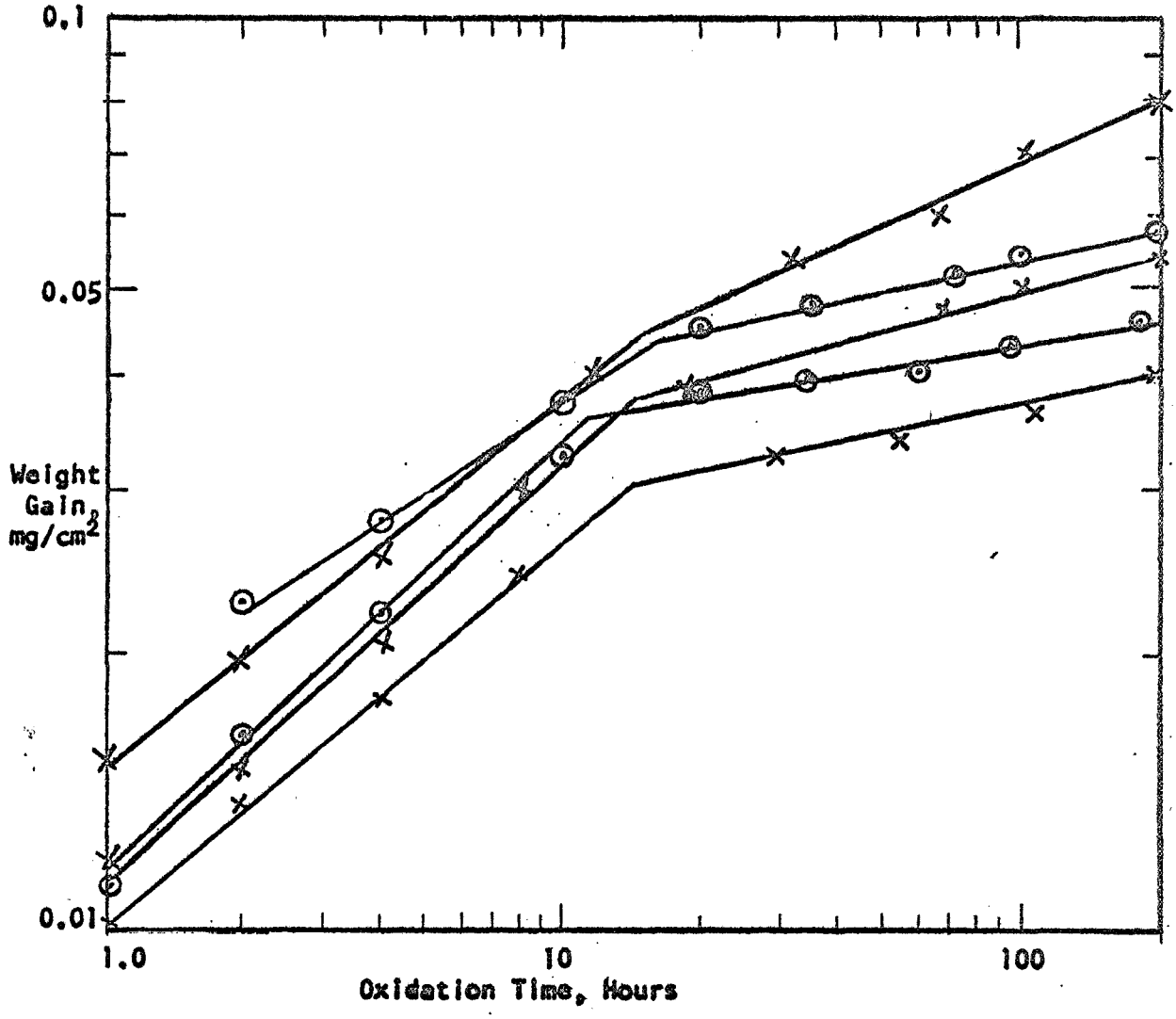

Figure 11. Weight Gain Data for $TiSi_2$ Oxidized at 600°C

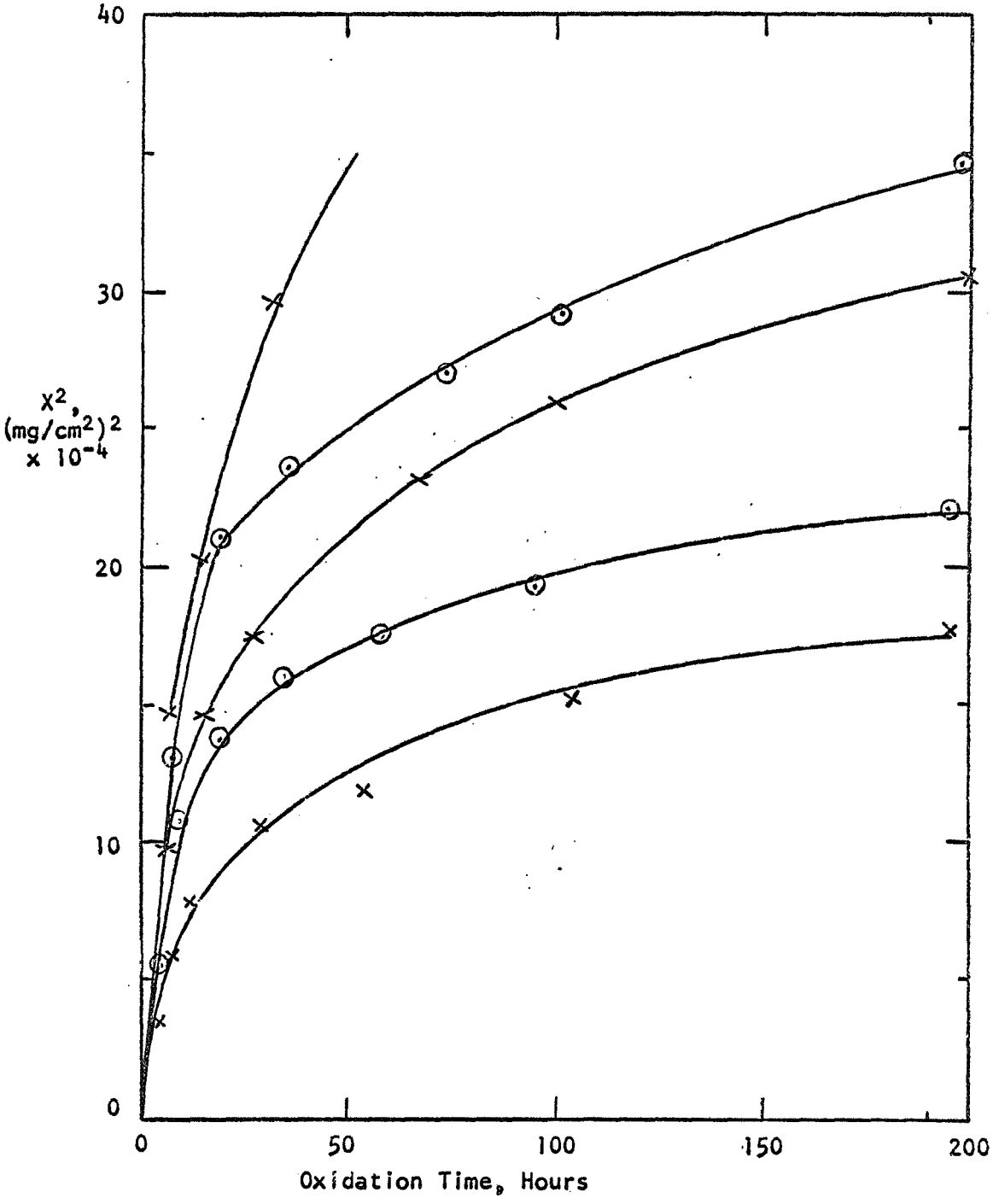

Figure 12. X^2 versus t for $TiSi_2$ Oxidized at 600°C

the rate of oxidation. While no effect was observed due to preparation methods, the variation in weight gain shown in Figure 11 is probably due to differences in surface quality.

At 800°C, results similar to those obtained at 600°C are observed. In this case, the break in weight gain curve occurs at about 6 hours compared to the 9 hours obtained at 600°C. Within experimental error, the magnitude of the observed weight gain for the first 50 hours is the same as that observed at 600°C. Beyond 50 hours, the weight gain at 800°C becomes greater.

Data at 800°C show similar behavior to those obtained at 600°C (75). No straight line regions are observed. If a straight line is assumed after 100 hours, a parabolic rate constant equal to 0.26×10^{-4} $(mg/cm^2)^2/hr$ is obtained. No change in rate is observed when the oxygen pressure is changed from 0.2 to 1.0.

As indicated earlier, the surface quality depends on the history of the $TiSi_2$ powder and its subsequent treatment. When oxidized at 1000°C, a significant difference in rate is observed depending on the powder used in the sample preparation.

Samples prepared with either CERAC $TiSi_2$ or Na-OH-washed CERAC powder gives similar rate data. Both sample types give higher weight gains due to imperfections in the surface. In the case of the samples prepared from NaOh-washed CERAC powder, there is a small amount of a second phase, Ti_5Si_3. This lower silicide oxidizes at a much faster rate than does $TiSi_2$. The samples prepared from unwashed CERAC powder have a greater number of holes. Oxidation would be expected to occur at a faster rate at these high energy sites. The presence of small amounts of Ti_5Si_3 appears to have an effect similar to the holes, i.e., to increase the crystallization of TiO_2 resulting in larger local weight gains. As indicated earlier, the amorphous region over the $TiSi_2$ in either sample is the same.

The average result obtained at 1000°C with wafers made from homemade $TiSi_2$ show an interesting contrast. In some cases, no difference in rate can be observed between these samples and samples made from the CERAC powder. In a few runs, lower initial weight gains and definite parabolic behavior in the entire region are indicated. This result is shown in Figure 13 where X^2 is plotted against t. In each case, extrapolation through the origin is observed. A summary of the rate constants obtained is given in Table XXI. A value of 3.52×10^{-4} $(mg/cm^2)^2/hr$ is obtained from the slope for the parabolic rate constant.

When the oxygen pressure is increased from 0.2 to 1.0, there is an increase in the oxidation rate. Parabolic behavior with a rate constant equal to 4.06×10^{-4} $(mg/cm^2)^2/hr$ is obtained. The samples for which these results were obtained appear to have better surfaces, i.e., fewer holes and no lower silicides.

The oxidation rate data at 1000°C obtained with samples prepared from either unwashed CERAC powder or NaOH-washed CERAC powder showed two major differences when compared to the homemade $TiSi_2$ data. As at 600 and 800°C, a break is observed when the log of the weight gain is plotted against the log of the time. At 1000°C, however, the break observed at 1 - 3 hours compared to 6 hours at 800°C and 9 hours at 600°C.

When the 1000°C data is plotted as X^2 versus t, a straight line is obtained for times greater than 5 hours. At times less than 5 hours, the values of X^2 are considerably below the straight line. In addition, the lines do not extrapolate through the origin, rather through positive values on the ordinate.

Also of significance is the total weight gain of the CERAC samples compared to the homemade. Higher weight gains are observed for samples made from the CERAC powder.

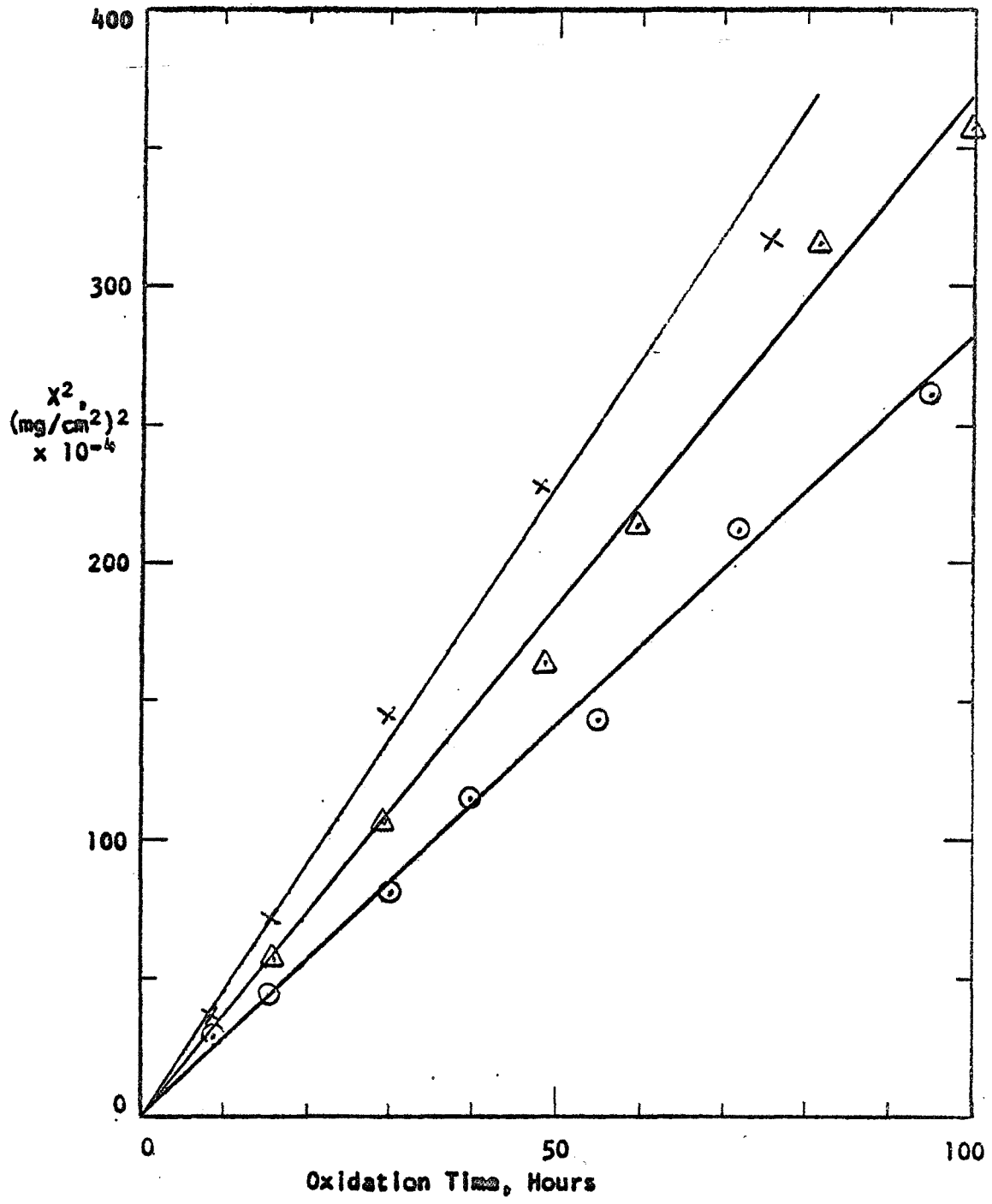

Figure 13. X^2 versus t for $TiSi_2$ Oxidized at 1000°C

Table XXI

Parabolic Rate Constants Obtained by Oxidizing Homemade $TiSi_2$ at 1000°C

Run Number	$kp, (mg/cm^2)^2/hr$	Standard Deviation
75	4.57×10^{-4}	0.09×10^{-4}
78	2.80×10^{-4}	0.04×10^{-4}
80	3.11×10^{-4}	0.03×10^{-4}
81	3.60×10^{-4}	0.05×10^{-4}

Average value of kp = 3.52×10^{-4} $(mg/cm^2)^2/hr$

Average deviation within runs = 0.05×10^{-4} $(mg/cm^2)^2/hr$

Standard deviation between runs = 0.77×10^{-4} $(mg/cm^2)^2/hr$

The kinetic data obtained at 1200 and 1300°C are similar to those obtained at 1000°C. Using wafers made from either untreated or NaOH-washed CERAC $TiSi_2$ gives a parabolic expression of the form $X^2 = kt + c$, where c is a positive number. When homemade $TiSi_2$ is used, parabolic behavior with $c = 0$ is observed. The average value for kp is 8.72×10^{-4} $(mg/cm^2)^2/hr$ with a standard deviation of 1.48×10^{-4} $(mg/cm^2)^2/hr$.

When the oxygen partial pressure is increased to 1.0 at 1200°C, the average value of kp obtained is 10.03×10^{-4} $(mg/cm^2)^2/hr$ with a standard deviation of 0.94×10^{-4} $(mg/cm^2)^2 hr$. This result indicates that there is a slight increase in the parabolic rate constant as the oxygen pressure is increased from 0.2 to 1.0 atmospheres. Data obtained with the CERAC $TiSi_2$ also show a slight increase in the oxidation rate when the oxygen pressure is increased from 0.2 to 1.0.

At 1300°C and an oxygen partial pressure of 0.2 atm., a value of 17.4×10^{-4} $(mg/cm^2)^2/hr$ is obtained for the parabolic rate constant. Only two short runs were made at this temperature since the vitreosil sample holder started to devitrify.

A summary of what appears to be the best rate data for the oxidation of $TiSi_2$ is shown in Figure 14. At temperatures of 600 and 800°C, the data are for all samples investigated. At 1000 - 1300°C, the results are given for samples made from homemade $TiSi_2$ powder.

An Arrhenius plot of the data at 1000 - 1300°C is shown in Figure 15. A straight line is obtained. The activation energy calculated from the slope is 21.3 kcal.

C. Other Silicides Studied

1. TiSi

In the titanium-silicon phase diagram shown earlier, there are

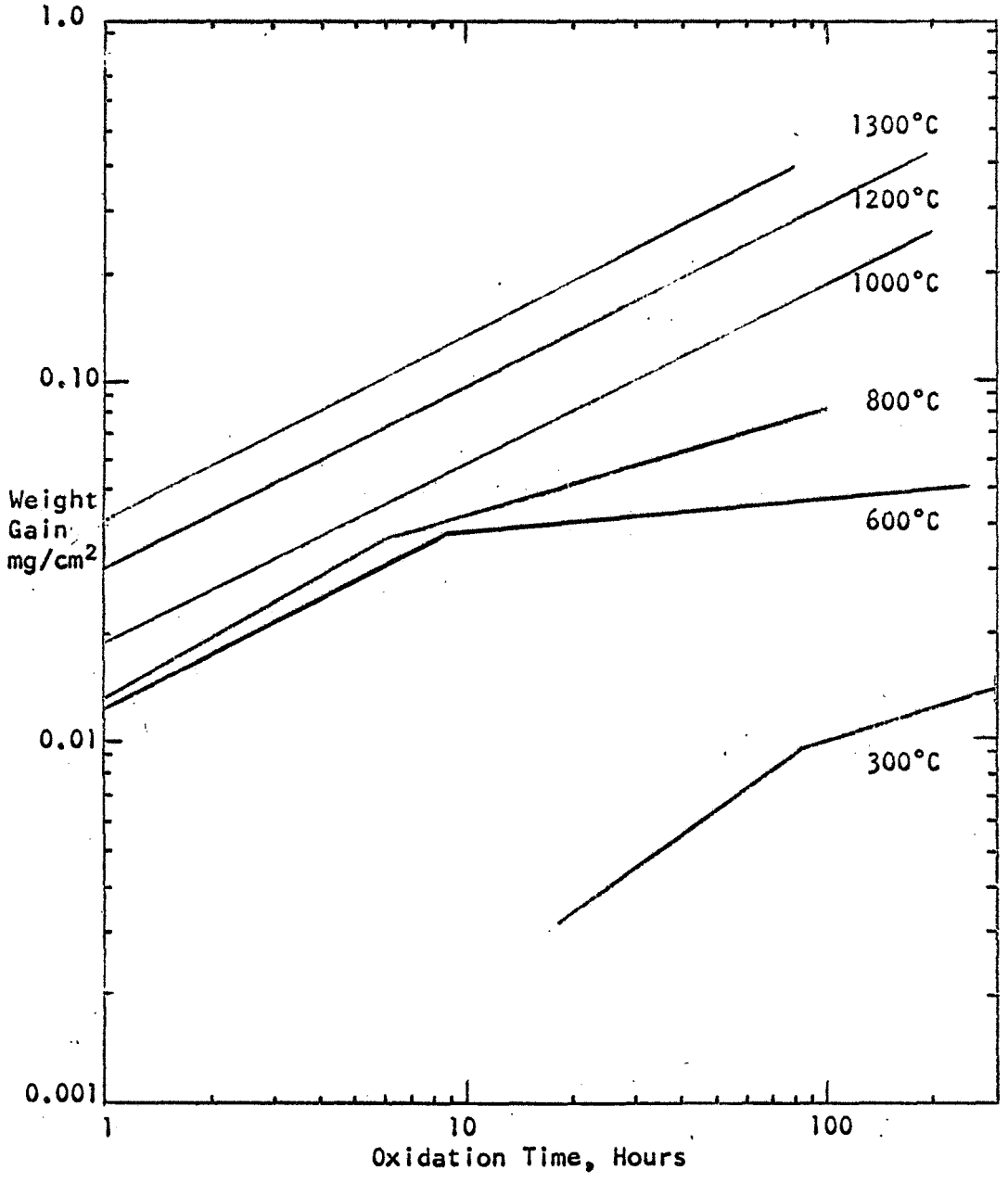

Figure 14. Summary of $TiSi_2$ Oxidation Rate Data: 300-1300°C

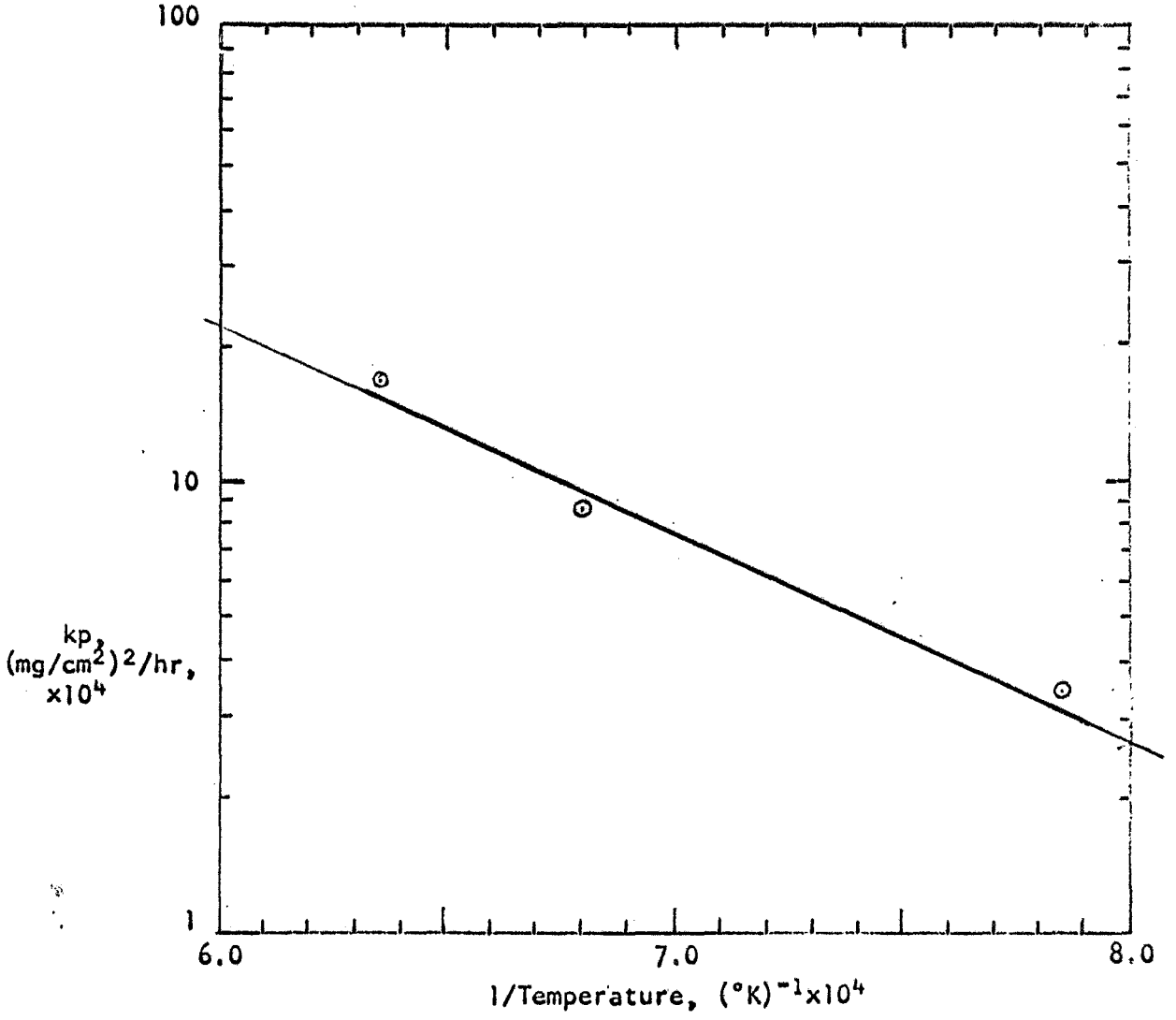

Figure 15. Arrhenius Plot of $TiSi_2$ Oxidation Data

two compounds in addition to $TiSi_2$. These are TiSi and Ti_5Si_3. Wafers of these lower silicides were prepared using the same technique that was used in preparing the disilicide.

Since TiSi is not commercially available, it was prepared by direct reaction of titanium and silicon at 1075°C and 10^{-4} Torr. A silicon excess of 0.5% of the stoichiometric value was used. The reaction product was ground, mixed with binder and pressed into 1 inch diameter disks. Sintering was achieved at 1350°C and 10^{-4} Torr.

Samples fabricated in this way have densities, as determined by water displacement of 90-97 percent of theoretical values. As is the case for $TiSi_2$, the density by direct measurement is 2 to 3 percent lower. The polished surfaces appear mirror-like.

Micrographs show considerable variation in surface quality. In addition to holes, there is also a fair amount of a second phase. X-ray analysis indicates TiSi with a small amount of $TiSi_2$. Since it is not possible to prepare a sample of TiSi alone, it is desirable to have $TiSi_2$ as the second phase rather than Ti_5Si_3. If TiSi forms a protective silica film on oxidation, $TiSi_2$, since it contains more silicon, would also form one, while Ti_5Si_3 would be more likely to form a titania rich oxide which might disrupt the silica film.

The X-ray diffraction results show that the interatomic spacings in the TiSi are greater than those reported in the ASTM data file. This is indicated by the data in Table XXII. Since these compounds probably exist over a range of compositions around TiSi, variation in the line positions is not unexpected.

Samples were oxidized at 1000°C in an atmosphere with an oxygen partial pressure of 0.2. The character of the growing oxide film was highly dependent on the composition and density of the

Table XXII

Comparison of Observed and ASTM X-ray Data for TiSi

Experimental		ASTM		
2θ	I/I_1	2θ	I/I_1	Identification(hkl)
23.85	50	-	-	*
30.05	50	-	-	*
33.41	66	33.66	70	TiSi
37.15	100	37.29	100	TiSi
38.56	93	38.85	70	TiSi
39.15	100	39.30	100	$TiSi_2$(311)
41.29	113	41.54	80	TiSi
42.35	150	42.40	70	$TiSi_2$(004)
42.98	250	43.46	90	$TiSi_2$(022)
45.35	20	45.72	60	TiSi
46.20	80	46.53	80	TiSi
50.12	47	50.52	80	TiSi
59.51	13	59.94	70	TiSi
64.65	13	65.28	80	TiSi
69.95	13	70.24	70	TiSi

*These peaks found in all $TiSi_2$ samples.

sample. A sample which had a density of 96 percent of theoretical value showed three distinct oxide regions on the surface during the initial oxidation period.

In the area of a hole, a large clump of yellow crystalline material forms after 15 minutes at temperature. On the $TiSi_2$ phase, a transparent vitreous film is observed. The TiSi region is covered with a film which appears transparent but does not show the bright interference colors observed with $TiSi_2$. Colors are observed; however, they are quite dull. X-ray analysis of the surface shows strong TiO_2 lines, TiSi and a small amount of $TiSi_2$.

As the time of oxidation increases, the color of the transparent region changes corresponding to changes in thickness. The number and size of the yellow crystalline islands increase with reaction time. After 100 hours, the sample is covered with an opaque, adherent, pale yellow oxide. On microscopic examination, there are bright yellow crystalline islands amidst the paler yellow matrix. These areas appear to correspond to the holes observed in the unoxidized sample. The pale yellow matrix also appears to be crystalline. X-ray analysis shows strong TiO_2 and weak TiSi peaks.

When a sample of lower density, 90% of theory, is oxidized, the surface is covered with the yellow crystalline oxide after about five hours. In the initial stage of oxidation, approximately 0.1 hours, a transparent, purple film is formed. As the time increases, the yellow crystalline areas form and increase in size. At 0.1 hour, TiO_2 is strongly observed in the X-ray pattern.

The infrared spectrum of the growing oxide was obtained at 0.2, 0.5, 1.0, 2.25 and 4.0 hours of oxidation. Using 5X ordinate expansion, the characteristic peaks of amorphous SiO_2 are observed at each time. The peaks are shifted however, to lower frequencies.

The absorption normally observed at 1250 cm^{-1} is shifted to 1180 cm^{-1} and that normally found at 1100 cm^{-1} is found at 1050 cm^{-1}. No absorption is observed at 800 cm^{-1}. The lower frequency of the Si-O absorption indicates a less dense, or more impure, SiO_2 film. The lack of Si-Si vibration at 800 cm^{-1} lends support to this conclusion. A broad absorption is also observed at 950 cm^{-1}. A small peak at 670 cm^{-1}, characteristic of TiO_2, is also obtained. The position of all the peaks remains fairly constant as the oxidation time is varied up to four hours. Beyond this time, a spectrum cannot be obtained as the film is opaque and rough, apparently giving rise to diffuse reflection which is not picked up by the detector.

Several significant observations can be made from these data. The most important is that TiSi forms a protective oxide layer at a temperature of 1000°C and an oxygen partial pressure of 0.20. The crystallization and growth rate of the TiO_2 is strongly dependent on the number of holes in the sample surface. No crystalline forms of SiO_2 are observed in the X-ray diffraction patterns even after 100 hours of oxidation.

The initial amorphous SiO_2 part of the film is quite impure and of low density. Apparently the SiO_2 remains amorphous but is surrounded by so much crystalline TiO_2 that is cannot be observed in the infrared after four hours. The presence of the absorption at 950 cm^{-1} indicates considerable Ti-O-Si bonding in the amorphous region.

The observed weight gain for the TiSi wafers is also strongly dependent on surface quality. The data indicated in Figure 16, by the upper curve, is for the low density sample, while the lower curve is for the high density sample. When the square of the weight gain is plotted against oxidation time, a straight line can be drawn.

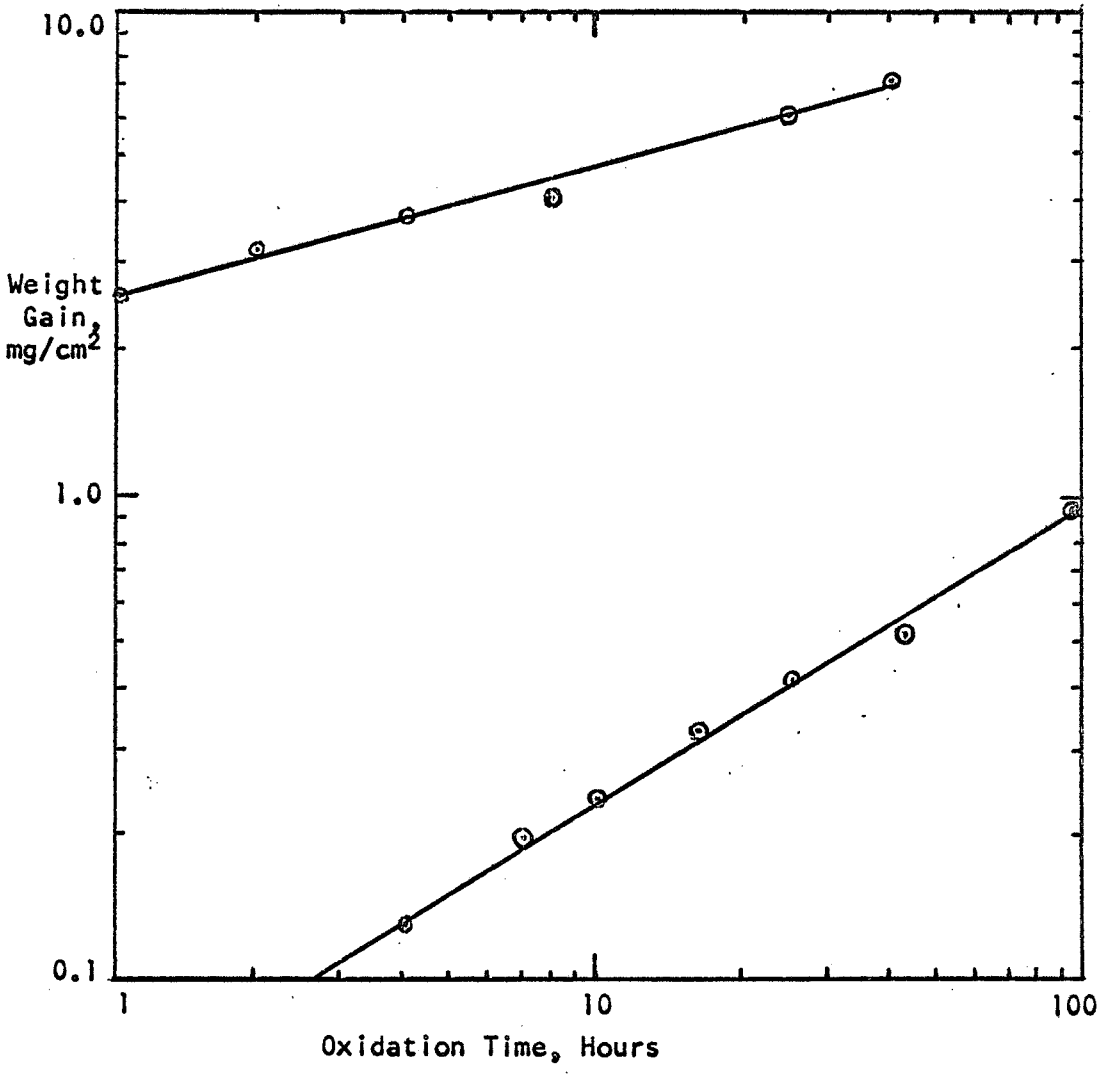

Figure 16. Oxidation Weight Gain Data for TiSi

The equations for the two runs are:

Sample with many holes: $X^2 = 0.10t + 0.80$

Sample with few holes: $X^2 = 0.0088t - 0.480$

The presence of a greater number of holes in the surface causes an increase in the rate constant by a factor of 10.

2. Ti_5Si_3

Ti_5Si_3 is commercially available from CERAC Inc. The technique used in preparing the disilicide proved to be unsuccessful for the Ti_5Si_3. With a sintering temperature as high as 1700°C for 15 minutes, wafers of low density ($\sim$75 percent of theory) are obtained. The addition of 0.5 percent titanium as a sintering aid does not result in any improvement of the density. When titanium is added, a layer of yellow TiO is formed on the bottom of the sample surface.

In order to get samples of reasonably high density, it was necessary to prepare Ti_5Si_3 directly from the elements. Titanium and silicon are reacted at 950-1100°C in a vacuum of 10^{-4} Torr. A vigorous exothermic reaction occurs. Heating is stopped when the temperature of the reactants reaches 950°C. Within a minute, the temperature climbs to 1100°C. The spongy product is ground, mixed with binder, compacted and sintered. Successful sintering of the pressed wafers is achieved at 1700°C. Sample density as determined by water displacement is 90 percent of theoretical. The polished surface appears mirror-like.

Microscopic examination shows more holes in these samples than in either the TiSi or $TiSi_2$. In addition, there are considerable microcracks in the surface. Only one phase can be observed in the hole-free region. X-ray analysis indicates Ti_5Si_3. Typical data are shown in Table XXIII. The peak positions vary slightly from

Table XXIII

Comparison of Observed and ASTM X-ray Data for Ti_5Si_3

Experimental		ASTM		Identification (hkl)
2θ	I/I_1	2θ	I/I_1	
27.71	6	27.68	7	Ti_5Si_3(200)
35.00	17	35.04	14	Ti_5Si_3(002)
37.12	39	37.24	47	Ti_5Si_3(210)
37.71	25	37.68	30	Ti_5Si_3(102)
41.06	100	41.02	100	Ti_5Si_3(211)
42.13	39	42.08	38	Ti_5Si_3(300)
42.80	93	42.76	98	Ti_5Si_3(112)
61.55	11	61.52	18	Ti_5Si_3(222)
66.81	18	66.76	29	Ti_5Si_3(213)
68.79	4	68.76	12	Ti_5Si_3(402)

the ASTM values while the intensities are almost identical. This is probably due to the fact that the Ti_5Si_3 grain size is quite small. For the larger grained $TiSi_2$, the orientation of the sample with respect to the beam changes in the reflected intensities.

Two wafers were oxidized at 1000°C in an oxygen-argon atmosphere with an oxygen partial pressure of 0.20. After about 0.5 hours at temperature, the sample is almost entirely covered with an opaque, yellow oxide. Microscopically, there are small areas where a transparent oxide film is present. X-ray analysis on the surface shows the Ti_5Si_3 substrate and the major TiO_2 (rutile) peak at $2\theta = 27.46^{\circ}$. This peak is due to constructive interference from the 110 plane.

The infrared spectrum at 0.5 hours is somewhat different from that obtained when $TiSi_2$ was oxidized. The usual SiO_2 absorption are observed at 1150, 1050 and 450 cm^{-1}. They are, however, extremely broad and of low intensity. The highest intensity absorption was observed at 885 cm^{-1}. This would appear to be the band due to the Ti-O-Si vibration observed at 940 cm^{-1} in the oxide on $TiSi_2$. The shift to the lower frequency could be due to the presence of a greater concentration of titanium, either in or around the amorphous SiO_2 regions.

After about 20 hours at temperature, the surface is completely covered by an opaque, yellow oxide. X-ray analysis indicates only TiO_2. In this case, the intensities of the low angles from $2\theta = 27^{\circ}$ to 35° are considerably lower than the standard values. The Ti_5Si_3 substrate lines are not observed. The peak positions of the TiO_2 in the X-ray also appear to be decreasing, indicating an increase in lattice spacing. Some typical data are shown below:

Oxidation Time, Hrs	2θ			
ASTM Standard	27.45	36.05	41.22	54.33
0.7	27.40	36.03	-	54.25
24.5	27.40	36.05	41.20	54.23
44.5	27.35	36.00	41.15	54.11
100.5	27.27	35.83	41.02	54.10

In addition to this shift to lower values of 2θ, the peaks are also very much broader. An infrared spectrum of the surface could not be obtained since it appears that diffuse reflection from the surface is occurring.

The weight gain data for the oxidation of Ti_5Si_3 at 1000°C and 0.2 atmospheres oxygen pressure is shown in Figure 17. Two samples were oxidized, one with a density of 82 percent of theory, the other 88 percent. Examination of the surfaces indicated about the same hole density. The weight gains observed agreed within 5 percent.

The value of the exponent in the equation $X^n = kt$ after approximately 0.5 hours of oxidation is 5.7. In the initial period, up to 0.5 hours, the slope is considerably greater with a value as high as 2 being obtained between 0.1 and 0.2 hours.

When the square of the weight gain is plotted against oxidation time, a straight line with the equation

$$X^2 = 0.65t + 84$$

can be obtained.

The important factor in the oxidation of Ti_5Si_3 is that it forms a protective oxide layer at 1000°C for oxidation times up to 120 hours.

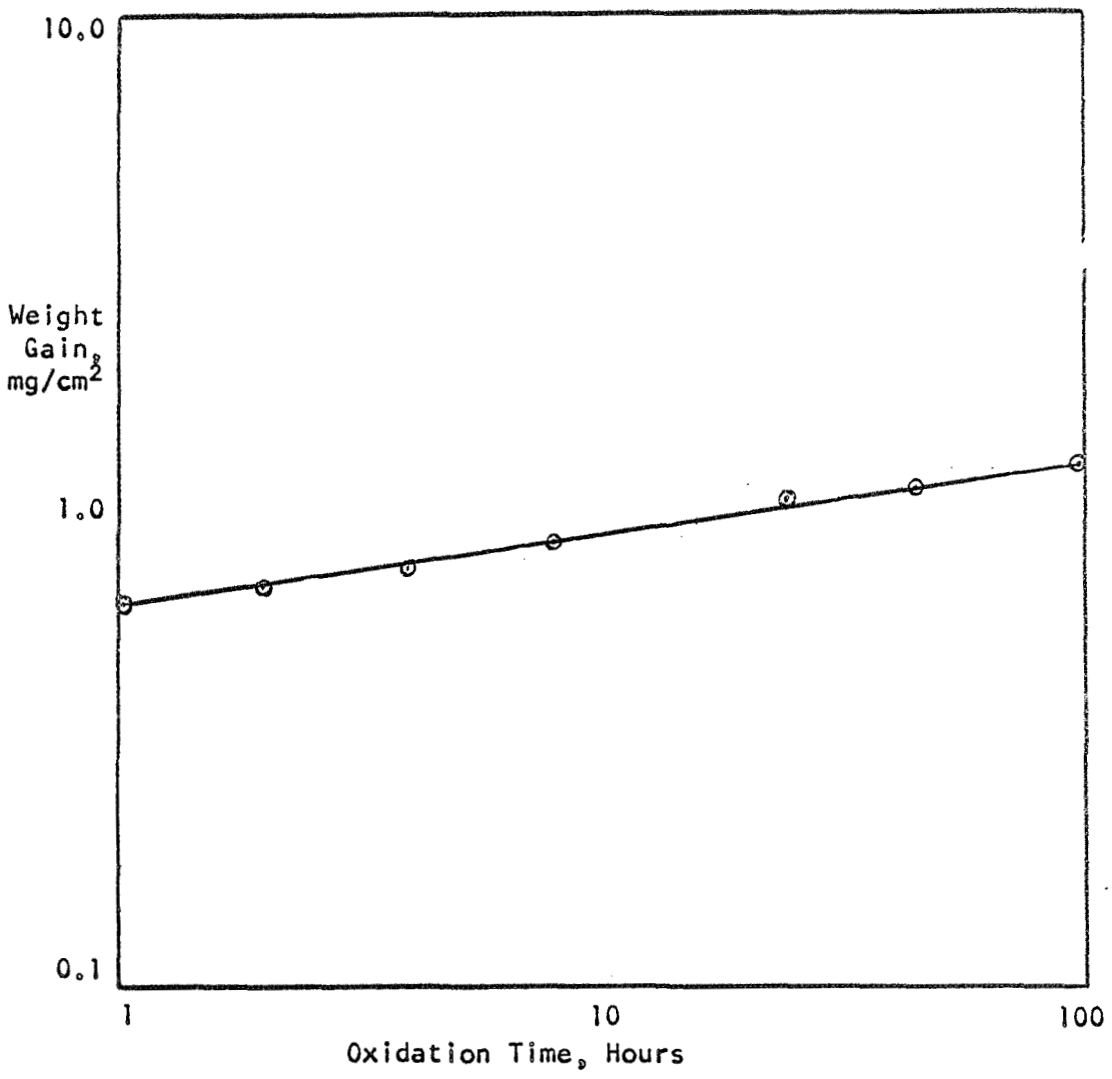

Figure 17 Oxidation Weight Gain Data for Ti_5Si_3

3. $TaSi_2$

An attempt was made to prepare wafers from $TaSi_2$ powder obtained from CERAC Inc. The density of the sintered samples was only 70 percent of the theoretical value. $TaSi_2$ was then prepared directly from tantalum and silicon powders at 1000°C in a vacuum of 10^{-4} Torr. Wafers made from this material had densities of 90 percent of the theoretical value. X-ray analysis indicates $TaSi_2$ with a trace of Ta_5Si_3.

Two samples were oxidized at 1000°C in an oxygen-argon atmosphere with an oxygen partial pressure of 0.2. After 1 hour at temperature, a yellow oxide is formed around the sample edges. The faces of the sample are covered by a blue, transparent film. After 5 hours, the oxide begins to spall from the edges, while the faces begin to show yellow oxide. After 10 hours, heavy spalling occurs on both the edges and faces. X-ray analysis of the surface indicates β-Ta_2O_5 and a trace of the $TaSi_2$ substrate. No weight gain data were obtained. It is not clear whether $TaSi_2$ is non-protective or whether the small amount of Ta_5Si_3 present in the sample causes the deterioration.

4. $TaSi_2$ - $TiSi_2$

Several wafers of a mixture 60 mole percent $TaSi_2$ and 40 mole percent $TiSi_2$ were prepared from homemade $TaSi_2$ and $TiSi_2$. Sintering at 1400°C yields a sample with a density of approximately 90 percent of the theoretical value. X-ray analysis of the polished surface indicates only $TaSi_2$ and $TiSi_2$. The $TaSi_2$ lines are identical to the ASTM values while the $TiSi_2$ lines are found at lower values of 2θ. This is consistent with the results obtained on the pure samples.

Two samples were oxidized at 1000°C and 1300°C in an oxygen-

argon atmosphere with an oxygen partial pressure of 0.20. At 1000°C and 45 hours of oxidation, a protective oxide layer is formed. X-ray analysis indicates the original substrate and TiO_2 (rutile). There is no evidence of crystalline Ta_2O_5 or SiO_2. The weight gain observed after 45 hours is approximately 1 mg/cm^2.

At 1300°C and 45 hours, a protective oxide layer is also formed. In this case, no regions of transparent oxide are present. X-ray analysis indicates the substrate, TiO_2 (rutile) and SiO_2 (α-cristobalite). No Ta_2O_5 is observed. The weight gain after 45 hours is approximately 1.5 mg/cm^2.

D. TiO_2-SiO_2 Solubility and Glass Formation

In order to be able to better characterize the oxide growing on $TiSi_2$, a study was made of the reactions occurring in the TiO_2-SiO_2 system at elevated temperatures. A detailed description of the results is given in reference (75). The results pertinent to the oxidation study will be described here.

The phase diagram for the TiO_2-SiO_2 binary system was shown earlier in Figure 8. These data indicate a maximum solubility of TiO_2 in SiO_2 of 10 wt. percent at the eutectic temperature of 1540°C. These studies were carried out in air.

In order to confirm these results and obtain samples for analysis, a number of wafers containing 10 wt. percent TiO_2 were heated at 1550°C for 15 minutes at 10^{-4} Torr. The sample coalesces but does not bond to the alumina support dish. X-ray analysis of the glassy-blue surface indicates the material is amorphous. The infrared spectrum is the same as the SiO_2 charged with one major exception. A broad absorption is observed at 935 cm^{-1}. If a solid solution or glass is formed, a Ti-O-Si vibration would be expected. Zeitler and Brown (77) have reported results on the infrared spectra

of organic-titanium-silicon compounds. They attribute an absorption at 919-925 cm^{-1} to a Ti-O-S vibration. They also show the Si-O stretching vibration at 1110 cm^{-1}, or nearly the same as in amorphous SiO_2. While this is not construed as positive proof, it appears likely that the absorption observed at 935 cm^{-1} in this study is due to a Ti-O-Si vibration. Since titanium is classified as a network modifier (78), it is likely that a substitutional solid solution or glass is formed.

When the concentration of TiO_2 is increased to 20 wt. percent and heated at 1550°C, TiO_2 is observed in the X-ray analysis. This confirms the solubility level of 10 wt. percent TiO_2 reported by Ricker and Hummel (56).

An interesting and unexplained result is obtained when a sample containing 10 wt. percent TiO_2 is heated in vacuum at 1200°C. While the TiO_2 lines disappear from the X-ray pattern, the infrared spectrum shows only the pure SiO_2. No absorption is observed at 925 cm^{-1}. Apparently, some type of physical segregation is occurring and not solution. When this sample is reheated in air at 1200°C, the color turns from blue to the original white and the TiO_2 lines reappear in the X-ray pattern.

4.5 Discussion

A. Introduction

The purpose of this study was to (1) obtain data on the oxidation of bulk $TiSi_2$ in the temperature region 300-1300°C, (2) develop a mechanism to describe the oxidation and (3) relate this mechanism to results obtained with other silicides and determine whether a consistent theory of oxidation protection can be applied to this general class of materials.

Suitable samples for oxidation studies were made using the techniques of powder matellurgy. The silicides are prepared by

direct reaction of the elements in vacuum at approximately 1000°C. The use of polymethylmethacrylate binder allows pressing of the powdered silicide into one inch diameter wafers at 5-10 tsi. Sintering at 1400°C in vacuum yields samples with densities of 95 percent of the theoretical value. Polishing with diamond paste results in mirror-like surfaces. Small holes and a trace amount of a second phase are usually observed upon metallographic examination. This cold pressing technique is superior to the hot pressing method previously used in preparing other silicide pellets (79) in that no carbon contamination of the sample occurs.

In an oxidation reaction, there are four steps which are involved before reaction can occur. Initially, there is transport of the oxygen from the gas phase to the solid surface followed by adsorption onto the surface. One or more species then diffuse through the oxide layer with subsequent reaction at an interface. Either of these steps may be rate controlling.

In this study, gas phase transport can be neglected since no difference in rate is observed between samples oxidized in stagnant and rapidly flowing gases. In addition, phase boundary reaction control is not likely since these phenomena normally give rise to reaction rates which are independent of film thickness. These data indicate, especially at low temperatures, that the reaction rate is highly dependent on film thickness. Some form of transport of one or both of the reacting species through the oxide film appears to be the rate controlling step. These conclusions are valid only for oxidation times which are greater than those for which a different initial mechanism may prevail. The rate at which diffusion through the oxide occurs depends on the structure of the oxide film.

B. High Temperature Model for $TiSi_2$ Oxidation

Between 1000 and 1300°C, the oxide structure consists of crystalline TiO_2 islands growing out of a slightly impure silica matrix. The rate data for samples with few holes indicate parabolic behavior with an activation energy of 21.3 kcal. The weight gain observed for $TiSi_2$ at any time of oxidation is approximately 50-70 percent greater than that obtained when silicon is oxidized. The question to be answered is how does diffusion occur through the oxide growing on $TiSi_2$.

Two cases can be considered. These are illustrated in Figures 18a and 18b. In Figure 18a, the entire silicide surface is covered by vitreous SiO_2 with the TiO_2 islands on top of the SiO_2 film only. In order for reaction to occur, it is necessary for diffusion to occur through the amorphous silica region. When compared to silicon oxidized for the same time, the thickness of the SiO_2 film on both the silicon and titanium disilicide would be the same since diffusion through the film is rate controlling. The weight gain for the silicide, however, would be 50 percent greater since for each silicon atom oxidized, 0.5 atoms of titanium are oxidized. The TiO_2 island growth would occur by diffusion of titanium through the silica to the TiO_2 islands. The weight gain calculated, assuming this mode of transport, is what is experimentally observed.

The growth mechanism of the film shown in Figure 18b would be by parallel diffusion through both the amorphous silica and crystalline TiO_2 regions. In this case, the TiO_2 islands extend through to the TiO_2 substrate. Kofstad (80) shows the parabolic constant for titanium oxidation at 1000°C as 0.6 $(mg/cm^2)^2/min$ $(3.6[mg/cm^2]^2/hr$. At this temperature, it appears that either the titanium or oxygen may be the diffusing species for titanium oxidation. The parabolic rate constant for silicon oxidation as reported by Deal

Figure 18

Possible Oxide Film Structures

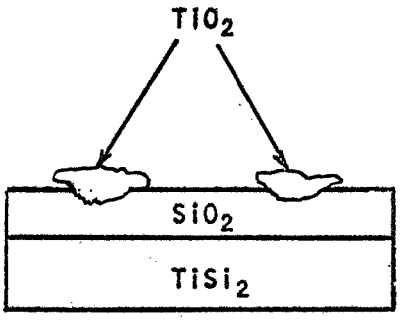

(a)

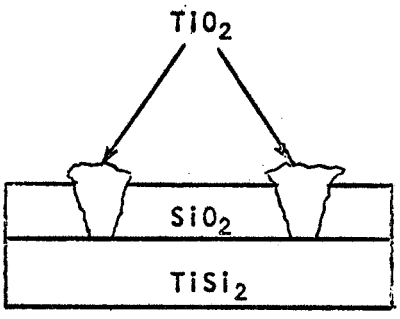

(b)

and Grove (64) has been given as 1.57×10^{-4} $(mg/cm^2)^2/hr$. If the TiO_2 covers 10 percent of the sample surface, the contribution to the overall rate through the TiO_2 would be greater than that through the SiO_2 by a factor of about 10^4. If there were pores or channels between the crystalline TiO_2 and the amorphous SiO_2, this ratio would be greater still. For the case described in Figure 18b then, the weight gain would be 100 times greater than that actually observed.

This calculation indicates that diffusion occurs through an amorphous silica film in which TiO_2 islands grow on the oxide-gas surface, as illustrated in Figure 18a. This is further confirmed by the fact that the activation energy for the reaction, 21.3 kcal, is very near the 28.5 reported for silicon oxidation (64).

Light microscope examination of a sample cross-section indicates TiO_2 growing on top of the film in the manner of Figure 18a and in some areas, particularly at holes, through the film, as in Figure 18b. The resolving power of the light microscope, however, is not sufficient to determine whether these islands do indeed go through the film to the substrate or whether they are separated from the substrate by a thin silica layer.

At 1000-1300°C, the number of holes in the sample greatly affects the oxidation rate. Observable crystallization of the TiO_2 occurs at an earlier time of oxidation when the number of holes is increased. When the square of the extended time weight data for samples with many holes is plotted against time, a straight line is obtained in most cases. The line does not pass through the origin. Apparently a two stage mechanism is involved: An initial rapid oxidation occurring before significant crystallization, followed by a slower parabolic reaction. If indeed the TiO_2 crystalline islands are nearly separated from the base by the

amorphous SiO_2, the initial rapid reaction could be due to TiO_2 channels through the film. Once significant growth has occurred, the crystalline TiO_2 would be forced up and onto the growing amorphous silica matrix. Diffusion would then be through a primarily silica film.

C. Low Temperature Model for $TiSi_2$ Oxidation

Measurable oxidation of $TiSi_2$ begins at approximately 300°C. The thin oxide film appears to be SiO_2 with isolated areas where impurities have oxidized. Since the weight gains are quite low and a competing reaction takes place, a quantitative interpretation is not justified.

At 600°C, an impure, amorphous SiO_2 film, exhibiting interference colors which vary with $TiSi_2$ grain orientation, is formed. Infrared analysis indicates the presence of Ti-O-Si bonding in the oxide film.

The kinetic data at 600°C are characterized by a rapid initial rate followed by extremely small reaction rates. No effect is observed as the number of holes in the surface is varied or as the partial pressure of oxygen is changed from 0.2 to 1.0.

Since the oxide thickness varies with surface orientation, the surface reaction between the silicide and oxygen is probably rate controlling for some initial period. Since the thickness at extended times does not change appreciably, this initial oxide makes a significant contribution to the optical interference.

These results appear to indicate that after the initial surface reaction control, some form of diffusion through the growing oxide film is the rate controlling step. For oxidation times of up to 300 hours, the plot of the square of the weight gain versus time for the 600°C data shows no straight line regions. This indicates that normal bulk diffusion is not rate controlling.

It is proposed that the mechanism of growth at 600°C after the initial rapid rate is one of diffusion control with a variable diffusivity. Initially, the oxide growth occurs by bulk and short circuit diffusion. As the oxidation time increases, the short circuit paths become blocked and bulk diffusion controls. If this were the mechanism, the plot of X^2 versus t would give a straight line at extended times. If it is assumed that the slope of the data obtained after 200 hours of oxidation is constant, a parabolic rate constant of 85×10^{-7} $(mg/cm^2)^2/hr$ is obtained.

Since the high temperature data are essentially for diffusion through a silica film, extrapolation using the Arrhenius plot should give an estimate of the parabolic rate constant at 600°C. These data, along with data for silicon oxidation, are shown in Table XXIV. The experimental value of 85×10^{-7} $(mg/cm^2)^2/hr$ is extremely close to the 40×10^{-7} $(mg/cm^2)^2/hr$ obtained by extrapolating the high temperature data. Since the low temperature silica is impure, i.e., contains TiO_2, diffusion would be easier giving a larger parabolic rate constant.

The values obtained for $TiSi_2$ cannot be compared directly with the results observed for silicon since the latter shows negligible oxidation at 600°C. However, extrapolating the data of Deal and Grove (64) to 600°C gives a value of 4.3×10^{-5} μ^2/hr or assuming an oxide density of 2.2 gms/cm^3, 5×10^{-7} $(mg/cm^2)^2/hr$ for the parabolic rate constant. This value is considerably smaller than that obtained experimentally or by extrapolation for $TiSi_2$. This could indicate that either the diffusivity through the low temperature oxide is greater due to the presence of titanium or that the slopes from the X^2 versus t plots are not constant. In either case, the consistency of the numerical values adds evidence to the proposed variable diffusivity model.

Table XXIV

Comparison of Parabolic Rate Constants for $TiSi_2$ and Silicon Oxidation

	kp $(mg/cm^2)^2/hr$		
	$TiSi_2$		Silicon*
Temp ^oC	Experimental	Extrapolated	
1300	17.4×10^{-4}	-	-
1200	8.72×10^{-4}	-	6.04×10^{-4}
1000	3.52×10^{-4}	-	1.57×10^{-4}
800	0.26×10^{-4}	0.7×10^{-4}	0.147×10^{-4}
600	85×10^{-7}	40×10^{-7}	5×10^{-7}

*Data from Deal and Grove (64). Calculated from ^{2}/hr assuming oxide density of 2.2 gms/cm^3.

A similar treatment was carried out on the data obtained at 800°C. These data are also shown in Table XXIV. These results are in line with those described for the 600° data.

Nothing definitive can be said concerning the mechanism by which the diffusivity decreases. This could be due to the closing of pores by reaction in the pores or by compressive stresses in the oxide. It could also be due to ageing of the oxide where interstitial spaces created at the time of oxidation are gradually closed. In either case, the presence of the short circuit paths is due to the low atomic mobility in the oxide at low temperature. While there is no evidence indicating the presence of pores in the oxide, the study of Ing, et.al. (56) on the structure of the oxide film on silicon indicates microchannels. This type of defect would be more likely to occur in the impure silica films considered here.

One of the most interesting and unique results in this study is the formation of an entirely amorphous film at 600°C. Since crystalline TiO_2 is not observed, the titanium is either trapped in the silica matrix or has formed a lower silicide layer beneath the growing oxide film or a combination of both. The possible reactions are:

$$TiSi_2 + 3O_2 = TiO_2\ 2SiO_2 \text{ (solid solution)} \qquad (1)$$

$$5TiSi_2 + 7O_2 = 7SiO_2 + Ti_5Si_3 \qquad (2)$$

$$TiSi_2 + O_2 = SiO_2 + TiSi \qquad (3)$$

$$Si \text{ (dissolved)} + O_2 = SiO_2 \qquad (4)$$

Little can be said about a preferred reaction from the thermodynamic data available. The free energy change of reactions (1) - (3) are almost identical. No thermodynamic data is available on silicon dissolution in titanium disilicide.

The infrared analysis indicates that reaction (1) to form a

$TiO_2 \cdot 2SiO$ solid solution is likely. The crystallization of TiO_2 observed when a sample oxidized at 600°C is heated to 1200°C in a reduced oxygen pressure atmosphere contributes to the validity of titanium trapped in the silica. The formation of a TiO_2-SiO_2 solution requires that 40 wt. percent TiO_2 (33 atomic percent) be dissolved if a stoichiometric reaction occurs. While the phase diagram for the system shows a maximum solubility of 10 wt. percent TiO_2 in SiO_2 at 1500°C, it is conceivable that in a solid-state reaction of this kind, 40 wt. percent TiO_2 could be retained in a metastable solution. The lack of crystallization indicates that the energy required for either nucleation or diffusion of the titanium is too great. If reaction (1) is correct, then the implication is that the energy required for oxygen diffusion and surface reaction is less than for titanium diffusion.

A combination of reactions (1) and (4) would result in a solution in which the TiO_2 concentration would be less than 40 percent. Reaction of dissolved silicon at the surface would also result in diffusion of dissolved silicon from the interior of the silicide. Whether this rate would be significant or whether there is sufficient dissolved silicon in the samples is not known. It is also not clear whether dissolved atomic silicon would be more active than bulk silicon which undergoes negligible oxidation at 600°C.

Were reactions (2) or (3) to occur, the oxide formed would be pure SiO_2. A combination of (1) and (2) or (3) would result in an oxide film with titanium dissolved in the film and a lower silicide layer beneath the oxide. The thickness of this lower silicide, assuming reaction (2) with some typical weight gain data is approximately 0.4 micron. Calculations (75) show that this thickness Ti_5Si_3 would diffract only 1 percent of the incident X-radiation. Almost all the diffracted energy is attributable to the $TiSi_2$

substrate. This would also be applicable to changes in the $TiSi_2$ lattice parameters as silicon is removed assuming reaction (4) is valid. The thickness of the silicon-free region would also probably be too small to be observed.

These considerations indicate that either reaction (1) or a combination of (1) with (2), (3) or (4) is occurring at 600°C.

D. TiSi and Ti_5Si_3 Studies

Wafers of TiSi and Ti_5Si_3 were prepared using the techniques of powder metallurgy. Purchased Ti_5Si_3 cannot be sintered to a sufficiently high density. Preparing the TiSi and Ti_5Si_3 directly from the elements by reaction in vacuum provides suitable material. TiSi contains small amounts of $TiSi_2$ while the Ti_5Si_3 surface has many holes and microcracks. On oxidation, these lower silicides form protective, opaque yellow oxide films. X-ray analysis indicates crystalline TiO_2 (rutile). A plot of the weight gain data as X^2 versus t, gives a straight line which does not extrapolate through the origin.

Since few runs were made, no model can be proposed for the oxidation although comparison can be made with titanium, $TiSi_2$ and silicon.

The parabolic rate constants for the straight line region of the weight gain data are shown in Table XXV along with those for silicon, $TiSi_2$ and titanium. The general trend is clear. The value for $TiSi_2$ is close to silicon. The value for TiSi is 30 times greater than for $TiSi_2$, although still quite small, while Ti_5Si_3 is approaching that for titanium. If the model proposed for $TiSi_2$ is correct, then as the amount of titanium in the substrate is increased, it might be expected that some of the islands would extend through the oxide to the substrate. This would result

Table XXV

Parabolic Rate Constants at 1000°C for Materials in the Titanium-Silicon System

Material Oxidized	kp, $(mg/cm^2)^2/hr$
Silicon	1.57×10^{-4}[a]
$TiSi_2$	3.52×10^{-4}
TiSi	90×10^{-4}
Ti_5Si_3	0.65
Titanium	3.6[b]

[a] Data of Deal and Grove (64)

[b] See Kofstad (81)

in a large increase in the parabolic rate constant. While TiSi is covered with an opaque yellow oxide, the low value for the rate constant indicates that there may be an amorphous SiO_2 layer below the TiO_2 covering most of the surface. Microscopic examination of the oxide on Ti_5Si_3 in cross-section does indicate a layered structure. The composition of this structure was not determined.

E. Mechanism for Protective Film Formation

The results of this study have indicated a mechanism which describes the growth rate of the oxide film formed on $TiSi_2$ during its oxidation. The characteristic or characteristics which account for the ability of this system to form a protective, adherent oxide are of primary importance.

The oxidation behavior of the titanium silicides stand in contrast to $MoSi_2$, which has been studied extensively, and also to most of the other silicides which have been given cursory examinations. In polycrystalline MoO_3 in the oxide at temperatures of 300-600°C results in rapid deterioration of the sample. Berkowitz-Mattuck, et.al. (53) attribute this "pest" phenomena to the pressure exerted by the growing oxide in cracks on the sample surface. Both MoO_3 and SiO_2 are formed. Above 600°C, the MoO_3 volatilizes and a protective silica film which bridges the cracks is formed. Berkowitz-Mattuck, et.al. suggest that the failure of some silicides, including $MoSi_2$, to form a protective film is due to microcracks in the substrate and the presence of a duplex film of both oxides.

For the case of $TiSi_2$, a protective film is formed even though both oxides are present. The presence of imperfections in the surface, particularly Ti_5Si_3 which has considerable holes and microcracks, results in an increase in the oxidation rate. However, an adherent oxide film is still formed. The present study suggests

that while the presence of cracks in the sample provides high energy nucleation sites which increases the reaction rate, the compatibility of the oxides is the more fundamental requirement for the formation of a protective oxide. The fact that TiO_2 is partially soluble in SiO_2 appears to be quite significant.

Two of the more important factors which determine whether a glass or solid solution can be formed are ionic size and charge. Titanium, a network modifier, has the same charge as silicon. The ionic size of titanium is greater than silicon and usually requires sixfold coordination. The solid solution studies on the TiO_2-SiO_2 system have indicated, however, that titanium can have fourfold coordination and replace silicon in the SiO_2 network. At low oxidation temperatures, this results in the formation of a titania-silica glass. At high temperatures, this allows titanium to diffuse through the silica film to the nucleation sites without disrupting the silica network. This probably occurs by a vacancy diffusion mechanism since the interstices are considerably smaller than could conveniently accommodate the titanium atom.

The infrared studies of the amorphous silica at temperatures over 800°C indicate that there is some titanium in the silica. The mobility of titania at temperatures over 1000°C is evidenced by the ease at which it sinters when fired in bulk form.

In addition to the solubility effect, the ability of the crystalline TiO_2 to exist and grow upward and out of the SiO_2 without cracking the film is critical.

The lack of compatibility of the oxides formed in the oxidation of $MoSi_2$ in the 300-600°C temperature region can be due to many factors. The inability of the molybdenum ion to form a glass or solid solution might be significant. The ionic radius of Mo^{5+} is 0.62 Å compared to 0.68 Å for Ti^{4+} (78). The ionic field

strength of the molybdenum ion classifies its function in glasses as an intermediate ion, i.e., it cannot usually form a glass but can take part in the network. Since titanium with a slightly larger ionic radius can replace silicon in the silica network, the size does not appear to hinder glass formation. The ionic charge of +5, however, would result in a structure which would not be neutral and hence unstable. This charge factor might also prevent tantalum and columbium from forming glasses. The silicides of these materials also form non-protective oxide films when oxidized.

In the preparation of silicide coatings on tantalum or columbium, it would seem desirable to add modifiers with a +3 charge in order to form an oxide with the capability of a neutral structure. The balancing of the charge, obviously, does not guarantee glass formation but would be desirable in the event the glass-forming ability were there.

The concept of oxide compatibility is quite complex. The structural considerations which result in the formation of a glass are still being debated. In the oxidation of the silicides, the compatibility involves both glass formation and coexistence of a glass with a crystalline oxide. An extensive study of the factors involved in the compatibility of binary oxides is beyond the scope of the present work.

References

1. N.E. Promisel, "The Science and Technology of Selected Refractory Metals", Macmillan Co. 1964.

2. C.D. Wirkus and D.R. Wilder, "High Temperature Oxidation of Molybdenum Disilicide", J. Am. Ceram. Soc. 49 (4), 173 (1966).

3. S.R. Levine, "The Thermodynamics of Refractory Metal Silicides by an EMF Method". Doctoral Thesis, The City University of New York, 1968.

4. S.R. Levine and M. Kolodney, "The Free Energy of Formation of Tantalum Silicides Using Solid Electrolytes", Jour. Electrochem. Soc., 116, 1420 (1969).

5. C.E. Wicks and F.E. Block, U.S. Bur. Mines Bull., 605 (1963).

6. L. Brewer and O. Krikorian, J. Electrochem. Soc. 103, 38-51, 701-3 (1956).

7. D.A. Robins and I. Jenkins, Acta. Met., 3, 598-604 (1955).

8. C.E. Myers and A.W. Searcy, J. Am. Chem. Soc., 79, 526-28 (1957).

9. A.W. Searcy and R.A. McNees, J. Am. Chem. Soc., 75, 1578-80 (1953).

10. A.W. Searcy and A.G. Thorp, J. Phys. Chem., 64, 1539-42 (1960).

11. A.W. Searcy and L.N. Finnie, J. Am. Ceram. Soc., 45, 268 (1962).

12. S.G. David, D.F. Anthrop, and A.W. Searcy, J. Chem. Phys., 34, 659-64 (1961).

13. K. Kiukkola and C. Wagner, J. Electrochem. Soc. 104, 308 and 379 (1957).

14. H. Schmalzried, Zeitschrift fur Electrochemie, 66, 572-6 (1962).

15. G.G. Charette and S.N. Flengas, J. Electrochem. Soc. 115, 795-804 (1968).

16. B.C.H. Steele and C.B. Alcock, Trans. Met. Soc. AIME, 233, 1359-67 (1965).

17. A.A. Vecher and D.V. Vecher, Russian J. Phys. Chem. (Engl. Transl.), 42, (3), 418 (1968).

18. R.A. Rapp, "Thermodynamics of Nuclear Materials, 1967", IAEA, Vienna, 1968.

19. L.S. Castleman, "An Analytical Approach to the Diffusion Bonding Problem", Nucl. Sci. and Eng., 4, 209 (1958).

20. G.V. Kidson, "Some Aspects of Growth of Diffusion Layers in Binary Systems", J. Nuclear Mat., 3(1), 21 (1961).

21. L.S. Darken, "Diffusion, Mobility and Their Interrelation Through Free Energy in Binary Metallic Systems", Trans. AIME, 175, 184 (1949).

22. M.M.P. Janssen and G.D. Riech, "Reaction Diffusion and Kirkendall Effect in the Ni-Al System", Trans. Met. Soc. AIME, 239, 1372 (1967).

23. G.B. Gibbs, "Diffusion Layer Growth in a Binary System", J. Nuclear Mat., 20, 303 (1966).

24. U. Roy, "Phase Boundary Motion and Polyphase Diffusion in Binary Metal - Interstitial Systems", Acta Met., 16, 243 (1968).

25. R. Resnick, R. Steinitz and L. Seigle, "Determination of the Diffusivity of C in Ta and Cb Carbides by Layer-Growth Measurements", Trans. Met. Soc. AIME, 233, 1915 (1965).

26. G. Kimmel, A. Bar-or and A. Rosen, "Interdiffusion Between Ni and U", Trans. ASM, 61, 703 (1968).

27. C. Wagner, "The Evaluation of Data Obtained with Diffusion Couples of Binary Single-phase and Multiphase Systems", Acta. Met., 17, 99 (1969).

28. W.C. Hagel, "Diffusion in Intermetallic Compounds", G.E. Res. Lab. Report No. 63-RL-3320 M (1963).

29. R.W. Bartlett, "Kinetics of Ta_5Si_3 and Cb_5Si_3 Growth in Disilicide Coatings on Ta and Cb", Trans. Met. Soc. AIME, 236, 1230 (1966).

30. J.J. English, "Binary and Ternary Phase Diagrams of Columbium, Molybdenum, Tantalum and Tungsten", DMIC Report 152 (1961).

31. H.W. Lavendel and A.G. Elliot, "Investigation of Modified Silicide Coatings for Refractory Metal Alloys with Improved Low-Pressure Oxidation Behavior", AFML-TR-65-344 (1965).

32. D.M. Koffman and R.E. Ogilvie, "Diffusion Studies in the Cb-Si and W-Si Binary Systems", AFML-TR-65-34 (1965).

33. R.W. Bartlett, P.R. Gage and P.A. Larssen, "Growth Kinetics of Intermediate Silicides in the $MoSi_2$/Mo and WSi_2/W Systems", Trans. Met. Soc. AIME, 230 1528 (1964).

34. P.R. Gage and R.W. Bartlett, "Diffusion Kinetics Affecting the Formation of Silicide Coatings on Mo and W", Trans. Met. Soc. AIME, 233, 832 (1965).

35. Norikazu Hashimoto, "Kinetics of WSi_2 Growth on Si", Trans. Met. Soc. AIME, 239, 1109 (1967).

36. G.V. Samsonov, et.al., "Diffusion of Si in Ti, Ta, Mo and Fe", Dop. Akad. Nauk. Ukr SSR, 1, (1959). Translation FTD-TT-63-262 (1963).

37. E.M. Passmore, J.E. Boyd, L.P. Neal, C.A. Anderson and B.S. Lement, "Investigation of Diffusion Barriers for Refractory Metals", WADD T.R. 60-343 (1960).

38. E.M. Passmore, J.E. Boyd and B.S. Lement, "Investigation of Diffusion Barriers for Refractory Metals", ASD-TDR-62-432 (1962).

39. "Powder Diffraction File", Compiled by the Joint Committee on Powder Diffraction Standards, American Society for Testing and Materials.

40. H. Nowotny, H. Schachner, R. Kiefer and F. Benesovsky, Monatsh. Chem., 84, 1 (1953).

41. A.G. Knapton, Nature, 175, 730 (1955).

42. E. Parthe, H. Nowotny and H. Schmid, Monatsh. Chem., 86, 385 (1955).

43. E. Parthe, B. Lux and H. Nowotny, Monatsh. Chem. 86, 359, (1955).

44. O.G. Karpinskii and B.A. Evseev, "Crystal Structure of the Compound Zr_5Si_4" Izv. Akad. Nauk SSSR, Neorg. Mat., 4 (#8), 1248 (1968).

45. M. Hansen, "Constitution of Binary Alloys", Second Edition, McGraw Hill, N.Y., 1958.

46. P.T.B. Shaffer, "Handbook of High-Temperature Materials, No. 1, Materials Index", Plenum Press, N.Y., 1964.

47. A.G. Knapton, Plansee Proc., 3rd Seminar, 1958, 42 (1959).

48. M. Semchyshen and J.J. Harwood, "Refractory Metals and Alloys", Interscience Pub., N.Y., 1961.

49. A.R. Stetson, H.A. Cook, V.S. Moore, "Development of Protective Coatings for Tantalum Base Alloys", Solar, AFML TR 65-205, Part 1, June (1965).

50. D.J. Bracco, P. Lublin, L. Sama, "Identification of Microstructural Constituents and Chemical Concentration Profiles in Coated Refractory Metal Systems", General Telephone and Electronics, AFML TR-66-126, May (1966).

51. R.T. Wimber, A.R. Stetson, "Development of Coatings for Tantalum Alloy Nozzle Vanes", Solar RDR 1396-2 for NASA, May (1966).

52. G.V. Samsonov, "Silicides and Their Uses in Engineering", Translation from Russian FTD-TT-62 430 1 & 2 (July 1962).

53. J.B. Berkowitz-Mattuck, P.E. Blackburn and E.J. Felten, "The Intermediate-Temperature Oxidation Behavior of Molybdenum Disilicide", Trans. Met. Soc. AIME, 233, 1093 (1965).

54. A.W. Searcy, "Predicting the Thermodynamic Stabilities and Oxidation Resistance of Silicide Cermets", J. Am. Ceram. Soc., 40 (12) 431-435 (1957).

55. E.N. Bunting, "Phase-Equilibria in the Systems TiO_2, TiO_2-SiO_2, TiO_2-Al_2O_3", J. Research Natl. Bur. Standards, 11 (5) 719-25.

56. R.W. Ricker and F.A. Hummel, "Reactions in the System TiO_2-SiO_2; Revision of the Phase Diagram", J. Am. Ceram. Soc., 34 (9) 271-79 (1951).

57. P.W. McMillan, "Glass Ceramics", Academic Press (1964), p. 60.

58. W.A. Pliskin and H.S. Lehman, "Structural Evaluation of Silicon Oxide Films", J. Elect. Soc., 112, 1013 (1965).

59. L.A. Murray and N. Goldsmith, "Nondestructive Determination of Thickness and Perfection of Silica Films", J. Elect. Soc., 113, 1297-1300 (1966).

60. K. Sato and M. Shibata, "Restrahl Reflection Characteristics of Amorphous Silica", J. Phys. Soc. Japan, 21, 1088-96 (1966).

61. B.E. Deal, "Oxidation of Silicon in Dry Oxygen, Wet Oxygen, Steam", J. Elect. Soc., 110, 527, 1292 (1963).

62. S.W. Ing, R.E. Morrison and J.E. Sandor, "Gas Permeation Study and Imperfection Detection of Thermally Grown and Deposited Thin Silicon Dioxide Films", J. Elect. Soc., 109, 221 (1962).

63. J.W. Evans and S.K. Chatterji, "Kinetics of the Oxidation and Nitridation of Silicon at High Temperatures", J. Phys. Chem., 62, 1064 (1958).

64. B.E. Deal and A.S. Grove, "General Relationship for the Thermal Oxidation of Silicon", J. Appl. Phys., 36, 3770 (1965).

65. F.J. Norton, "Permeation of Gaseous Oxygen Through Vitreous Silica", Nature, 191, 701 (1961).

66. E.N. Sucov, "Diffusion of Oxygen in Vitreous Silica", J. Am. Ceram. Soc., 46, 14 (1963).

67. P.J. Jorgensen, "Effect of an Electric Field on Silicon Oxidation", J. Chem. Phys., 37, 874 (1962).

68. W.A. Pliskin and R.P. Gnall, "Evidence for the Oxidation Growth at the Oxide-Silicon Interface from Controlled Etch Studies", J. Elect. Soc., 111, 872 (1964).

69. P.S. Flint, "The Rates of Oxidation of Silicon", Paper presented at the Spring Meeting of the Electrochemical Society, Abstract No. 94, Los Angeles, 6-10 (May 1962).

70. R.J. Ligenza, "Effect of Crystal Orientation on Oxidation Rates of Silicon in High Pressure Steam", J. Phys. Chem., 65, 2011 (1961).

71. G.V. Samsonov, "Plenum Press Handbooks of High Temperature Materials - Properties Index", (1964) p. 373.

72. G.V. Samsonov, "Plenum Press Handbooks of High Temperature Materials - Properties Index", (1964) (a) p. 28, (b) p. 98, (c) p. 186, (d) p. 51, (e) p. 68, (f) p. 129, (g) p. 144, (h) p. 160, (i) p. 163.

73. M. Tannenbaum, "Film Stripping Technique for Making Thin Silica Windows", J. App. Phys., 31, 940 (1960).

74. W.A. Pliskin and E.E. Conrad, "Nondestructive Determination of Thickness and Refractive Index of Transparent Films", IBM J. Res. and Dev., 8, 43 (1964).

75. F.N. Schwettmann, "Mechanism of the Oxidation of Titanium Disilicide: 300-1300°C", Doctoral Thesis, The City University of New York, 1969.

76. I. Simon and H.O. McMahon, "Study of Some Binary Silicate Glasses by Reflection in Infrared", J. Am. Cer. Soc., 36(5), 160-64 (1953).

77. V.A. Zeitler and C.A. Brown, "The Infrared Spectra of Some Ti-O-Si, Ti-O-Ti and Si-O-Si Compounds", J. Phys. Chem., 61, 1174-77 (1957).

78. P.W. McMillan, "Glass Ceramics", Academic Press (1964) p. 16.

79. R.W. Bartlett, et.al., "Investigation of Mechanisms for Oxidation Protection and Failure of Intermetallic Coatings for Refractory Metals", Aeronutronic ASD-TDR 63-753, Part I, June 1963, Part II, July 1964, Part III, September 1965.

80. P. Kofstad, "High Temperature Oxidation of Metals", John Wiley & Sons, Inc. (1966) p. 175.

81. P. Kofstad, "High Temperature Oxidation of Metals", John Wiley & Sons, Inc. (1966) p. 175.

DISTRIBUTION LIST FOR RESEARCH GRANT NGR-33-013-017

	ADDRESSEE			NUMBER OF COPIES
1.	NASA Headquarters 600 Independence Avenue S.W. Washington, D.C. 20546			
	Attention: N.F. Rekos (RAP)			1
	G. Deutsch (RRM)			1
	Winnie M. Morgan (Y)			10
2.	NASA-Lewis Research Center 21000 Brookpark Road Cleveland, Ohio 44135			
	Attention: Technology Utilization Office	M.S.	3-19	1
	Report Control Office	M.S.	5-5	1
	Fluid System Components Division			
	I.I. Pinkel	M.S.	5-3	1
	P.T. Hacker	M.S.	5-3	1
	Airbreathing Engines Division			
	J. Howard Childs	M.S.	60-4	1
	R.E. Oldrieve	M.S.	60-6	2
	Dr. W.H. Roudebush	M.S.	60-6	1
	A. Anglin	M.S.	60-6	1
	Airbreathing Engines Procurement Section			
	John H. Deford	M.S.	60-5	1
	Materials & Stresses Division			
	S.J. Grisaffe	M.S.	49-1	2
	G.M. Ault	M.S.	105-1	1
	R.W. Hall	M.S.	105-1	1
	J. Johnston	M.S.	49-1	1
	J.W. Weeton	M.S.	49-1	1
	H.B. Probst	M.S.	49-1	
	J.W. Fresche	M.S.	49-1	1
	Library	M.S.	60-3	2
3.	FAS Headquarters 800 Independence Avenue, S.W. Washington, D.C. 20553			
	Attention: F.B. Howard/SS-210			1
	Brig. Gen. J.C. Maxwell			1

	ADDRESSEE	NUMBER OF COPIES
4.	Supersonic Transport Office Wright-Patterson Air Force Base, Ohio 45433 Attention: SESHS, J.L. Wilkins	2
5.	Batelle Memorial Institute 505 King Avenue Columbus, Ohio 43201 Attention: Defense Metals Information Center (DMIC)	1
6.	Boeing Company P.O. Box 733 Renton, Washington 98055 Attention: W.E. Binz, Jr. SST Unit Chief	1
7.	Chromalloy Corporation 169 Western Highway West Nyack, New York 10994 Attention: L. Miasel	1
8.	General Electric Company Materials Devel. Lab. Oper. Advanced Engine & Technology Dept. Cincinnati, Ohio 45215 Attention: L.P. Jahnke	1
9.	IIT Research Institute Technology Center Chicago, Illinois 60616 Attention: V. Hill	1
10.	Pratt & Whitney Aircraft Division United Aircraft Corporation 400 Main Street East Hartford, Connecticut 06108 Attention: E.F. Bradley	
11.	Solar, A Division of International Harvester 2200 Pacific Highway San Diego, California 92112 Attention: A.R. Stetson	1

	ADDRESSEE	NUMBER OF COPIES
12.	Sylvania Electric Products Sylcor Division Cantiague Road Hicksville, Long Island, New York 11802 Attention: L. Sama	1
13.	Texas Instruments P.O. Box 5303 Dallas, Texas 75222 Attention: Materials R & D Lab.	1
14.	University of Washington Ceramics Department Seattle, Washington 98101 Attention: Dr. J. Mueller	1
15.	Spartan Aviation, Inc. Aviation Service Division P.O. Box 51239 Dawson Station Tulsa, Oklahoma 07052	1
16.	Westinghouse Electric Corporation Research Laboratories Pittsburgh, Pennsylvania 15235 Attention: R. Grekila	1
17.	Headquarters, USAF Air Force Office of Scientific Research Propulsion Research Division Washington, D.C. 20025 Attention: Dr. M. Slawsky	1
18.	Defense Documentation Center (DDC) Cameron Station 5010 Duke Street Alexandria, Virginia 22314	1
19.	AFML Wright-Patterson AFB, Ohio 45433 Attention: N. Geyer (MAMP) E. Beardslee (MAAE)	1 1

	ADDRESSEE	NUMBER OF COPIES
20.	Department of the Navy ONR Code 429 Washington, D.C. 20025 Attention: Dr. R. Roberts	1
21.	NASA-Langley Research Center Langley Station Hampton, Virginia 23365 Attention: Technical Library E.E. Mathauser	1 1
22.	NASA-Manned Spacecraft Center Structures & Mechanics Division 2101 Webster-Seabrook Road Houston, Texas 77058 Attention: Branch Chief (ES441)	1
23.	SAAMA (SA-NLP) Kelly Air Force Base San Antonio, Texas 78241 Attention: Michael Claypool	1
24.	Westinghouse Astronuclear Laboratory P.O. Box 10864 Pittsburgh, Pennsylvania 15236 Attention: Mr. R. Begley	1